AUG 29 '45

UNITED STATES DEPARTMENT OF COMMERCE

Journal of Research

of the

National Bureau of Standards

Vol. 35, No. 1 July 1945

CONTENTS

RP	TITLE AND AUTHOR	Page
1660.	Single-cylinder engine tests of substitute motor fuels. Donald B. Brooks.....[Price 10 cents]	1
1661.	Thermodynamic properties of 1.3-butadiene in the solid, liquid, and vapor states. Russell B. Scott, Cyril H. Meyers, Robert D. Rands, Jr., Ferdinand G. Brickwedde, and Norman Bekkedahl .....[Price 10 cents]	39
1662.	Effects of some oxide additions on the thermal length changes of zirconia. R. F. Geller and Paul Yavorsky.....[Price 10 cents]	87
1663.	Acetyl derivatives of certain heptoses, of gulose, and of lactulose. Harriet L. Frush and Horace S. Isbell.....[Price 5 cents]	111

The articles listed may be purchased separately (see cover page II) at the prices stated

A monthly periodical of pure and applied science published by our National Government

Journal of Research of the National Bureau of Standards

The July 1945 issue of the JOURNAL OF RESEARCH of the National Bureau of Standards begins the thirty-fifth semiannual volume of this periodical. Fundamental researches in progress in the Bureau's laboratories are reported in this JOURNAL. If you are interested in new developments in science and technology, you should receive the JOURNAL. If you are not already a subscriber, you are invited to send in your subscription.

Technical News Bulletin

This is a monthly publication containing short articles reporting progress of work in the Bureau laboratories, abstracts of papers which appear in the JOURNAL OF RESEARCH, accounts of scientific and technical meetings in which the Bureau has taken part, a list of all publications by members of the staff, and other items within the Bureau's fields. The BULLETIN is designed primarily to give a general and timely review of the activities of the Bureau in brief form. It is a prompt and reliable source of official information. If you have not already subscribed for the BULLETIN, you are invited to do so.

ANNUAL SUBSCRIPTION	Price	
	United States, Canada, Cuba, Mexico, Newfoundland, Republic of Panama	Other countries
JOURNAL OF RESEARCH of the National Bureau of Standards:		
12 monthly issues (2 volumes), paper covers	$3.50	$4.50
Bound volume (½ year, 1 volume), blue buckram	3.00	3.50
Technical News Bulletin, 12 monthly issues	.50	.70

Research Papers, reprinted individual articles appearing in the JOURNAL OF RESEARCH, are available from the Superintendent of Documents shortly after appearance of monthly issues of the JOURNAL.

B9

Address orders only to
Superintendent of Documents, U. S. Government Printing Office
Washington 25, D. C.

UNITED STATES DEPARTMENT OF COMMERCE
HENRY A. WALLACE, Secretary
NATIONAL BUREAU OF STANDARDS
Lyman J. Briggs, Director

✦

Journal of Research

of the

National Bureau of Standards

✦

Volume 35, Number 1

July 1945

[Published with approval of the Director of the Budget]

UNITED STATES
GOVERNMENT PRINTING OFFICE
WASHINGTON : 1945

For sale by the Superintendent of Documents, U. S. Government Printing Office
Washington 25, D. C. - Price 30 cents, $3.50 per year on subscription

The prices of the separate Research Papers appearing in this JOURNAL are given on the front cover page. If 100 or more copies of any separate are ordered, a discount of 25 percent is allowed. Those who desire copies of separate Research Papers should send their orders and remittances without delay to the Superintendent of Documents, U. S. Government Printing Office, Washington 25, D. C. Research Papers are not printed from electrotypes, and usually no more reprints can be had when the first and only printing is exhausted.

MATHEMATICAL TABLES

A list of the mathematical tables now obtainable from the National Bureau of Standards is printed on pages 3 and 4 of the JOURNAL cover. New tables will be announced from time to time as they become available. An order blank is available on the last page of this issue.

Engine lib.
Direct

U. S. DEPARTMENT OF COMMERCE · NATIONAL BUREAU OF STANDARDS

RESEARCH PAPER RP1660

Part of Journal of Research of the National Bureau of Standards, Volume 35, July 1945

SINGLE-CYLINDER ENGINE TESTS OF SUBSTITUTE MOTOR FUELS

By Donald B. Brooks

ABSTRACT

Single-cylinder-engine tests of nonhydrocarbon fuels and gasoline, at fixed compression ratio and at the compression ratio for trace knock for each fuel, show no material differences in performance other than those associated with differences in heats of combustion and vaporization. All the nonhydrocarbon fuels could be operated at compression ratios higher than was permissible with the gasoline, with corresponding increases in power and thermal efficiency.

CONTENTS

	Page
I. Scope of investigation	1
II. Fuels, test equipment, and procedure	2
III. Test results	3
IV. Discussion of test results	26
1. Power at constant compression ratio	26
2. Comparison of power with calculated values	26
3. Optimum spark advance	28
4. Power at compression ratio for trace knock	28
5. Combustion performance of fuels	29
(a) Relative power versus heat input	29
(b) Rate of burning	31
(c) Thermal-plug temperatures	33
6. Power at constant spark advance	34
7. Power–mixture–spark-advance relationship	36
V. Conclusions	36
VI. Appendix	37

I. SCOPE OF INVESTIGATION

The work reported herein is a portion of an extensive investigation of substitute motor fuels conducted by the National Bureau of Standards for the United States Foreign Economic Administration. The Bureau's part in this investigation, begun in 1942, was to develop technical information on the utilization of substitute fuels that could be produced in foreign countries where petroleum products were scarce and where military exigencies required the use of automotive transport. Considerations of economics and production specifically were not part of the investigation as assigned to this Bureau, although

it was understood that no data were to be developed on materials the production of which would involve unreasonable costs.

The objective of the work covered by this report was to determine on a precision test engine, the power, thermal efficiency, and combustion performance of each of a series of substitute fuels and of gasoline, both at the compression ratio giving trace knock on gasoline and at the compression ratio at which trace knock prevailed with each fuel.

II. FUELS, TEST EQUIPMENT, AND PROCEDURE

The fuels used in this work were selected from those used in the liquid-fuels phase of the major investigation, and included only non-hydrocarbon fuels, with the exception of the reference gasoline. Table 1 gives the composition, knock rating, and experimental heat of combustion as determined by bomb calorimeter of each fuel used in this part of the work. The heat of combustion values were determined by R. S. Jessup of this Bureau, and are believed to be accurate to 0.1 percent.

TABLE 1.—*Data on test fuels*

Fuel	Composition	Heat of combustion, Btu/lb at at 30° C		Octane number	
		Higher	Lower	ASTM motor	CFR research
A	Reference gasoline	(a)	(a)	70	72
B	190-proof ethyl alcohol	11,760	10,570	94	a 2.7
C	200-proof ethyl alcohol	12,720	11,520	92	a 1.4
D	75 percent ethanol, 25 percent diethyl ether	13,410	12,850	89	b 0.3
E	Reference gasoline	20,170	18,810	70	72
1	50 percent acetone, 50 percent butanol	14,380	13,270	90	b 0.2
2	27 percent acetone, 6 percent ethanol, 67 percent butanol.	14,650	13,500	88	b 1
3	28.5 percent acetone, 71.5 percent butanol	14,860	13,690	87	100

a Assumed to be same as for fuel E.
b Milliliters of tetraethyl lead per gallon of isooctane.

The test apparatus consisted of a CFR (Coordinating Fuel Research Committee) single-cylinder variable-compression engine direct-connected to an essentially constant-speed alternating-current dynamometer, and provided with all necessary test instruments. Fuel was injected into the intake pipe, the stroke of the injector being controlled with a micrometer screw. Spark advance was indicated by the capacitance discharge of a neon tube mounted in an insulating disk attached to the crankshaft. The temperature of a thermal plug screwed into the cylinder head was shown on an automatic-indicating potentiometer graduated in degrees Fahrenheit. As the engine is in effect hopper-cooled, coolant temperature is automatically maintained at the boiling point. Fuel consumption was determined by noting the time required to use one-fourth pound of fuel.

With the engine operating at best-power mixture ratio and optimum spark advance on gasoline (reference fuel blend) of 70 motor octane number, the compression ratio was adjusted to give trace knock. The ratio so found was 5.11. Each fuel was tested under this condition; each fuel was also tested under the compression ratio at which the fuel itself gave trace knock at best-power mixture ratio and optimum spark advance.

The same test procedure was followed with each fuel. The fuel flow was adjusted initially to approximately the least rate at which consistent firing could be obtained. While operating at this rate, two or more measurements of fuel consumption were made. Coincidentally, observations of power and of thermal-plug temperature were made at a series of spark settings from full retard to full advance, a range of about 40 degrees. At the conclusion of these readings, the fuel flow was increased and the observations were repeated. This was continued, in appropriate steps, to a fuel flow about 50 percent greater than that giving maximum power. Readings of barometric pressure, ambient temperature, atmospheric humidity, and engine friction were taken frequently throughout the tests.

Power and fuel-consumption rates were corrected to standard conditions of 59° F. and 29.53 in. Hg dry air pressure by the formula

$$P_s = P_0 \frac{29.53}{B-h}\sqrt{\frac{460+t}{519}},$$

where

P_0 = observed power or fuel consumption
P_s = corrected power or fuel consumption
B = barometric pressure, in. Hg
h = pressure of water vapor, in. Hg
t = intake air temperature, °F.

III. TEST RESULTS

The sum of the brake and friction power readings at each rate of fuel flow was plotted against the respective spark advance. A sample of the resulting curves is shown in figure 15. The coordinates of the peak of each curve were determined and tabulated, together with the faired values of indicated power at each 5 degrees of spark advance. These values are given in tables 2 to 15.

TABLE 2.—*Power and economy tests on reference gasoline—first run*

The lower set of data was obtained on a different day from the upper set

[Compression ratio 5.11]

Fuel consumption	Fuel heat input	Indicated horsepower at spark advance of—							Maximum indicated horse power	Optimum spark advance	Specific fuel consumption
		40°	45°	50°	55°	60°	65°	70°			
lb/hr	*Btu/hr×10⁻³*									*Degrees*	*lb/ihp-hr*
5.66	114.2	12.08	12.34	12.46	12.48	12.45	12.36	12.25	12.49	53.9	0.453
5.98	120.6	12.42	12.64	12.71	12.71	12.65	12.54	12.38	12.72	52.2	.470
6.49	130.9	12.65	12.78	12.79	12.73	12.62	12.45	12.24	12.80	49.0	.507
6.75	136.1	12.64	12.78	12.80	12.68	12.49	12.27	12.00	12.80	47.7	.527
7.28	146.8	12.55	12.63	12.64	12.57	12.42	12.19	11.93	12.64	47.6	.576
5.21	105.1	9.90	10.39	10.76	10.81	10.70	10.55	10.38	10.83	53.0	.481
5.98	120.6	12.31	12.49	12.58	12.59	12.56	12.49	12.39	12.59	54.5	.475
6.56	132.3	12.42	12.54	12.58	12.55	12.46	12.33	12.14	12.58	50.6	.521
6.83	137.8	12.54	12.68	12.72	12.69	12.59	12.44	12.25	12.72	50.6	.537
7.84	158.1	12.38	12.51	12.56	12.50	12.37	12.17	11.83	12.56	50.0	.624
8.56	172.7	12.04	12.26	12.40	12.36	12.19	11.96	11.69	12.42	51.0	.689
9.43	190.2	11.60	11.90	12.09	12.12	12.03	11.88	11.65	12.12	53.7	.778
10.18	205.3	10.94	11.32	11.60	11.74	11.78	11.77	11.70	11.78	61.1	.864
Maximum power.....12.80 at 6.60 lb/hr. Minimum values.....										47.5	0.452

TABLE 3.—*Power and economy tests on 190-proof ethyl alcohol*

[Compression ratio 5.11]

Fuel consumption	Fuel heat input	Indicated horsepower at spark advance of—							Maximum indicated horsepower	Optimum spark advance	Specific fuel consumption	Thermometer plug temperature at optimum spark advance
		40°	45°	50°	55°	60°	65°	70°				
lb/hr	*Btu/hr* $\times 10^{-3}$									*Degrees*	*lb/ihp-hr*	°*F*
8.18	96.2	8.65	9.10	9.47	9.76	9.98	10.13	10.22	10.28	76.0	0.796	<600
8.71	102.4	10.70	11.10	11.36	11.52	11.62	11.63	11.52	11.64	62.6	.749	617
9.93	116.8	12.59	12.83	12.94	12.97	12.92	12.81	12.61	12.97	54.3	.766	711
11.10	130.5	13.31	13.45	13.46	13.39	13.25	13.04	12.76	13.47	48.2	.824	744
12.53	147.4	13.29	13.40	13.40	13.29	13.12	12.90	12.63	13.41	47.0	.934	728
13.87	163.1	13.15	13.24	13.27	13.22	13.09	12.89	12.63	13.27	49.1	1.045	684
15.23	179.1	12.67	12.90	13.02	13.05	13.01	12.91	12.76	13.05	54.6	1.167	635
16.19	190.4	12.26	12.49	12.65	12.75	12.76	12.72	12.62	12.76	59.0	1.269	610
16.71	196.5	11.62	12.12	12.31	12.41	12.44	12.44	12.38	12.44	61.6	1.343	<600
Maximum power.....13.46 at 11.40 lb/hr. Minimum values.....										47.0	0.746	.....

TABLE 4.—*Power and economy tests on 200-proof ethyl alcohol*

[Compressed ratio 5.11]

Fuel consumption	Fuel heat input	Indicated horsepower at spark advance of—							Maximum indicated horsepower	Optimum spark advance	Specific fuel consumption	Thermometer plug temperature at optimum spark advance
		40°	45°	50°	55°	60°	65°	70°				
lb/hr	*Btu/hr* $\times 10^{-3}$									*Degrees*	*lb/ihp-hr*	°*F*
7.58	96.4	9.00	9.44	9.75	9.96	10.12	10.20	10.22	10.22	69.0	0.742	<600
8.09	102.9	10.78	11.03	11.25	11.43	11.56	11.62	11.63	11.64	67.4	.695	<600
8.76	111.4	11.91	12.20	12.35	12.41	12.41	12.35	12.20	12.42	57.3	.705	681
10.34	131.5	13.27	13.36	13.37	13.30	13.16	12.92	12.60	13.38	48.0	.773	740
11.59	147.4	13.28	13.37	13.35	13.23	13.01	12.74	12.41	13.37	46.6	.867	723
13.14	167.1	13.18	13.31	13.32	13.24	13.07	12.85	12.60	13.33	48.0	.986	700
14.59	185.6	12.77	13.04	13.16	13.15	13.03	12.87	12.67	13.16	51.7	1.109	654
15.61	198.6	12.30	12.59	12.76	12.82	12.84	12.82	12.76	12.84	60.5	1.216	610
16.08	204.5	11.87	12.23	12.39	12.45	12.46	12.44	12.36	12.46	59.2	1.291	<600
Maximum power.....13.38 at 11.00 lb/hr. Minimum values.....										46.9	0.695	.....

TABLE 5.—*Power and economy tests on ether blend, fuel D*

[Compression ratio 5.11]

Fuel consumption	Fuel heat input	Indicated horsepower at spark advance of—							Maximum indicated horsepower	Optimum spark advance	Specific fuel consumption	Thermometer plug temperature at optimum spark advance
		40°	45°	50°	55°	60°	65°	70°				
lb/hr	*Btu/hr* $\times 10^{-3}$									*Degrees*	*lb/ihp-hr*	°F
7.19	96.4	8.58	9.23	9.62	9.88	10.05	10.14	10.13	10.15	67.4	0.708	<600
7.60	101.9	10.44	10.72	10.93	11.07	11.17	11.21	11.19	11.21	66.2	.678	612
8.58	115.1	12.49	12.72	12.84	12.84	12.76	12.61	12.41	12.85	52.6	.668	720
9.45	126.7	13.25	13.35	13.35	13.28	13.13	12.90	12.60	13.36	47.4	.707	755
10.64	142.7	13.35	13.40	13.36	13.23	13.02	12.68	12.31	13.40	44.9	.794	739
11.60	155.6	13.31	13.36	13.31	13.16	12.94	12.67	12.32	13.34	44.6	.870	716
12.84	172.2	13.12	13.24	13.23	13.13	12.92	12.68	12.39	13.25	47.1	.969	687
13.81	185.2	12.89	13.05	13.09	13.06	12.93	12.76	12.57	13.07	50.0	1.057	662
15.01	201.3	12.27	12.59	12.78	12.86	12.85	12.78	12.67	12.86	57.3	1.167	625
15.77	211.5	11.71	12.08	12.32	12.48	12.57	12.60	12.56	12.60	64.8	1.252	616
Maximum power.....		13.41 at 10.00 lb/hr. Minimum values..								44.5	0.663	.....

TABLE 6.—*Power and economy tests on blend 1*

[Compression ratio 5.11]

Fuel consumption	Fuel heat input	Indicated horsepower at spark advance of—							Maximum indicated horsepower	Optimum spark advance	Specific fuel consumption	Thermometer plug temperature at optimum spark advance
		40°	45°	50°	55°	60°	65°	70°				
lb/hr	*Btu/hr* $\times 10^{-3}$									*Degrees*	*lb/ihp-hr*	°F
7.05	101.4	8.95	9.48	9.94	10.30	10.56	10.76	10.89	11.00	78	0.641	631
7.65	110.0	11.14	11.38	11.58	11.74	11.86	11.94	11.93	11.95	67.5	.640	703
8.61	123.8	12.62	12.86	12.97	12.96	12.86	12.70	12.49	12.98	52.0	.663	736
10.30	148.1	12.90	13.07	13.08	12.98	12.81	12.58	12.30	13.09	48.1	.787	725
11.42	164.2	12.81	12.97	12.98	12.89	12.74	12.54	12.28	12.99	47.8	.879	699
12.41	178.5	12.59	12.77	12.80	12.71	12.56	12.38	12.18	12.80	48.4	.969	669
13.24	190.4	12.10	12.46	12.60	12.62	12.57	12.48	12.33	12.62	54.3	1.049	641
14.32	205.9	11.72	12.10	12.26	12.32	12.33	12.31	12.25	12.33	59.3	1.161	610
Maximum power.....		13.15 at 9.50 lb/hr. Minimum values..								47.8	0.639	.....

TABLE 7.—*Power and economy tests on blend 2*

[Compression ratio 5.11]

Fuel consumption	Fuel heat input	Indicated horsepower at spark advance of—							Maximum indicated horsepower	Optimum spark advance	Specific fuel consumption	Thermometer plug temperature at optimum spark advance
		40°	45°	50°	55°	60°	65°	70°				
lb/hr	*Btu/hr* $\times 10^{-3}$									*Degrees*	*lb/ihp-hr*	°F
6.61	96.8	8.63	9.10	9.46	9.74	9.94	10.07	10.09	10.09	68.5	0.655	<600
6.77	99.2	9.54	10.04	10.44	10.76	10.98	11.13	11.14	11.16	68.5	.607	611
7.25	106.2	10.84	11.20	11.48	11.68	11.81	11.88	11.87	11.88	67.2	.610	690
7.84	114.9	11.98	12.26	12.42	12.50	12.51	12.45	12.32	12.52	58.2	.626	710
8.27	121.2	12.66	12.94	13.07	12.99	12.83	12.63	12.41	13.07	50.2	.633	725
9.29	136.1	13.04	13.19	13.19	13.09	12.90	12.68	12.42	13.20	47.9	.704	732
10.39	152.2	12.99	13.08	13.08	13.00	12.84	12.61	12.29	13.09	47.6	.794	713
11.37	166.6	12.82	12.97	13.00	12.95	12.82	12.60	12.27	13.00	49.4	.875	660
12.64	185.2	12.50	12.73	12.81	12.81	12.74	12.62	12.40	12.82	52.7	.986	655
13.62	199.5	12.01	12.29	12.45	12.54	12.53	12.45	12.32	12.54	57.4	1.086	633
14.49	212.3	11.48	11.82	12.03	12.15	12.20	12.20	12.15	12.20	63.0	1.188	<600
Maximum power..... 13.21 at 9.15 lb/hr. Minimum values.....										47.5	0.607	.....

TABLE 8.—*Power and economy tests on blend 3*

[Compression ratio 5.11]

Fuel consumption	Fuel heat input	Indicated horsepower at spark advance of—							Maximum indicated horsepower	Optimum spark advance	Specific fuel consumption	Thermometer plug temperature at optimum spark advance
		40°	45°	50°	55°	60°	65°	70°				
lb/hr	*Btu/hr* $\times 10^{-3}$									*Degrees*	*lb/ihp-hr*	°F
6.37	94.7	7.88	8.56	9.02	9.33	9.54	9.65	9.60	9.66	66.4	0.659	<600
6.64	98.7	9.30	10.10	10.53	10.79	10.95	11.04	11.04	11.04	67.4	.601	<600
7.18	106.7	11.07	11.41	11.66	11.79	11.83	11.82	11.75	11.83	60.5	.607	666
7.57	112.5	12.06	12.36	12.49	12.50	12.42	12.30	12.13	12.51	52.5	.605	717
8.08	120.1	12.44	12.69	12.81	12.83	12.75	12.60	12.36	12.83	53.2	.630	727
8.94	132.8	12.84	13.03	13.12	13.03	12.85	12.61	12.33	13.12	49.6	.681	732
9.83	146.1	12.85	13.04	13.07	12.98	12.78	12.53	12.22	13.08	49.0	.752	725
10.69	158.9	12.68	12.87	12.93	12.87	12.72	12.52	12.24	12.93	49.9	.827	696
11.72	174.2	12.45	12.70	12.83	12.77	12.66	12.46	12.22	12.83	51.6	.913	660
12.87	191.2	11.98	12.25	12.46	12.52	12.50	12.44	12.35	12.52	56.0	1.028	627
13.88	206.3	11.30	11.70	11.91	11.98	12.00	11.97	11.92	12.00	58.6	1.157	<600
Maximum power..... 13.10 at 8.95 lb/hr. Minimum values.....										49.0	0.600	.....

TABLE 9.—*Power and economy tests of 190-proof ethyl alcohol*

[Compression ratio 9.91]

Fuel consumption	Fuel heat input	Indicated horsepower at spark advance of—								Maximum indicated horsepower	Optimum spark advance	Specific fuel consumption	Thermometer plug temperature at optimum spark advance
		25°	30°	35°	40°	45°	50°	55°	60°				
lb/hr	*Btu/hr* $\times 10^{-3}$										*Degrees*	*lb/ihp-hr*	°*F*
8.64	101.6	13.32	13.88	14.32	14.52	14.47	14.26	13.88	13.13	14.53	41.6	0.595	727
9.09	106.9	13.98	14.70	15.12	15.20	14.99	14.63	14.16	13.58	15.22	38.7	.597	766
9.71	114.2	14.82	15.29	15.64	15.74	15.52	15.10	14.65	14.18	15.75	39.0	.617	798
10.56	124.2	15.12	15.85	16.04	16.05	15.90	15.48	14.97	14.42	16.06	37.7	.658	799
11.37	133.7	15.31	15.83	16.13	16.17	15.94	15.59	15.17	14.70	16.18	37.1	.703	771
12.21	143.6	15.15	15.76	16.07	16.16	16.06	15.78	15.36	14.81	16.16	39.8	.756	751
13.14	154.5	14.70	15.42	15.79	15.94	15.87	15.69	15.44	15.12	15.94	40.7	.824	727
14.08	165.6	14.37	15.03	15.40	15.58	15.63	15.58	15.47	15.25	15.63	44.9	.901	711
15.03	176.8	13.43	14.28	14.71	14.93	15.02	15.01	14.93	14.79	15.02	47.8	1.001	662
Maximum power . . . 16.18 at 11.45 lb/hr. Minimum values											37.3	0.595	.....

TABLE 10.—*Power and economy tests of 200-proof ethyl alcohol*

[Compression ratio 9.91]

Fuel consumption	Fuel heat input	Indicated horsepower at spark advance of—								Maximum indicated horsepower	Optimum spark advance	Specific fuel consumption	Thermometer plug temperature at optimum spark advance
		25°	30°	35°	40°	45°	50°	55°	60°				
lb/hr	*Btu/hr* $\times 10^{-3}$										*Degrees*	*lb/ihp-hr*	°*F*
7.48	95.1	11.44	12.37	12.96	13.24	13.35	13.29	12.99	12.50	13.35	46.0	0.560	702
7.90	100.5	12.75	13.67	14.02	14.16	14.12	13.84	13.35	12.56	14.17	41.4	.558	760
8.76	111.4	14.82	15.21	15.31	15.26	15.03	14.61	14.01	13.31	15.31	35.7	.572	785
9.73	123.8	15.77	16.03	16.10	16.03	15.76	15.28	14.71	14.13	16.10	35.0	.604	805
10.48	133.3	15.91	16.11	16.17	16.09	15.83	15.30	14.67	14.00	16.17	34.6	.648	800
11.68	148.6	15.66	16.02	16.12	16.09	15.80	15.38	14.82	14.09	16.12	35.7	.725	762
12.78	162.6	15.16	15.55	15.83	15.92	15.81	15.55	15.16	14.64	15.92	39.9	.803	708
13.79	175.4	14.26	15.05	15.46	15.59	15.57	15.38	15.04	14.63	15.60	41.5	.884	693
15.04	191.3	13.69	14.67	14.99	15.13	15.18	15.14	15.02	14.79	15.18	44.8	.991	648
15.80	201.0	13.58	14.41	14.76	14.91	14.97	14.94	14.83	14.64	14.97	45.6	1.055	<600
Maximum power . . . 16.18 at 10.65 lb/hr. Minimum values											34.7	0.558	.....

TABLE 11.—*Power and economy tests of ether blend, fuel D*

[Compression ratio 8.60]

Fuel consumption	Fuel heat input	Indicated horsepower at spark advance of—								Maximum indicated horsepower	Optimum spark advance	Specific fuel consumption	Thermometer plug temperature at optimum spark advance
		25°	30°	35°	40°	45°	50°	55°	60°				
lb/hr	*Btu/hr* $\times 10^{-3}$										*Degrees*	*lb/ihp-hr*	°*F*
7.24	97.1	11.38	12.25	12.93	13.25	13.28	13.12	12.82	12.36	13.30	43.4	0.544	699
7.92	106.2	13.20	13.77	14.18	14.26	14.23	14.04	13.66	13.20	14.26	41.0	.555	703
8.61	115.5	14.34	14.99	15.18	15.17	14.92	14.56	14.07	13.46	15.20	36.5	.566	728
9.21	123.5	14.99	15.44	15.63	15.60	15.35	14.95	14.45	13.84	15.64	36.6	.589	736
9.75	130.7	15.03	15.48	15.68	15.65	15.37	14.99	14.49	13.90	15.70	36.7	.621	785
10.43	139.9	14.95	15.41	15.62	15.58	15.37	15.03	14.53	13.86	15.64	36.6	.667	772
11.65	156.2	14.53	15.10	15.41	15.47	15.34	15.09	14.73	14.23	15.48	39.0	.753	730
12.68	170.0	13.96	14.64	15.06	15.21	15.22	15.06	14.85	14.56	15.22	42.4	.833	697
13.84	185.6	13.35	13.96	14.52	14.84	14.90	14.87	14.76	14.53	14.90	45.6	.929	653
14.21	190.6	12.44	13.58	14.24	14.50	14.61	14.63	14.53	14.25	14.64	48.1	.971	646
Maximum power . . . 15.70 at 9.70 lb/hr. Minimum values											36.5	0.545	

TABLE 12.—*Power and economy tests of blend 1*

[Compression ratio 8.18]

Fuel consumption	Fuel heat input	Indicated horsepower at spark advance of—								Maximum indicated horsepower	Optimum spark advance	Specific fuel consumption	Thermometer plug temperature at optimum spark advance
		25°	30°	35°	40°	45°	50°	55°	60°				
lb/hr	*Btu/hr* $\times 10^{-3}$										*Degrees*	*lb/ihp-hr*	°*F*
6.25	89.9	8.57	9.82	10.72	11.32	11.73	12.00	12.12	12.04	12.12	55.5	0.516	657
6.61	95.1	10.46	11.53	12.15	12.52	12.75	12.83	12.70	12.34	12.83	50.0	.515	696
6.96	100.1	11.78	12.93	13.32	13.47	13.47	13.30	12.99	12.61	13.48	42.2	.516	725
7.48	107.6	12.94	13.59	14.13	14.30	14.23	13.89	13.49	13.06	14.30	40.6	.523	778
8.42	121.1	14.34	14.74	14.98	15.04	14.87	14.49	14.05	13.58	15.05	39.0	.559	837
9.44	135.7	14.36	14.82	15.04	15.10	14.91	14.60	14.19	13.70	15.11	38.2	.625	771
10.37	149.1	14.16	14.74	14.98	15.04	14.96	14.67	14.27	13.82	15.04	39.5	.689	747
11.52	165.5	13.62	14.30	14.67	14.82	14.82	14.68	14.37	13.93	14.84	42.7	.776	711
12.48	179.5	12.92	13.73	14.23	14.47	14.58	14.59	14.46	14.16	14.60	47.9	.855	695
13.39	192.5	11.96	13.09	13.66	13.94	14.09	14.15	14.11	14.00	14.15	50.3	.946	654
Maximum power . . . 15.11 at 9.15 lb/hr. Minimum values											38.2	0.514	

TABLE 13.—*Power and economy tests of blend 2*

[Compression ratio 7.81]

Fuel consumption	Fuel heat input	Indicated horsepower at spark advance of—								Maximum indicated horse power	Optimum spark advance	Specific fuel consumption	Thermometer plug temperature at optimum spark advance
		25°	30°	35°	40°	45°	50°	55°	60°				
lb/hr	*Btu/hr* $\times 10^{-3}$										*Degrees*	*lb/ihp-hr*	°F
6.98	102.3	11.69	12.45	13.06	13.43	13.50	13.31	12.97	12.57	13.51	43.7	0.517	737
7.38	108.1	13.10	13.55	13.97	14.27	14.11	13.82	13.48	13.10	14.27	40.6	.517	775
8.28	121.3	14.12	14.66	14.91	14.93	14.81	14.48	14.08	13.66	14.94	38.1	.554	780
9.36	137.1	14.16	14.66	15.02	15.04	14.88	14.66	14.32	13.83	15.05	38.1	.622	760
9.98	146.2	13.90	14.56	14.91	14.95	14.85	14.67	14.41	14.05	14.96	39.4	.668	742
11.03	161.6	13.59	14.24	14.58	14.70	14.72	14.62	14.41	14.07	14.72	42.9	.749	714
12.03	176.2	12.70	13.42	13.98	14.34	14.46	14.46	14.33	13.93	14.48	47.5	.831	689
12.56	184.0	12.20	12.92	13.56	14.03	14.18	14.21	14.13	13.93	14.21	48.9	.884	659
Maximum power, 15.06 at 9.10 lb/hr. Minimum values											37.8	0.514	

TABLE 14.—*Power and economy tests of blend 3*

[Compression ratio 7.43]

Fuel consumption	Fuel heat input	Indicated horsepower at spark advance of—								Maximum indicated horse power	Optimum spark advance	Specific fuel consumption	Thermometer plug temperature at optimum spark advance
		25°	30°	35°	40°	45°	50°	55°	60°				
lb/hr	*Btu/hr* $\times 10^{-3}$										*Degrees*	*lb/ihp-hr*	°F
6.74	100.2	10.81	11.43	12.00	12.48	12.70	12.77	12.75	12.59	12.77	51.2	0.528	716
7.30	108.5	12.32	12.99	13.52	13.75	13.82	13.77	13.60	13.14	13.82	45.8	.528	769
8.28	123.0	13.82	14.31	14.68	14.73	14.61	14.34	13.94	13.45	14.74	39.4	.562	784
9.04	134.3	14.09	14.52	14.76	14.80	14.68	14.36	13.96	13.52	14.80	38.6	.611	770
9.90	147.1	13.97	14.46	14.69	14.73	14.61	14.27	13.86	13.40	14.73	38.7	.672	729
11.05	164.2	13.58	14.02	14.40	14.52	14.49	14.29	13.97	13.60	14.53	41.7	.760	683
12.31	182.9	12.92	13.64	13.97	14.15	14.20	14.15	13.97	13.63	14.20	45.1	.867	662
13.30	197.6	11.94	12.88	13.45	13.71	13.82	13.82	13.71	13.45	13.84	47.5	.961	625
Maximum power, 14.80 at 8.80 lb/hr. Minimum values											38.6	0.525	

TABLE 15.—*Power and economy tests of reference gasoline—second run*

[Compression ratio 5.11]

Fuel consumption	Fuel heat input	Indicated horsepower at spark advance of—						Maximum indicated horsepower	Optimum spark advance	Specific fuel consumption	Thermometer plug temperature at optimum spark advance
		30°	40°	50°	60°	70°	80°				
lb/hr	*Btu/hr* $\times 10^{-3}$								*Degrees*	*lb/ihp-hr*	°F
4.74	95.6	.....	.....	8.40	8.97	9.22	9.30	9.30	83.	0.510	<60
4.95	99.8	.....	.....	10.22	10.58	10.65	10.63	10.65	72.2	.465	67
5.04	101.7	.....	.....	10.69	10.98	11.01	10.92	11.02	66.8	.457	65
5.33	107.5	.....	.....	11.38	11.56	11.56	11.46	11.58	64.5	.460	75
5.35	107.9	.....	10.92	11.40	11.55	11.53	11.39	11.56	63.0	.463	-----
5.63	113.6	.....	11.72	12.08	12.04	11.89	.....	12.08	52.1	.466	78
5.94	119.8	.....	11.95	12.30	12.18	11.89	.....	12.30	51.0	.483	81
6.26	126.3	11.53	12.22	12.34	12.12	11.79	.....	12.35	47.2	.507	80
6.64	133.9	11.72	12.28	12.29	12.03	.....	.....	12.32	45.5	.539	78
7.24	146.0	11.63	12.25	12.21	11.86	.....	.....	12.30	44.1	.589	75
8.22	165.8	.....	11.90	12.16	11.92	11.34	.....	12.16	49.5	.676	71
9.19	185.4	.....	11.46	11.89	11.90	11.61	.....	11.94	55.3	.770	66
10.07	203.1	.....	10.88	11.27	11.66	11.57	.....	11.66	61.4	.864	62
11.09	223.7	.....	.....	9.80	10.58	11.05	10.99	11.09	74.0	1.000	<60
Maximum power....12.34 at 6.40 lb/hr. Minimum values.....									45.0	0.458	.....

Maximum indicated power and optimum spark advance were then plotted against fuel consumption, as was the derived function, indicated specific fuel consumption. Figures 1 to 14 show these curves. The first runs were made on a reference gasoline of 70 motor octane number, composed of standard reference fuels C–12 and A–6. As the engine operators were not familiar with the test method, the readings were somewhat erratic and did not adequately cover the mixture-ratio range, as shown in figure 1. For this reason, the gasoline run was repeated some months later, and is shown in figure 14. In the interim several changes had been made in the test engine, including the installation of a new camshaft, and reference fuels C–12 and A–6 were no longer available. A blend of C–13 and M–4, of 70 motor octane number, was therefore used. The maximum power shown in figure 14 is consequently about 3½ percent below that shown in figure 1. As the engine changes are believed to be responsible for this difference, the power and fuel-consumption values shown in figure 14 were corrected accordingly.

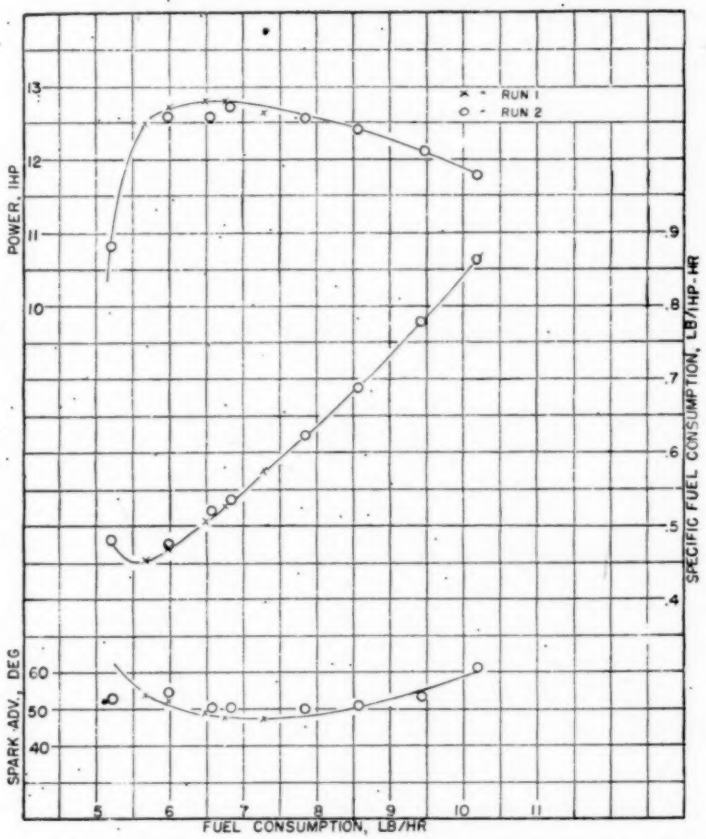

FIGURE 1.—*Power, specific fuel consumption, and optimum spark advance for reference gasoline.*

The engine was operated at a compression ratio of 5.11, which gave trace knock on this reference gasoline of 70 motor octane number. The two runs were made on successive days.

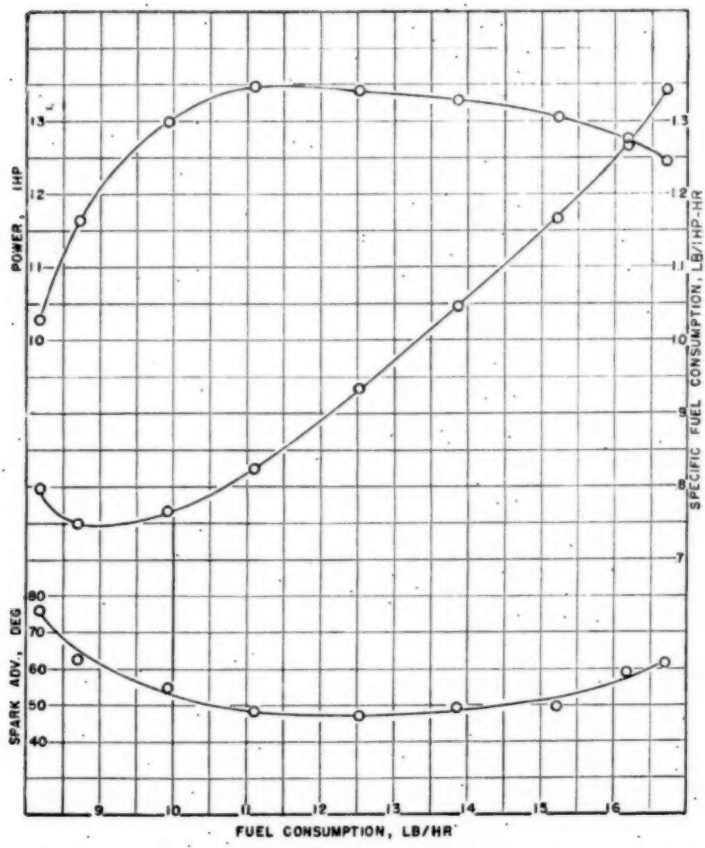

FIGURE 2.—*Power, specific fuel consumption, and optimum spark advance for 190-proof ethyl alcohol.*

The engine was operated at a compression ratio of 5.11, which gave trace knock on the reference gasoline of 70 motor octane number.

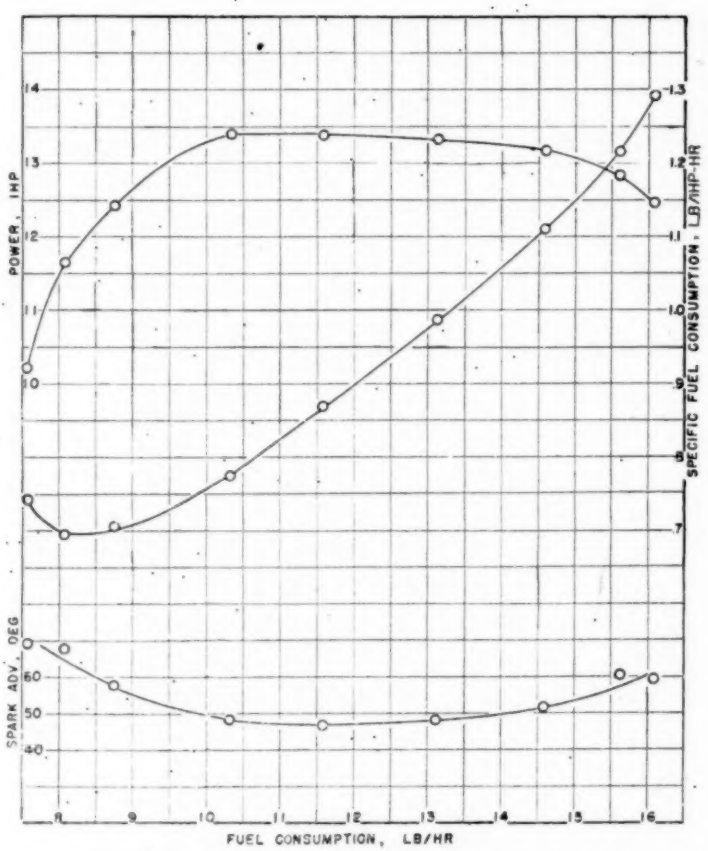

FIGURE 3.—*Power, specific fuel consumption, and optimum spark advance for 200-proof ethyl alcohol.*

The engine was operated at a compression ratio of 5.11, which gave trace knock on the reference gasoline of 70 motor octane number.

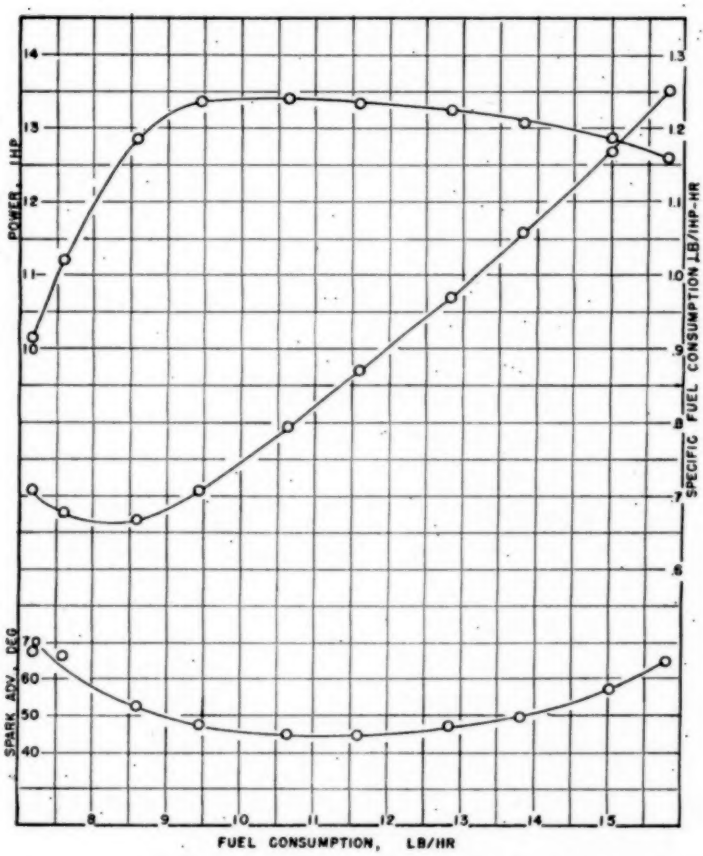

FIGURE 4.—*Power, specific fuel consumption, and optimum spark advance for a blend of 75 percent ethanol and 25 percent diethyl ether.*

The engine was operated at a compression ratio of 5.11, which gave trace knock on the reference gasoline of 70 motor octane number

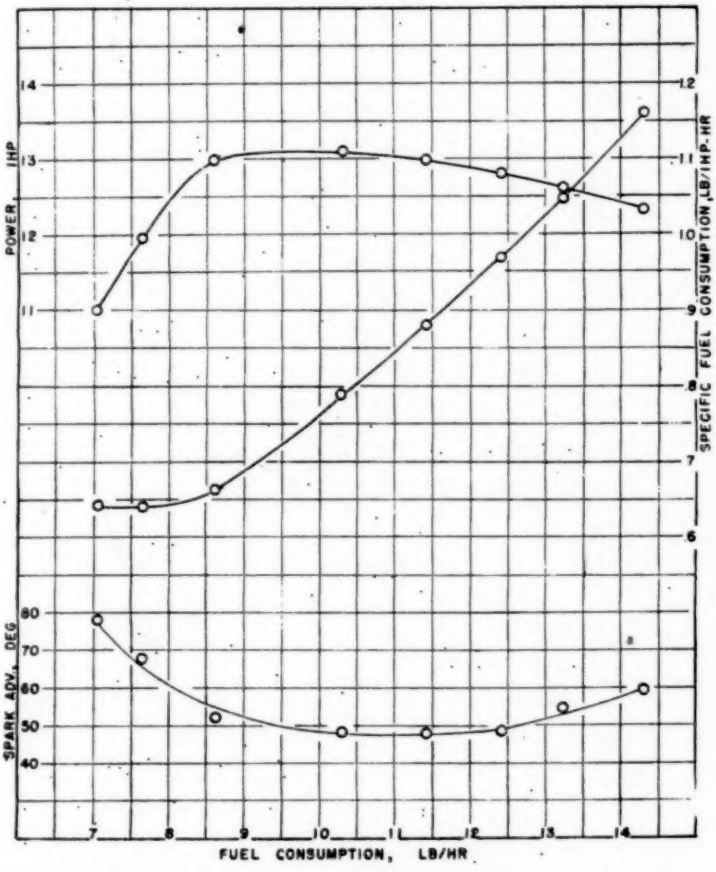

FIGURE 5.—*Power, specific fuel consumption, and optimum spark advance for a blend of 50 percent acetone and 50 percent butanol.*

The engine was operated at a compression ratio of 5.11, which gave trace knock on the reference gasoline of 70 motor octane number.

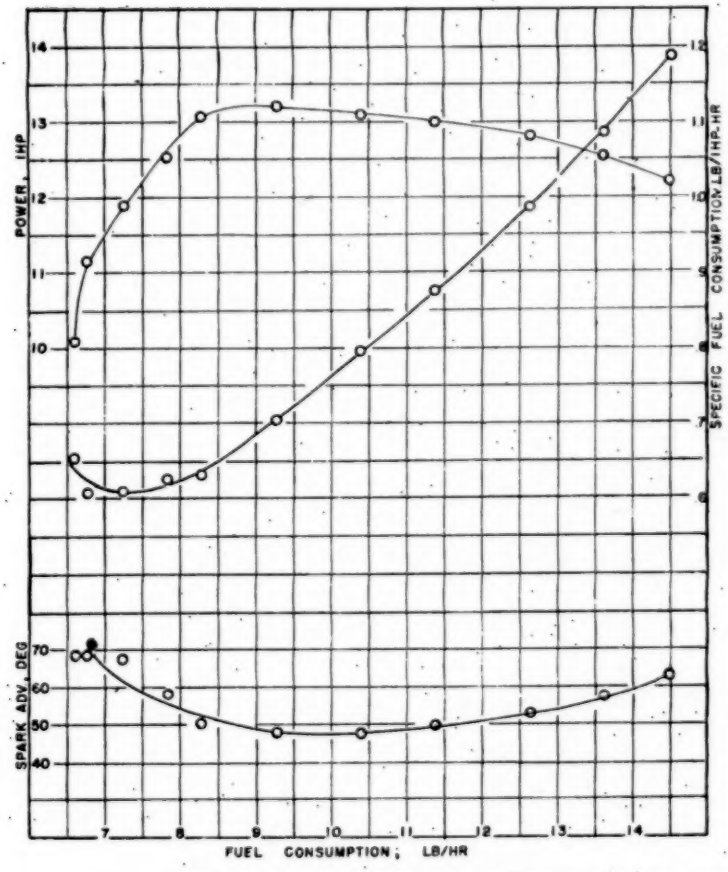

FIGURE 6.—*Power, specific fuel consumption, and optimum spark advance for a blend of 27 percent acetone, 6 percent ethanol, and 67 percent butanol.*

The engine was operated at a compression ratio of 5.11, which gave trace knock on the reference gasoline of 70 motor octane number.

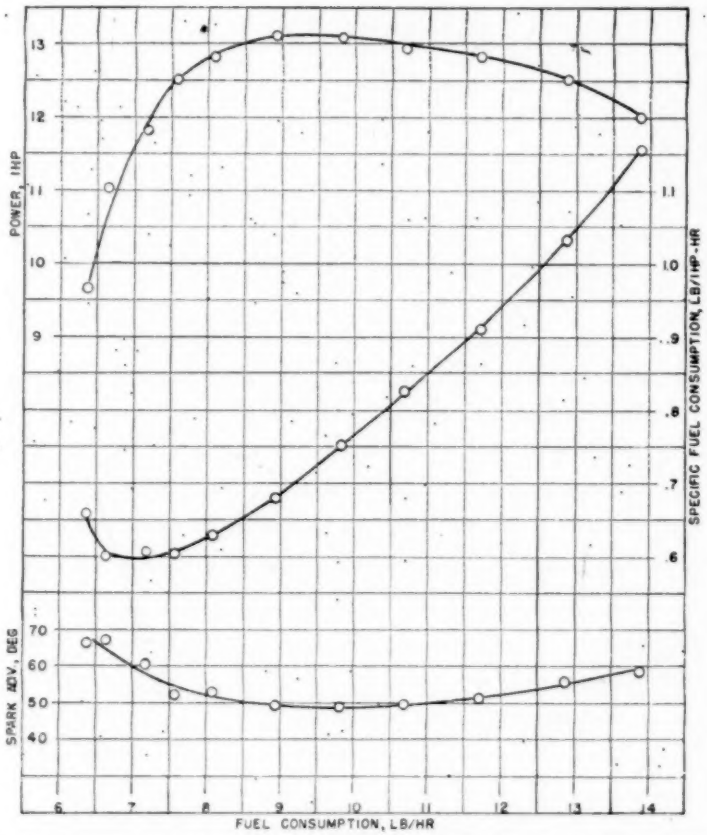

FIGURE 7.—*Power, specific fuel consumption, and optimum spark advance for a blend of 28.5 percent acetone and 71.5 percent butanol.*

The engine was operated at a compression ratio of 5.11, which gave trace knock on the reference gasoline of 70 motor octane number.

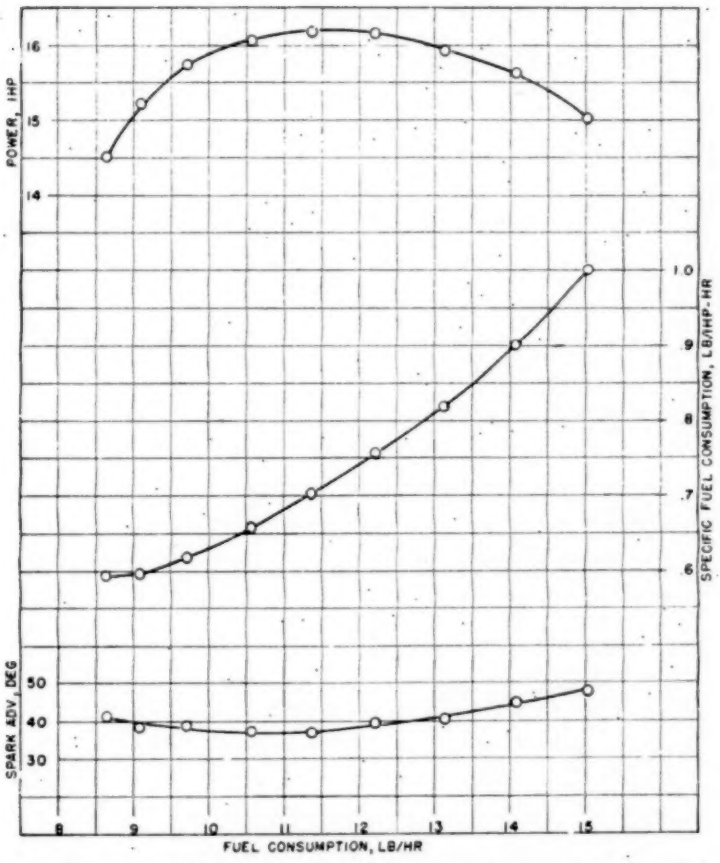

FIGURE 8.—*Power, specific fuel consumption, and optimum spark advance for 190-proof ethyl alcohol.*

The engine was operated at a compression ratio of 9.91, which gave trace knock on this fuel.

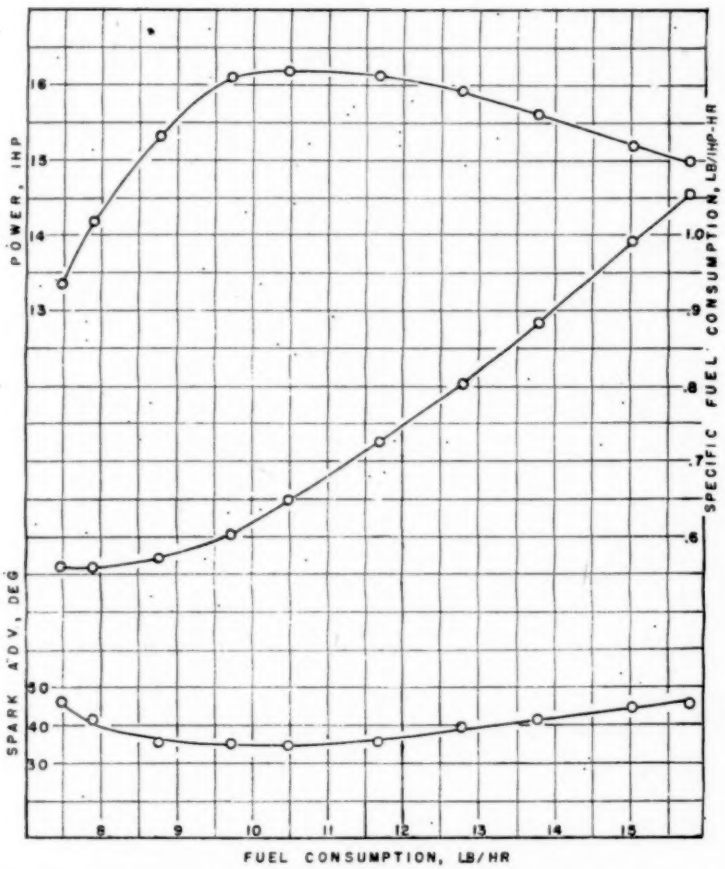

FIGURE 9.—*Power, specific fuel consumption, and optimum spark advance for 200-proof ethyl alcohol.*

The engine was operated at a compression ratio of 9.91, which gave trace knock on this fuel.

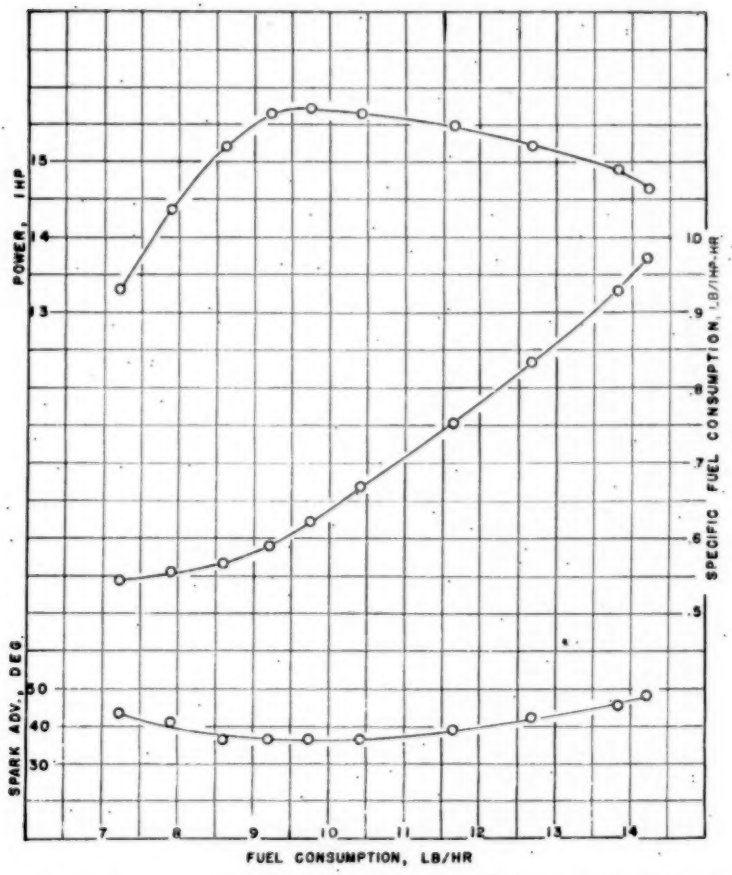

FIGURE 10.—*Power, specific fuel consumption, and optimum spark advance for a blend of 75 percent ethanol and 25 percent diethyl ether.*

The engine was operated at a compression ratio of 8.60, which gave trace knock on this fuel.

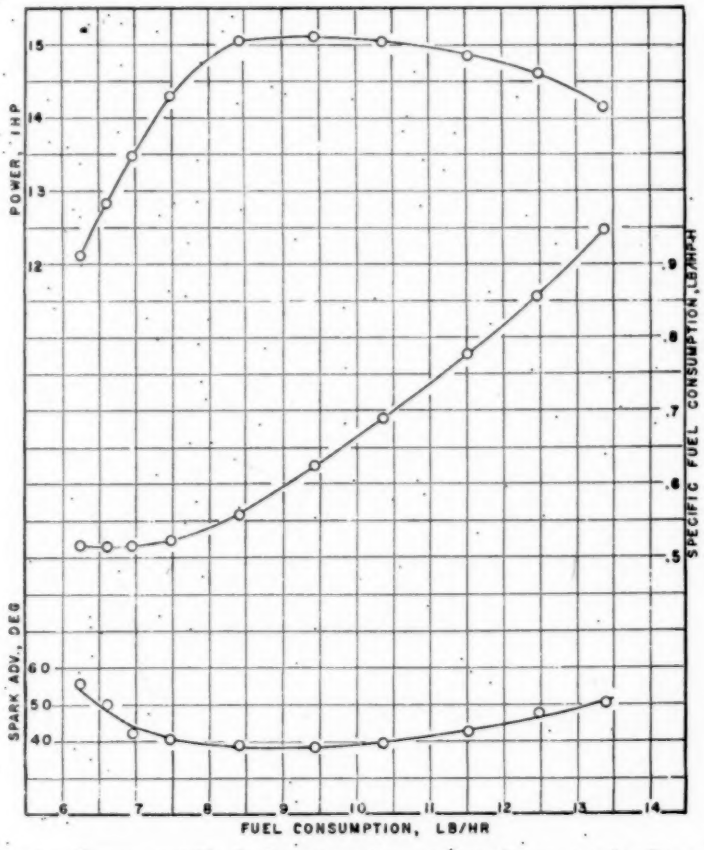

FIGURE 11.—*Power, specific fuel consumption, and optimum spark advance for a blend of 50 percent acetone and 50 percent butanol.*

The engine was operated at a compression ratio of 8.17, which gave trace knock on this fuel.

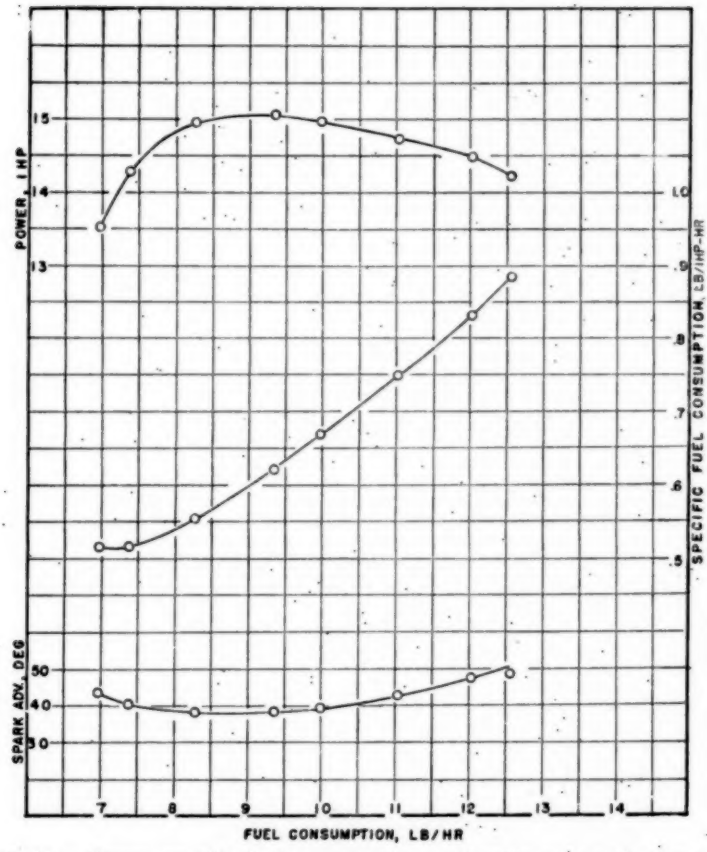

FIGURE 12.—*Power, specific fuel consumption, and optimum spark advance for a blend of 27 percent acetone, 6 percent ethanol, and 67 percent butanol.*

The engine was operated at a compression ratio of 7.80, which gave trace knock on this fuel.

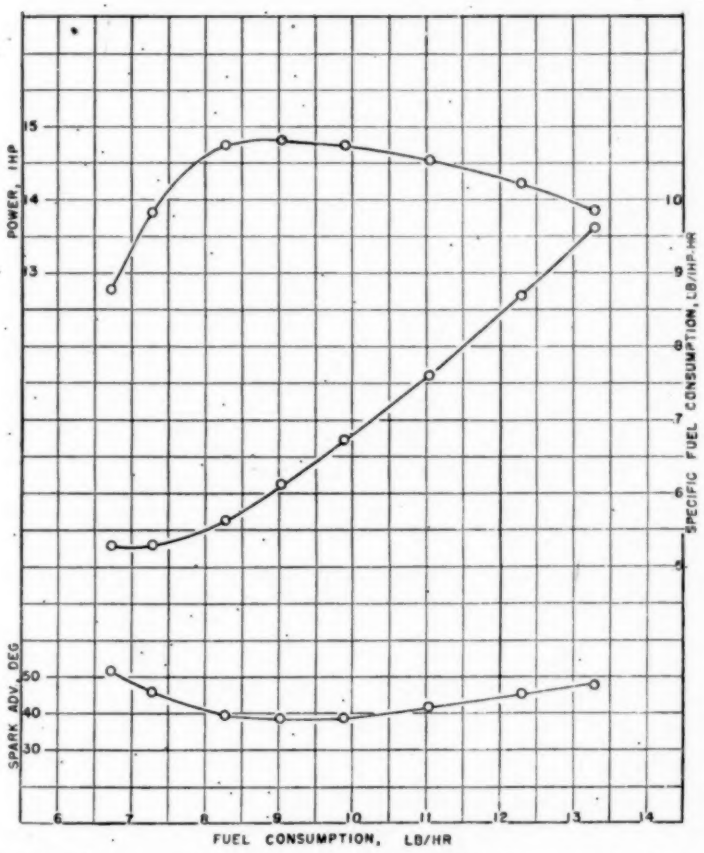

FIGURE 13.—*Power, specific fuel consumption, and optimum spark advance for a blend of 28.5 percent acetone and 71.5 percent butanol.*

The engine was operated at a compression ratio of 7.43, which gave trace knock on this fuel.

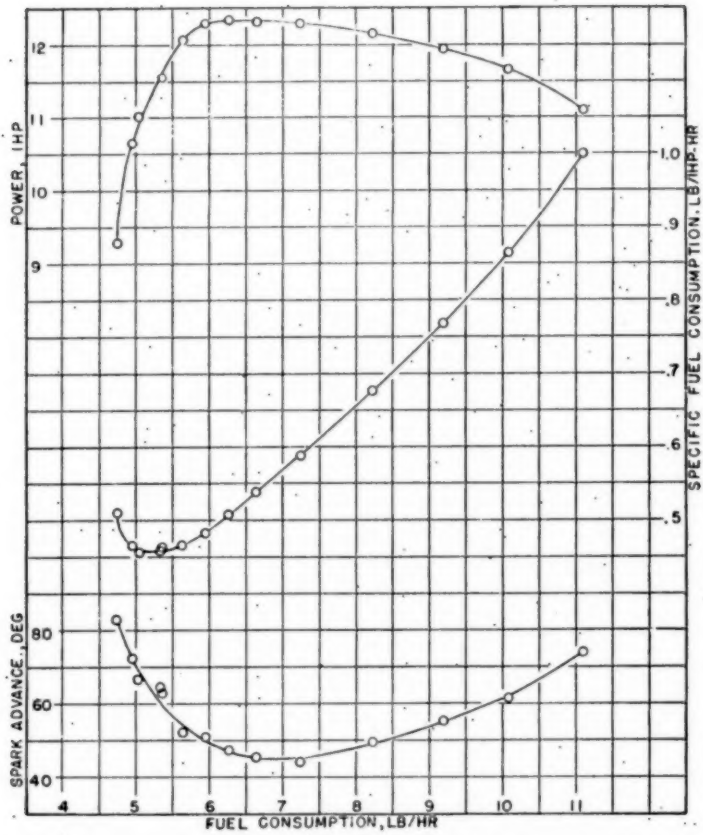

FIGURE 14.—*Power, specific fuel consumption, and optimum spark advance for second reference gasoline.*

The engine was operated at a compression ratio of 5.11, which gave trace knock on this reference gasoline of 70 motor octane number. This run, a repetition of that shown in figure 1, was made in order to cover more adequately the air-fuel range of interest. Several months elapsed between the test shown in figure 1 and this test, and interim engine changes altered the maximum power by about 3½ percent. The results were therefore corrected by an appropriate factor for all subsequent use.

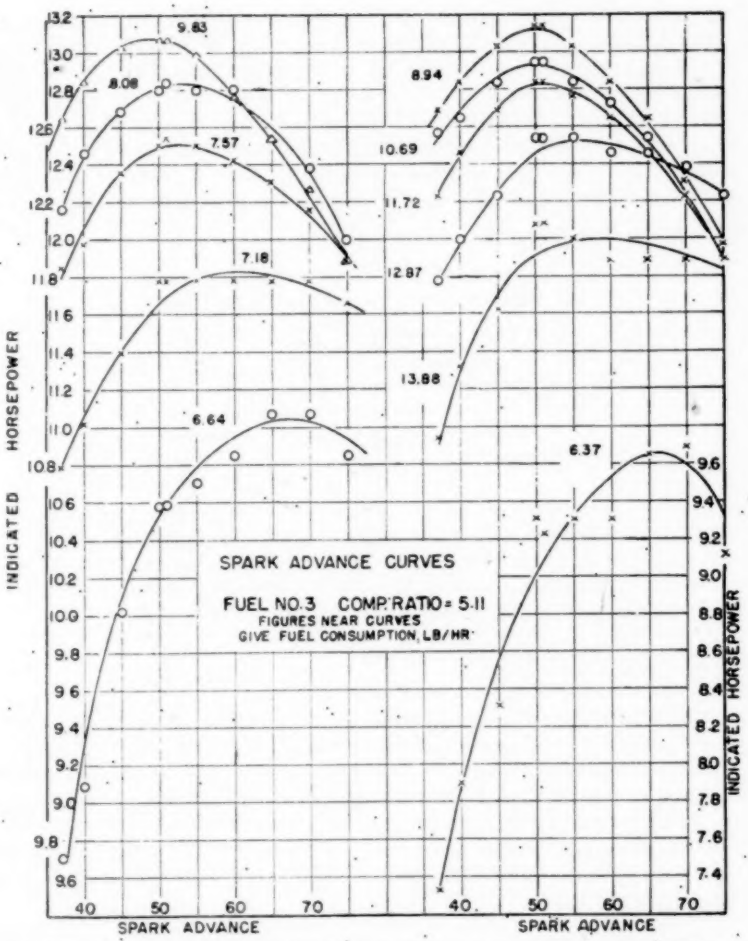

FIGURE 15.—*Power versus spark advance at a series of fuel consumption rates.*

These data, obtained at a compression ratio of 5.11, are typical for all of the fuels. The plotted points in figures 1 to 14 are the peaks of curves such as these.

IV. DISCUSSION OF TEST RESULTS

1. POWER AT CONSTANT COMPRESSION RATIO

For the purpose of facilitating comparison of performance over the mixture-ratio range, power was plotted against fuel heat input, calculated from the higher heating value [1] of the fuel. This eliminates the horizontal displacement of the performance curves that would result from the different heating values of the fuels, if power were plotted against weight of fuel burned, as in figures 1 to 14. The curves obtained at a compression ratio of 5.11 are shown in figure 16. It will be seen that the power developed with each of the three acetone blends is 2 to 3 percent greater than that with gasoline, whereas the increase with alcohol is about twice as much. A tabular comparison of the power developed by these fuels is given in the second and third columns of table 16.

TABLE 16.—*Comparison of fuels at a compression ratio of 5.11*

Fuel	Indicated horsepower	Power ratio to that of gasoline	Minimum specific fuel consumption	Maximum thermal efficiency (high heating value)	Optimum spark advance	Humidity	Corrected[1] advance
		Percent	*lb/ihp-hr.*	*Percent*	*Degrees*	*in. Hg*	*Degrees*
A	12.80	100.0	0.452	27.9	47.5	0.47	47.7
B	13.46	105.2	.746	29.0	47.0	.54	46.7
C	13.38	104.5	.695	28.8	46.9	.54	46.6
D	13.41	104.8	.663	28.6	44.5	.55	44.1
E [2]	12.80	100.0	.458	27.6	45.0	.23	47.0
1	13.15	102.7	.639	27.7	47.8	.67	46.6
2	13.21	103.2	.607	28.6	47.5	.58	46.9
3	13.10	102.3	.600	28.5	49.0	.63	48.0
Standard deviation (excluding fuel D)							.5

[1] Corrected to 0.50 in. Hg humidity, basis 7.3°/in. Hg.
[2] Corrected as stated in text.

The minimum specific fuel consumption, and the maximum thermal efficiency, based on the higher heating value, are given in the fourth and fifth columns of table 16. To facilitate examination of the thermal efficiencies in the lean mixture range, lines of constant thermal efficiency have been plotted in figure 16. It will be seen that all the substitute fuels have better thermal efficiencies [2] throughout this range than does gasoline. The differences, although consistent, in no case exceed 1½ percent.

2. COMPARISON OF POWER WITH CALCULATED VALUES

Table 17 gives the calculated properties of theoretical mixtures of each of the fuels. The second column gives the calculated air-fuel ratio, and the third column gives the fuel heat per pound of dry air. The fourth column gives the relative heat per unit volume of charge at standard temperature and pressure, based on gasoline as unity. It can been seen from this column that the heating values of these fuel-air mixtures are essentially equal. The next four columns are steps in the computation of the potential cooling of the charge by fuel vaporiza-

[1] See Appendix for values based on lower heating value.
[2] It should be understood that a conventionalized calculation such as thermal efficiency does not accurately describe the thermodynamic processes actually occurring in the engine.

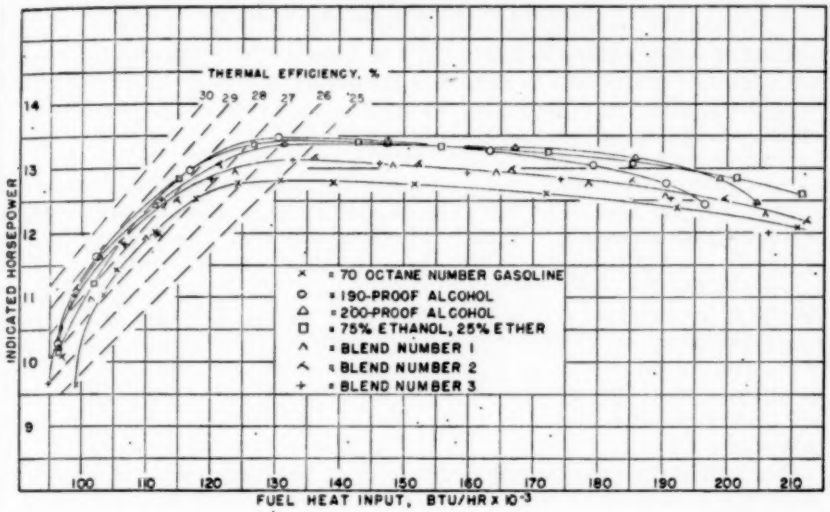

FIGURE 16.—*Power and thermal efficiency of the test fuels at a compression ratio of 5.11.*

When fuel consumption of dissimilar fuels is expressed in terms of fuel heat input, comparison of the power curves is facilitated. This also permits superposition of a scale of thermal efficiency.

tion. From this is found the volume of air that would be inducted if all of the fuel were vaporized, in terms of the gasoline-air mixture as unity. For comparison, the observed maximum power at equal compression ratio is tabulated in the last column, as the power obtainable from an engine has been shown[3] to be determined by the air consumption of the engine. The agreement between the values in the last two columns is apparently a measure of the relative fuel vaporization at the moment of closure of the intake valve, as subsequent fuel vaporization would not affect air induction. Thus fuels 1 and 2 are nearer complete vaporization than is gasoline; fuel 3 and fuel D are about the same; and the alcohols, fuels B and C, are less so, presumably because of the large potential cooling involved in their vaporization.

TABLE 17.—*Properties of theoretical fuel-air mixtures*

Fuel	Theoretical air-fuel ratio	Btu per pound of air at theoretical air-fuel ratio	Relative heat per unit volume of charge	Air (percentage of volume of charge)	Latent heat of fuel vaporization *	Specific heat of fuel	Specific heat of charge	Potential cooling of charge	Air (calculated percentage of volume of charge)	Observed
			Percent	*Percent*	*cal/g*	*cal/g*	*cal/g of fuel*	*°C*	*Percent*	*Percent*
B	8.19	1,436	100.2	92.0	238	0.41	2.37	100	110.8	105.2
C	9.00	1,413	100.3	93.5	204	.41	2.56	80	107.4	104.5
D	9.51	1,410	101.0	94.3	176	.42	2.69	65	104.8	104.8
E	15.09	1,337	100.0	98.5	75	.61	4.22	18	100.0	100.0
1	10.36	1,388	101.1	95.9	127	.38	2.86	44	102.2	102.7
2	10.61	1,380	100.7	96.1	133	.40	2.93	45	102.6	103.2
3	10.72	1,386	101.4	96.2	128	.40	2.96	43	102.2	102.3

* From International Critical Tables.

[3] Nat. Advisory Comm. Rep. No. 426 (1932).

3. OPTIMUM SPARK ADVANCE

Earlier work at this Bureau [4 5 6 7] and elsewhere [8] showed that spark advance for maximum power was markedly affected by atmospheric humidity. The sixth and seventh columns of table 16 list the observed optimum spark advances for the several fuels, and the atmospheric humidity prevailing during the test. An analysis of these data indicates that the optimum spark advance increases with humidity at the rate of 7.3°/in. Hg. The correlation coefficient of advance and humidity for these values is +0.944, which shows that the values unquestionably were affected by humidity. On this basis the optimum spark advances for the fuels, when corrected to a humidity of 0.50 in. Hg, are as given in the last column of table 16. Excluding fuel D the standard deviation of the corrected values is 0.5°. As the spark quadrant was graduated only to 1 degree, the deviation of 0.5 degree is accounted for adequately by experimental error. This means that all of the fuels, except the ether blend, have equal optimum spark advances, and hence equal rates of burning in this engine.

The optimum spark advance for fuel D, the ethanol-ether blend, is 3 degrees less than the average for the other fuels. The chance of so large a deviation occurring through the operation of the factors that caused the experimental error for the other fuels is exceedingly small. It therefore appears that the ether blend actually burns some 7 percent faster than the other fuels.

4. POWER AT COMPRESSION RATIO FOR TRACE KNOCK

In figure 17 are plotted the runs in which each fuel was tested at the compression ratio for trace knock (for best-power mixture and optimum spark advance) and tabular values are given in the third to sixth columns of table 18. As in figure 16, lines of constant thermal efficiency are shown in figure 17. At the same heat input, a considerable increase in power and in thermal efficiency is shown by the substitute fuels, chiefly because of the permissible increase in compression ratio. The increase in power is approximately 83 percent of that calculated on an air-cycle basis, from the change of compression ratio. The apparent reason for the departure from air cycle is a decrease in the volumetric efficiency of the test engine with increase in compression ratio, the magnitude of the decrease being sufficient to account for the observed departure.

TABLE 18.—*Comparison of fuels at compression ratio giving trace knock*

Fuel	Compression ratio	Indicated horse power	Power ratio to that of gasoline	Minimum specific fuel consumption	Maximum thermal efficiency	Optimum spark advance	Humidity	Corrected advance [1]
			Percent	*lb/ihp-hr*	*Percent*	*Degrees*	*in. Hg*	*Degrees*
A	5.11	12.80	100.0	0.452	27.9	47.5	0.47	47.7
B	9.91	16.18	126.4	.595	36.4	37.3	.64	36.3
C	9.91	16.18	126.4	.558	35.9	34.7	.56	34.3
D	8.60	15.70	122.7	.545	34.8	36.5	.75	34.7
E [2]	5.11	12.80	100.0	.458	27.6	45.0	.23	47.0
1	8.18	15.11	118.0	.514	34.4	38.2	.59	37.3
2	7.81	15.06	117.7	.514	33.8	37.5	.77	36.3
3	7.43	14.80	115.6	.525	32.6	38.6	.67	36.6

[1] Corrected to 0.50 in. Hg humidity, basis 7.3°/in. Hg.

[2] Corrected as stated in text.

[4] Nat. Advisory Comm. Rep. No. 426 (1932).
[5] Nat. Advisory Comm. Note No. 309 (1929).
[6] SAE Journal **25**, 277 (September 1929).
[7] BS J. Research **3**, 795 (1929) RP118.
[8] SAE Journal **24**, 155 (February 1929).

The observed optimum spark advances and prevailing humidities are given in the seventh and eighth columns of table 18, and the advances corrected to a humidity of 0.50 in. Hg, by the correction factor deduced above, in the last column of this table. These corrected advances vary, of course, with compression ratio. However, ethanol fuel, C, and its ether blend, fuel D, are somewhat below the mean line for the other fuels.

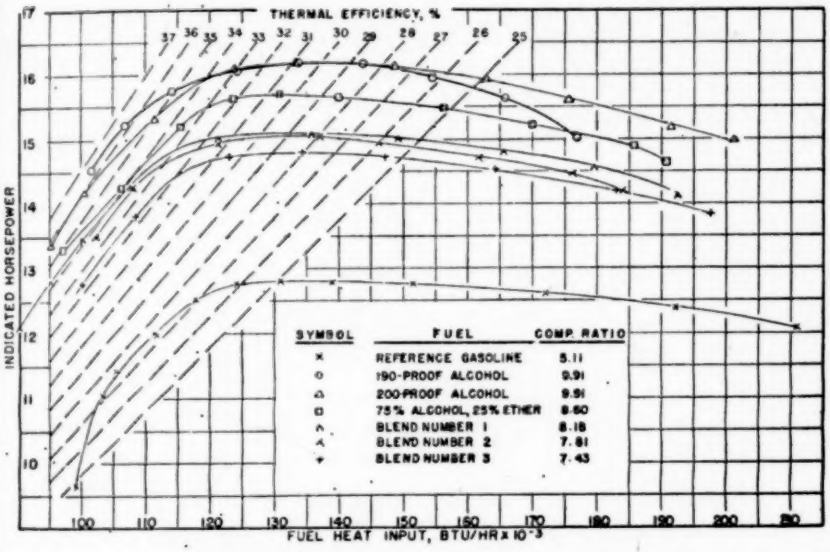
THERMAL EFFICIENCY, %
37 36 35 34 33 32 31 30 29 28 27 26 25
INDICATED HORSEPOWER
17 16 15 14 13 12 11 10
SYMBOL FUEL COMP. RATIO
× REFERENCE GASOLINE 5.11
○ 190-PROOF ALCOHOL 9.91
△ 200-PROOF ALCOHOL 9.91
□ 75% ALCOHOL, 25% ETHER 8.60
∩ BLEND NUMBER 1 8.18
∧ BLEND NUMBER 2 7.81
+ BLEND NUMBER 3 7.43
100 110 120 130 140 150 160 170 180 190 200 210
FUEL HEAT INPUT, BTU/HR x 10⁻³

FIGURE 17.—*Power and thermal efficiency of the test fuels at the compression ratio giving trace knock.*

The peaks of the power curves occur at an essentially constant fuel heat input, although the compression ratios vary from 5.11 to 9.91.

5. COMBUSTION PERFORMANCE OF FUELS

(a) RELATIVE POWER VERSUS HEAT INPUT

As a means of further comparing the combustion performance of the fuels, the data plotted in figures 16 and 17 have been transformed to percentages of maximum indicated power (for each fuel and test condition) and heat input in Btu per pound of dry air. The results are shown in figure 18, in which the upper curve is fitted to the data obtained on the substitute fuels when operating at trace knock, and the lower curve is fitted to the data obtained on all fuels when operating at 5.11 compression ratio.

With two exceptions, it is apparent that the performances of these fuels are identical, within experimental error, at equal heat-input rates over the full range of mixture ratios. The performance of gasoline is slightly below the average at mixtures leaner than that giving maximum power, and slightly better at richer mixtures. The opposite is true of the 190-proof ethyl alcohol, which shows a marked deterioration in performance at rich mixtures. The behavior of the gasoline is consistent with the assumption that some of its less volatile components pass through the engine without being burned.

In figure 19 the curves of figure 18 are compared. The differences are very slight and do not exceed the probable experimental error of air-flow measurement at the two conditions. If the measured air flow at 5.11 compression ratio were 1 percent low, for example, then the two curves are really coincident. The conclusion drawn is, that the relative performances of these fuels are essentially identical under both test conditions.

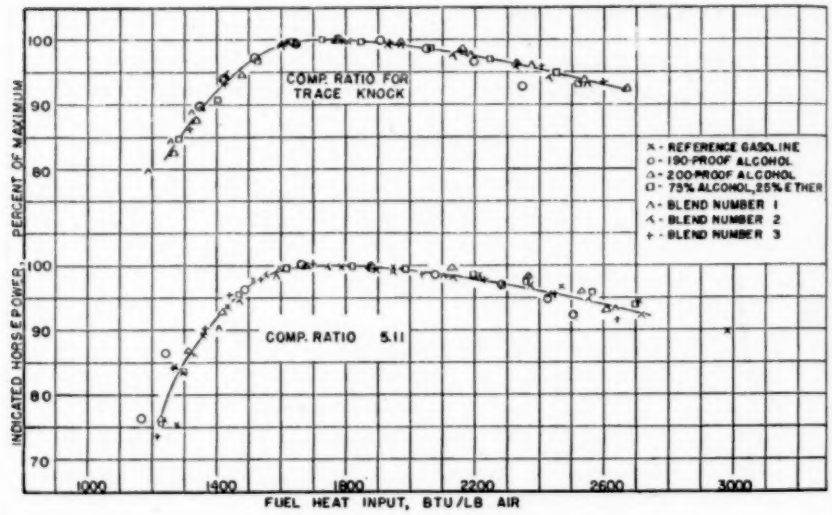

FIGURE 18.—*Relative power versus fuel heat input.*

When the power data of each curve on figures 16 and 17 are expressed as percentage of maximum power, the curves for each fuel coincide.

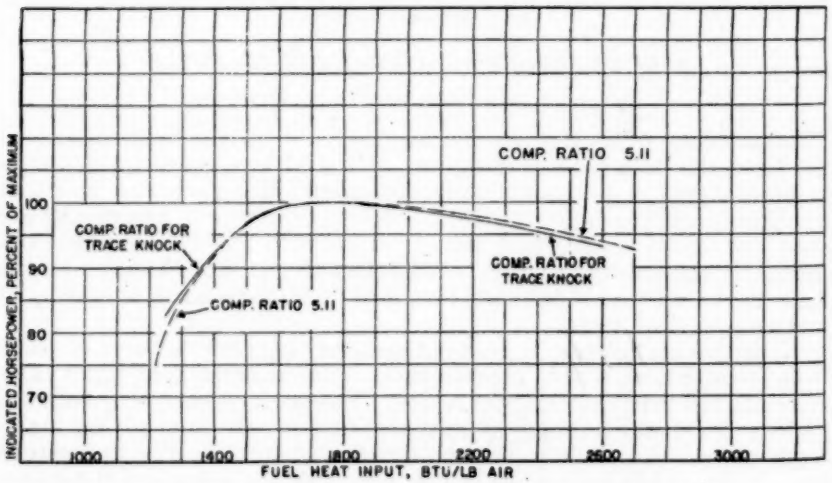

FIGURE 19.—*Relative power versus fuel heat input.*

The curves of figure 18 are shown by superposition to differ by no more than the experimental error. Thus hydrocarbon and nonhydrocarbon fuels, at compression ratios from 5.11 to 9.91, show essentially the same response to mixture ratio.

(b) RATE OF BURNING

Another means of comparing the combustion performance of the fuels is by a study of the combustion times as indicated by the optimum spark advances. In figure 20, the optimum spark advances observed for each fuel at each mixture ratio when operating at a compression ratio of 5.11 have been corrected to a mean value of humidity of 0.50 in. Hg and plotted against fuel heat input in Btu per pound of dry air. Except at the leaner mixtures, the points do not show large scatter. The ether blend, fuel D, exhibits a definite tendency to require less advance than the other fuels. Gasoline appears to require a slightly higher advance than the other fuels at lean and at rich mixtures. It is noteworthy that, whereas maximum power is reached at 1,760 Btu per pound of air (fig. 18), the minimum advance, hence maximum combustion rate, occurs at 1,890 Btu per pound of air.

In order to compare the relation of optimum spark advance to mixture ratio at the lower and higher compression ratios used in the tests, the values shown in figure 20 and those obtained when operating at trace knock are plotted in figure 21 in percentage of minimum optimum spark advance. The curves of figure 21 are superposed in figure 22. This figure shows that at the higher compression ratios, the curve of relative optimum spark advance versus specific heat input is displaced in the direction of lower heat input, in this case by about 10 percent. This tendency is apparent also on closer examination of the upper plot on figure 21, in which it can be noted that the points for fuels giving trace knock at the lower compression

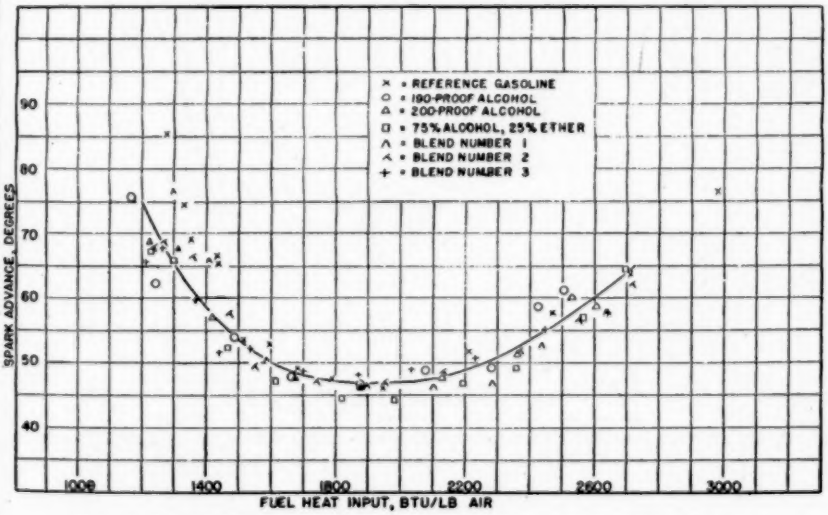

FIGURE 20.—*Relation of optimum spark advance to fuel heat input.*

In these tests at a compression ratio of 5.11, the observed optimum advances have been corrected to a standard pressure of water vapor (atmospheric humidity) of 0.50 in. Hg. Only the ether blend appears to differ substantially from the mean curve.

649238—45——3

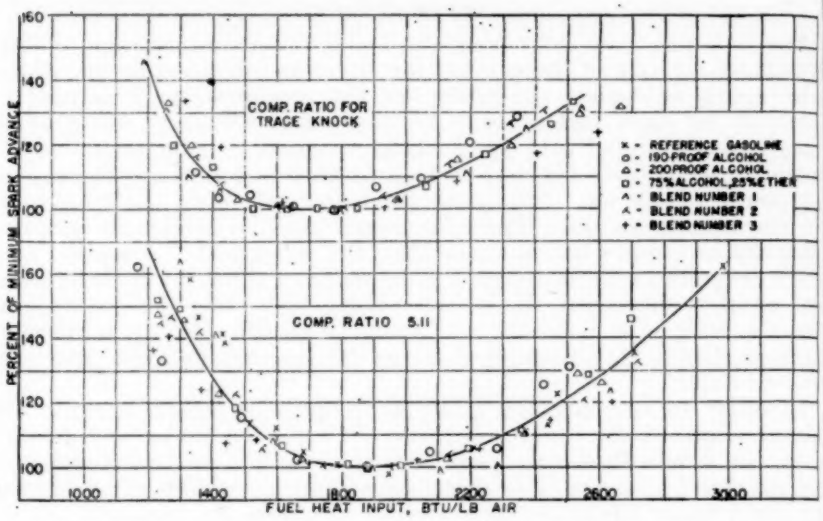

FIGURE 21.—*Relative optimum spark advances.*

When the optimum spark advances for each fuel are expressed in terms of the minimum optimum advance, the values are nearly coincident at the lower compression ratio, and in good agreement at the higher compression ratios.

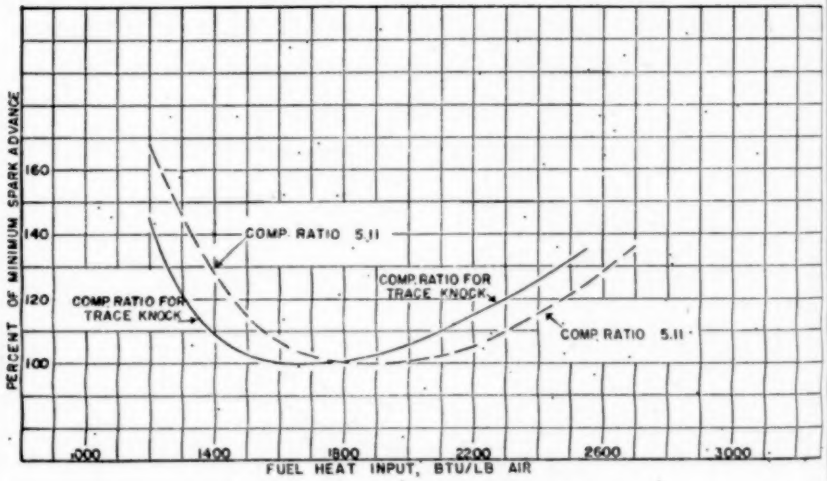

FIGURE 22.—*Comparison of relative optimum spark advances at compression ratio of 5.11 and at compression ratio giving trace knock.*

The tendency of the minimum point to shift toward the stoichiometric equivalent (about 1,400 Btu/lb of air) at the higher compression ratios can be noted also in the departures of the observed points from the upper curve of figure 21.

ratios fall at higher fuel heat input than the curve, and vice versa. The significance of this fact can be expressed in several ways:

1. With increase of compression ratio, the *actual* optimum spark advance for lean mixtures decreases more rapidly than that for rich mixtures.

2. With increase of compression ratio, the *relative* optimum spark advance for lean mixtures decreases and that for rich mixtures increases.

3. With increase of compression ratio, the mixture requiring minimum spark advance (presumably maximum rate of burning) approaches the stoichiometric equivalent.

The last statement follows from the fact that the heat input at the stoichiometric mixture ratio is roughly 1,400 Btu per pound of air for these fuels, as shown in table 17.

It is of interest to note that whereas at 5.11 compression ratio minimum optimum spark advance occurs at a mixture about 7 percent richer than that for maximum power, at the higher compression ratios used for trace knock with the substitute fuels it occurs at a mixture roughly 4 percent leaner than that for maximum power.

(c) THERMAL-PLUG TEMPERATURES

As mentioned earlier, the engine was equipped with a thermal plug mounted in the cylinder head to be flush with the combustion-chamber surface. This plug was connected to a direct-reading indicator. Temperatures were noted at each test condition.

The readings obtained over the range of spark advance at each mixture ratio were plotted. The thermal plug temperature at optimum spark advance was then read from the resulting curve. Figure 23 shows these readings plotted against fuel heat input, a convenient basis for expressing mixture ratio in terms common to all fuels. Within experimental error, the observed temperatures for the various substitute fuels are equal, at comparable mixtures, both at 5.11 compression ratio and at trace knock. The temperatures observed for

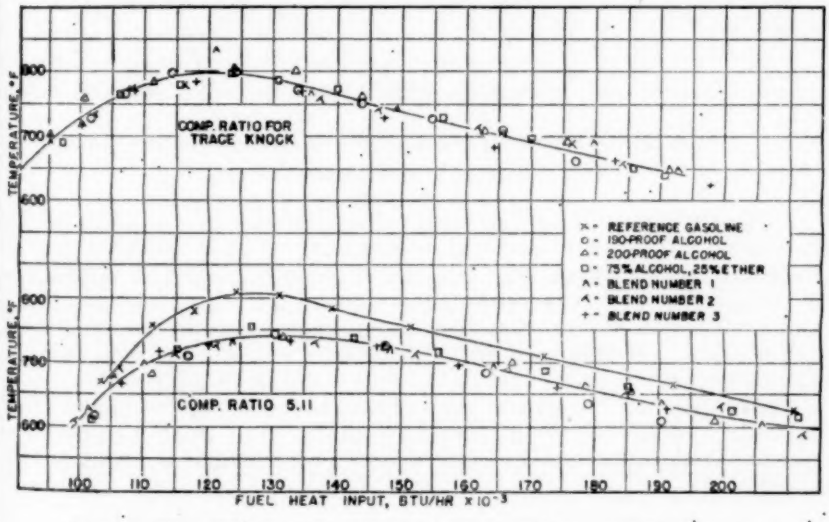

FIGURE 23.—*Thermal plug temperatures at optimum spark advance.*

The lowest curve is for the nonhydrocarbon fuels at a compression ratio of 5.11, at which ratio these fuels did not knock. The curve immediately above is for gasoline, which gave trace knock at this ratio. The upper curve, on a different scale of ordinates, is for the nonhydrocarbon fuels at the compression ratio which gave trace knock with the fuel.

gasoline, however, are decidedly higher than those for the substitute fuels at 5.11 compression ratio.

When the curves of this figure are superposed, as in figure 24, it is seen that a considerable rise in temperature in the region lean of maximum power occurs when the substitute fuels are tested at trace knock instead of the lower compression ratio of 5.11. That most of this rise is connected with the phenomenon of knock and can be attributed to the occurrence of "incipient" knock is suggested by the fact that at richer mixtures, where no knock would be audible even at considerably higher compression ratios, the two curves for the substitute fuels differ by only about 12 degrees Fahrenheit, although the average compression ratio for trace knock for these fuels was 8.6 as compared with the value of 5.11 for the lower curve.

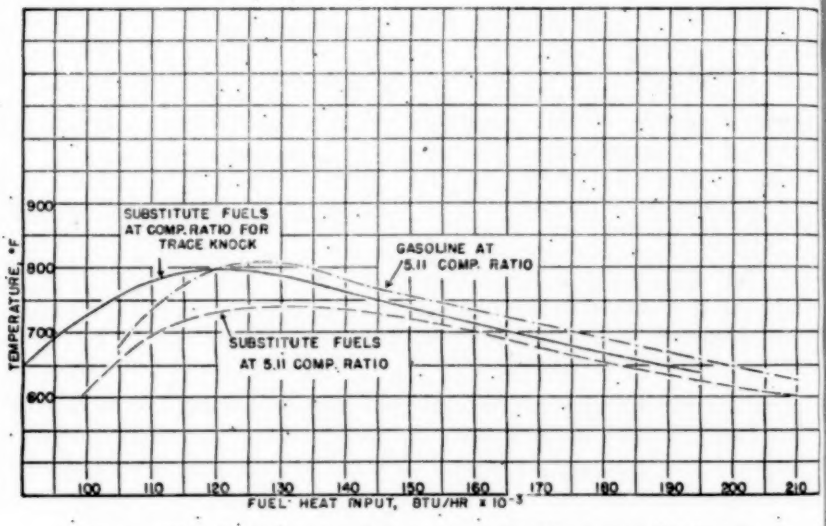

FIGURE 24.—*Thermal plug temperatures at optimum spark advance.*

The curves of figure 23 are superposed in this figure.

In figure 24, as in figure 18, the curve for gasoline appears as if it had been displaced toward higher fuel heat input by about 7 percent from that of the substitute fuels at trace knock. Such an appearance is compatible with the assumption that a portion of the gasoline is sufficiently nonvolatile that it does not participate in the reaction of combustion. If this assumption be made, and the gasoline curve be displaced toward lower fuel heat input accordingly, the temperatures for gasoline then fall within the band of those for the substitute fuels at trace knock. It would therefore appear that in this respect also no essential difference in combustion performance is exhibited by these fuels.

6. POWER AT CONSTANT SPARK ADVANCE

A plot of the data given in table 5 is shown for selected spark advances in figure 25, which is typical of power versus fuel-consumption curves at fixed spark advances. At the least-advanced spark, 40

legrees, power is lower than with the other settings at lean and rich mixtures but approaches the best power obtained at the mixture ratio giving maximum power. At a setting of 50 degrees, power is considerably improved at lean and rich mixtures and is highest of any of the curves at best mixture. An advance of 60 degrees improves the power at lean and rich mixtures, but causes a material loss of power in the intermediate range. The highest advance, 70 degrees, gives the highest power of any of these settings at the leanest mixture, and

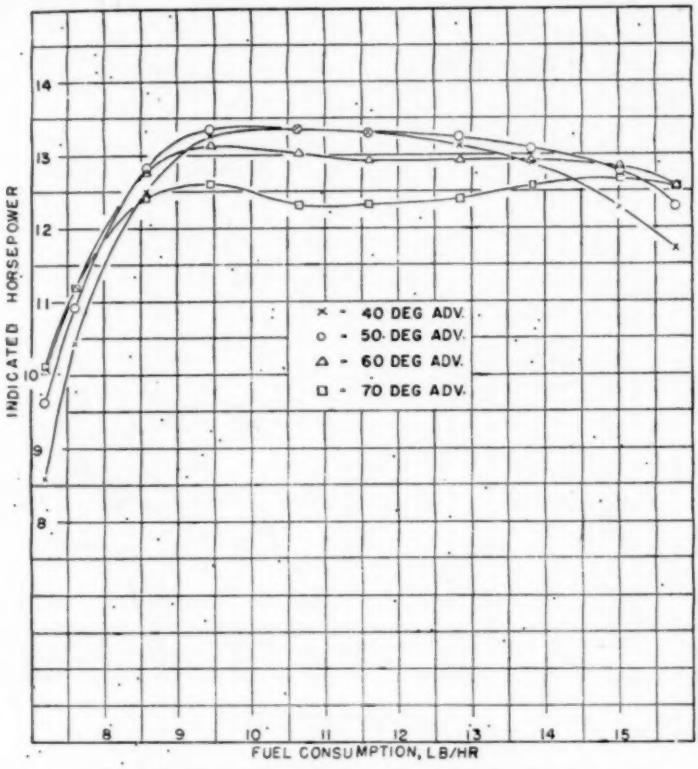

FIGURE 25.—*Power curves at fixed spark advances.*

Curves are shown for spark advances of 40°, 50°, 60°, and 70°. The reason for the double peak at 70° is explained in the text.

would do so at a mixture slightly richer than any which were run, but gives a pronounced loss of power at normal mixtures.

The double peak shown by the power curve for 70-degree spark advance is typical of high spark advances. As can be seen in figures 1 to 14, the optimum spark advance increases at lean and at rich mixtures. At high spark advances, the loss of power occasioned by going rich or lean from the best mixture is at first less than the gain of power resulting from the fact that at the richer or leaner setting the spark advance is closer to the optimum. This is the reason for the double peak of the power curve at high spark advances. Close examination of figure 25 will show that this double peak is foreshadowed in the curve for 60-degree advance.

7. POWER–MIXTURE–SPARK-ADVANCE RELATIONSHIP

It was shown earlier in this analysis that when the data obtained on all fuels were plotted as percent maximum power versus fuel heat input in Btu per pound of air, the relations were essentially identical (figs. 18 and 19). The power–mixture–spark-advance surface for fuel D at 5.11 compression ratio, figure 26, is therefore closely representative of that for all of these fuels, and the relations depicted therein may be considered as typical.

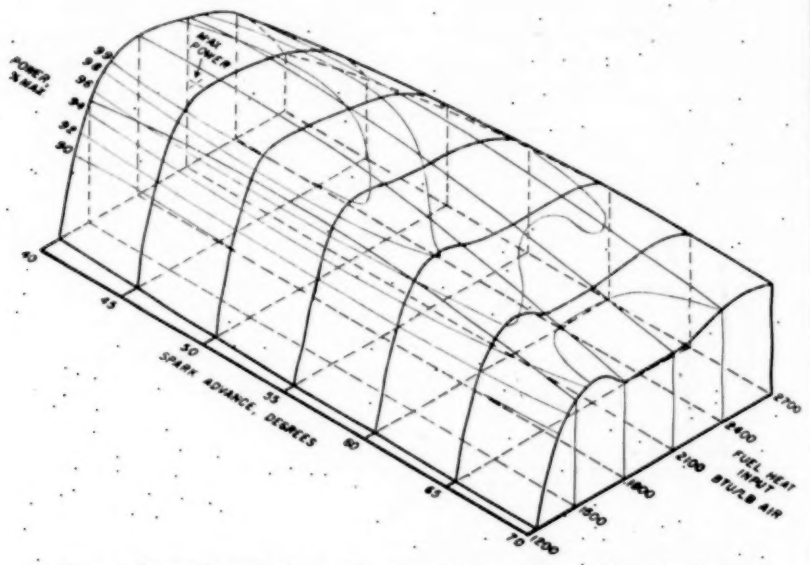

FIGURE 26.—*Interrelations of power, mixture ratio, and spark advance.*

When power was expressed in percentage of maximum power, and mixture ratio in terms of fuel heat input, the behavior of all fuels tested was essentially identical. This figure is therefore valid for all of these fuels. The light lines are vertical contours, their values being given in percentage of maximum power at the left of the chart. The point of maximum power, in the upper left part of the figure, is marked with a cross.

V. CONCLUSIONS

These tests on a single-cylinder CFR engine lead to the following conclusions, which are believed to be of general applicability in a qualitative sense:

1. At constant compression ratio, slightly more power (2 to 3 percent) is obtained with the acetone blends, whereas with 190- or 200-proof ethyl alcohol the increase is somewhat larger (4 to 5 percent). At lean mixtures the substitute fuels have slightly better thermal efficiencies than does gasoline.

2. Analysis of the optimum spark advances of these fuels indicates that their rates of burning are equal at best mixture ratio, with the exception of the ether blend, which may burn a few percent faster.

3. All the substitute fuels are capable of use at compression ratios yielding more power than that allowable for the gasoline, with a corresponding increase in thermal efficiencies. The permissible increases in power range up to one-quarter for ethyl alcohol, the thermal efficiency of which is 36 percent, based on the higher heating value.

4. Analyses of power, rate of burning as indicated by optimum spark advance, and thermal plug temperatures, versus fuel heat input, reveal no material differences in the combustion performances of these fuels.

5. Relative power at equal heat input per pound of air is the same for these fuels at both compression ratios used.

V. APPENDIX

THERMAL EFFICIENCIES BASED ON LOWER HEATING VALUE

The consensus of authorities in this country favors the use of the higher heating value of fuels in reckoning the thermal efficiency of an engine, although the lower heating value is preferred by some, and was standard practice in Germany. Although it may be considered improper to charge a noncondensing type of engine with the latent heat of vaporization of the water formed, it has been found that greater consistency of values results when the higher heating value of the fuels is used. For information, the thermal efficiencies of the several fuels, based on the lower heating values are given in table 19.

TABLE 19.—*Maximum thermal efficiency*

[Based on lower heating value]

Fuel	Thermal efficiency		Compression ratio for trace knock
	At 5.11, compression ratio	At compression ratio for trace knock	
	Percent	*Percent*	*Percent*
A	29.9	29.9	5.11
B	32.3	40.5	9.91
C	31.8	39.6	9.91
D	29.9	36.3	8.60
E	29.5	29.5	5.11
1	30.0	37.3	8.18
2	31.1	36.7	7.81
3	31.0	35.4	7.43

WASHINGTON, March 21, 1945.

U. S. DEPARTMENT OF COMMERCE · NATIONAL BUREAU OF STANDARDS

RESEARCH PAPER RP1661

Part of Journal of Research of the National Bureau of Standards, Volume 35, July 1945

THERMODYNAMIC PROPERTIES OF 1,3-BUTADIENE IN THE SOLID, LIQUID, AND VAPOR STATES

By Russell B. Scott, Cyril H. Meyers, Robert D. Rands, Jr., Ferdinand G. Brickwedde, and Norman Bekkedahl

This paper presents a detailed description of apparatus used and the results obtained in the following measurements relating to the thermodynamic properties of 1,3-butadiene in the solid, liquid, and vapor states: (1) Specific heats from −258° to +30° C, (2) heat of fusion, (3) heats of vaporization from −26° to +23° C; (4) vapor pressures from −78° to +110° C, (5) liquid densities from −78° to +95° C, (6) vapor densities from 30° to 150° C, and (7) the critical pressure, volume, and temperature of 1,3-butadiene. Tables embodying the results of these measurements are included for specific heats, enthalpy, and entropy of the solid, liquid, and vapor.

CONTENTS

	Page
I. Introduction	40
II. Preparation of samples	40
III. Calorimetric measurements	44
1. Apparatus	44
(a) Calorimeter	44
(b) Electric control circuits	47
(c) Measuring circuits	49
2. Specific heat	51
(a) Method of measurement	51
(b) Method of calculation	51
(c) Results	52
3. Heat of fusion	55
(a) Method of measurement	55
(b) Results	55
4. Heat of vaporization	55
(a) Method of measurement	55
(b) Results	56
5. Accuracy of calorimetric measurements	57
IV. Pressure-volume-temperature measurements	58
1. Vapor pressure	58
(a) Measurements from 195° to 288° K	58
(b) Measurements from 0° to 152° C	59
(c) Vapor-pressure equation	64
(d) Comparison with data of other observers	64
2. Density of superheated vapor	65
(a) Method and apparatus	65
(b) Results of measurements and their formulation	66
3. Density of saturated liquid	68
(a) Method and apparatus	68
(b) Results of measurements and their formulation	69
(c) Comparison with other data	71
4. Rate of polymerization	72
5. Critical constants	72

Page
V. Purity of samples and melting point of pure butadiene 74
VI. Derived properties and formulated tables of the thermodynamic properties of 1,3-butadiene 78
1. Entropy and enthalpy of solid and liquid 1,3-butadiene from 15° to 300° K 78
2. Thermodynamic properties of liquid and vapor 1,3-butadiene from −109° to +150° C 81
VII. References 85

I. INTRODUCTION

The measurements of the thermodynamic properties of 1,3-butadiene described in this paper were undertaken in response to requests for data needed in the Government's synthetic-rubber program. Most of the experimental data were made available previously to the synthetic-rubber industry in the form of reports [1, 2] [1] submitted to the Office of the Rubber Director and in a National Bureau of Standards Letter Circular [3]. As these reports were rather brief, more detailed descriptions of the apparatus, methods, and results are given here.

Empirical equations were constructed to represent the experimental results and used to calculate a thermodynamically consistent set of tables of various derived properties, including enthalpy and entropy of 1,3-butadiene in the solid, liquid, and vapor state. In these calculations use was made of measurements of the specific heat of 1,3-butadiene vapor previously published [4] and an equation of state for the vapor that represents measurements over a wide range of temperature and pressure.

II. PREPARATION OF SAMPLES

The butadiene from which the samples were prepared was furnished by the Dow Chemical Co. It was shipped in a steel cylinder refrigerated with solid carbon dioxide (−78° C). After it was received it was kept at or near −78° C, except while being transferred from one container to another. The butadiene was removed from the cylinder by evaporating it into one-half-liter Pyrex flasks at −78° C. These were provided with seals that could later be broken with magnetic plungers so that all the handling of the material could be carried out in the absence of air. The supply of butadiene, somewhat less than 2 liters, was stored in four such flasks.

It appeared that a small amount of carbon dioxide had leaked into the cylinder during transit while it was in a CO_2 atmosphere at such a low temperature that the pressure inside the cylinder was less than atmospheric. The carbon dioxide impurity was noticed during the transfer as it caused blocking by not condensing with the butadiene. It did condense readily in a liquid-air trap, which fact led to the belief that it was carbon dioxide and not air. The blocking occurred three times during the filling of the first half-liter flask. When it occurred, the flask and cylinder were connected through a stopcock to a vacuum system and pumped for a few seconds. In this way most of the carbon dioxide was removed, together with some butadiene. No difficulty was experienced during the filling of the three other half-liter flasks. These flasks are designated by the numbers 1, 2, 3, and 4 in the order of their filling.

[1] Figures in brackets indicate the literature references at the end of this paper.

During the course of the experiments four *samples* were prepared. Sample 1 was prepared by evaporating the 450-ml contents of flask 3 at about −30° C, separating a middle fraction of about 110 ml. This fraction was frozen with liquid air with the intention of pumping off any air that may have been present. However, a pressure measurement, made with a McLeod gage, showed this pumping to be unnecessary. The butadiene seemed to be free of any impurity that had an appreciable vapor pressure at the temperature of liquid air. After melting the butadiene, another evaporation was carried out, and the middle 95 ml was collected. This constituted sample 1. The unused material from both evaporations was returned to the half-liter flask.

The material from which sample 2 was prepared consisted of about 100 ml of butadiene also taken from flask 3. The distillate was separated into five fractions. Fraction 1, about 10 ml of liquid, was discarded. Fraction 2 was a very small amount, about 0.2 ml of liquid. Fraction 3 was the main body of the material, about 80 ml of liquid, which constituted sample 2. Fraction 4 was another small sample about the same size as fraction 2. Fraction 5, about 10 ml of liquid, was discarded.

The vapor pressures of fractions 2 and 4 were compared at a pressure of about 1 atm by means of a differential vapor-pressure apparatus similar to that described by Shepherd [5]. No difference in vapor pressures was detected, although a difference of 0.05 mm Hg could have been noticed. This equality of vapor pressures indicated that further distillation of fraction 3 would have little effect.

Sample 2 was prepared by fractional distillation by the use of a still with a rectifying column. This apparatus is shown in figure 1. The boiling reservoir, *A*, is surmounted by a rectifying column, *B*, consisting of a monel tube with a deep helical groove. The Pyrex container surrounding the rectifying column fits so closely that, during operation, the liquid sealed the space between the glass and the metal, causing all the vapor and most of the refluxing liquid to traverse the helical groove, a path of about 6 m. The evacuated space between the two walls of the Pyrex container insulated the boiler and rectifying column. The heat required for the boiling is supplied by the heater, *C*, consisting of 34 ohms of fiber-glass-insulated constantan wire wound on the stem of the copper piece, *D*. The inverted mushroom of copper conducts the heat from the constantan heater to the bottom of the boiling reservoir. The walls of the condenser, *E*, are in contact with the stirred alcohol bath in which the still is immersed. The bath is refrigerated by means of a copper coil into which high-pressure carbon dioxide expands. An electric heater is provided so that excess refrigeration can be compensated and a constant bath temperature maintained. During the operation of the still the temperature of the bath was kept at about −25° C and manually controlled so as not to vary more than 0.05 degree. The butadiene vapor was withdrawn at *F*. The withdrawal rate and the boiling rate were adjusted so that the reflux ratio was about 15.

Sample 3 was prepared by fractional crystallization of material from flask 2. The apparatus used is shown in figure 2. The butadiene in flask *A* was partially frozen by cooling produced by the liquid air surrounding tube *C*. The air space separating flask *A* and tube *C* provided enough insulation to prevent too rapid freezing. About 20 minutes were required to freeze 150 ml of butadiene. While the

freezing proceeded, the magnetic stirrer, *D*, kept the liquid agitated so that there would not be a concentration of impurity at the surface of the solid as it formed. Two fractional crystallizations were performed. After the first, about 50 ml remained liquid and was poured into flask *B*. The remaining solid was melted and again fractionally crystallized, this time discarding into flask *B* about 75 ml of unfrozen

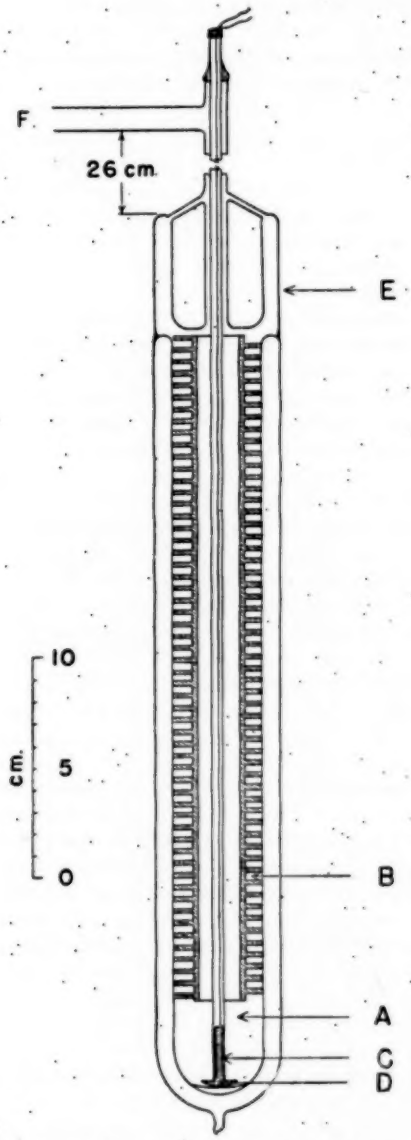

FIGURE 1.—*Still with rectifying column used to purify butadiene.*

A, boiling reservoir; *B*, rectifying column; *C*, heater; *D*, copper conductor; *E*, condenser; *F*, withdrawal line.

material. Flask *B* was then sealed off, and the 125 ml of butadiene remaining in flask *A* constituted sample 3.

Sample 4 was prepared by passing the butadiene, from flask 4, as a vapor over freshly outgassed silica gel. After condensing, the buta-

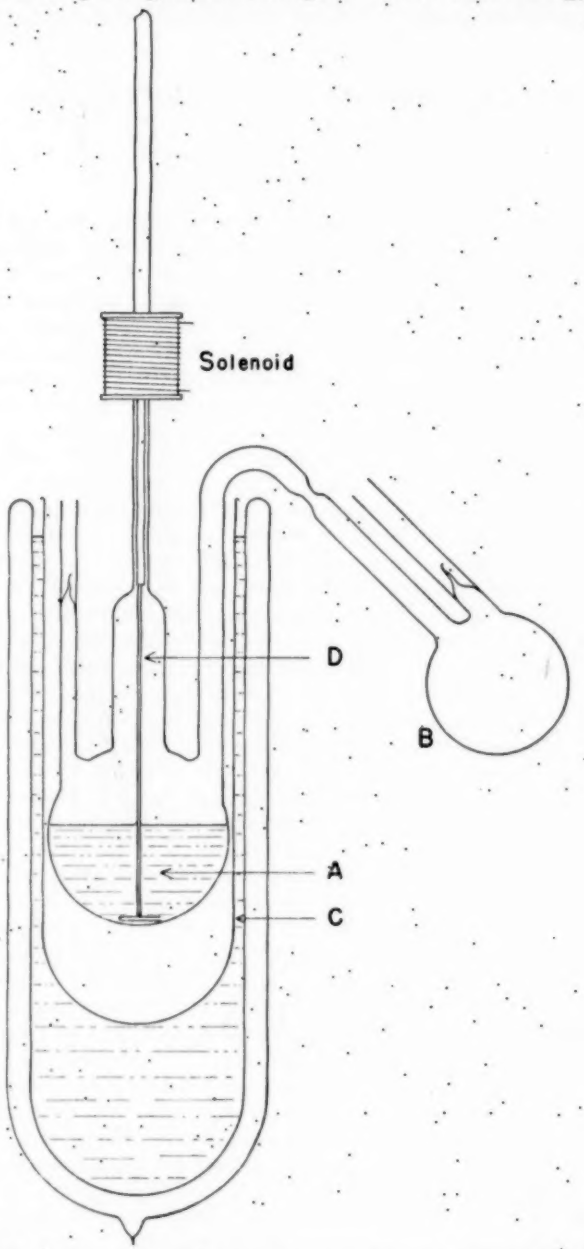

FIGURE 2.—*Fractional cystallization apparatus used to purify butadiene.*

A, butadiene in freezing flask; *B*, waste flask; *C*, tube providing air space around freezing flask; *D*, stirrer.

diene was fractionally crystallized three times, and finally the recrystallized material was distilled twice. In this process only about 60 ml of butadiene was obtained from an initial supply of 400 ml.

Estimates of purity of the various samples, based on melting data and vapor-pressure measurements, are given in section V.

III. CALORIMETRIC MEASUREMENTS

1. APPARATUS

(a) CALORIMETER

The calorimeter was of the adiabatic vacuum type, similar to one described by Southard and Brickwedde [6] for the measurement of the specific heats of nonvolatile solids. It was designed for the measurement of the specific heat and latent heats of a material that can be introduced into the calorimeter as a vapor and there condensed. Although the principal features are the same as those described by Southard and Brickwedde, several changes were necessary to adapt the design to the present use. Some changes were also made in the electric controls, by means of which adiabatic conditions are maintained. Because of these modifications and other differences in constructional detail, a description of the apparatus will be given here.

The term "calorimeter" may be properly applied to the complete apparatus with which thermal measurements are made, but for convenience in the following and later discussions in this paper, the word "calorimeter" will be used to designate that part of the apparatus containing the material being investigated, including all parts in intimate thermal contact with the material. The calorimeter is shown in vertical section at C, figure 3, and in horizontal section at C'. It consists of a cylindrical container of copper 1 mm in wall thickness, with domed ends of the same thickness, and contains two sets of vanes, V_1 and V_2, 0.2 mm thick, for the distribution of heat. The heater, H_1, by means of which measured amounts of electric energy were added, consists of two lengths of No. 34 AWG constantan wire with fiber-glass insulation. The wire was inserted into copper tubing, and then the tubing was drawn down snugly on the wire. The outside diameter of the tubing was about 1 mm after drawing. The tubing was wound in a single layer on the outside of vanes V_1. The heater is in two parts, the section nearer the bottom of the calorimeter having a resistance of about 28 ohms and the upper part having a resistance of about 37 ohms. The four ends of the copper tubes, with the projecting ends of the constantan wire, were brought out through the bottom of the calorimeter. Vanes V_2 are W-shaped pieces of copper formed to fit closely between the heater tubing and the wall of the calorimeter. The cone, B, just above the vanes, is a baffle intended to prevent droplets of liquid from being carried out of the calorimeter during vaporization experiments. The vanes, heater tubes, and inside surfaces of the calorimeter shell were tinned before assembling and the completed assembly heated to solder the parts together. About 2 mm of each end of the cylindrical wall was spun over the edge of the end cap to increase the strength of the calorimeter. The thermometer, T, used to determine the temperature of the calorimeter is a four-lead, strain-free, platinum resistance thermometer in a platinum

tube. This type of thermometer has been described by Southard and Milner [7]. The calibration of the thermometer used in this investigation has been described by Hoge and Brickwedde [8]. The thermometer contains helium and is sealed at the bottom by a soft glass cap, through which the platinum leads pass. Intimate thermal contact

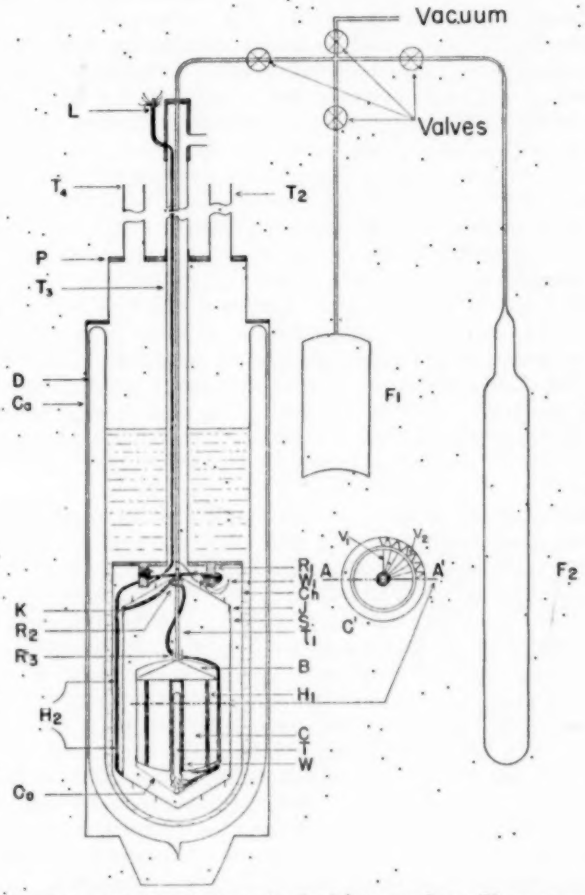

FIGURE 3.—*Sectional view of calorimeter and auxiliary apparatus.*

L, electrical leads; *P*, top plate of hydrogen container; T_2 monel tube for evacuation; *D*, Dewar flask; *Ca*, brass case; *K*, point at which leads pass through shield; R_2 and R_3, copper rings; H_2, cable heater; *Co*, aluminum cone; T_3, monel tube for exhausting over bath; R_1, brass ring; W_1, wire for thermal shunt; *Ch*, vacuum chamber; *J* sliding joint between top and side of shield; *S*, shield; T_1, filling tube; *B*, baffle; H_1, heater; *C*, calorimeter; *T*, resistance thermometer; *W*, thermometer well; F_1, weighing flask; F_2 reservoir; V_1 and V_2, copper vanes.

between the thermometer and the well, *W*, was attained by filling the excess space around the thermometer with low-melting (90° C) solder. The cone, *Co*, is a piece of aluminum foil 0.001 in. thick to trap heat radiated from the exposed ends of the heaters. The calorimeter is supported by the monel tube, T_1, through which the calorimeter was filled and emptied.

The radiation shield, *S*, is made of sheet copper 0.4 mm thick. It is cylindrical with conical ends. The bottom is soldered to the

cylindrical side, and the joint, *J*, at the top is a close sliding fit between the side and a flange on the top. Electric heaters on the shield and differential thermocouples between the calorimeter and shield were provided so that all parts of the shield could be kept at the temperature of the calorimeter. The heater on the side of the shield consists of a single layer of No. 30 AWG double silk-covered constantan wire entirely covering the side. Two wires were wound side by side and connected in parallel so as to obtain the desired resistance. The heaters on the top and bottom cones of the shield were wound on the projecting cylindrical copper rings shown in the figure. Although these heaters do not achieve as uniform distribution of heat as does the side winding, a calculation showed that errors arising from the nonuniformity of temperature would be negligible. Glyptal lacquer applied to the heater wires as they were wound served to cement them in place and to improve their thermal contact with the shield. After the heaters were wound, the shield was covered with aluminum foil to reduce radiation. The heater and thermocouple circuits and the distribution of the thermocouple junctions will be described later.

The radiation shield is supported by the tube, T_1, and the assembly thus far described hangs in the evacuated chamber, *Ch*. There is an opening in the shield through which the electric leads pass so that the space between the calorimeter and the shield is also evacuated. However, aluminum foil was placed over this opening so that there would be no direct path for radiation to leave the space inside the shield.

The temperature of tube T_1 was controlled by means of a heater of constantan wire wound in a single layer from a point about 2 cm above the top of the shield to a point level with the top of the Dewar flask, *D*. At the lower end of this heater was soldered a copper wire, W_1, No. 18 AWG, which provides a thermal path to the cold ring, R_1. The wire is in two parts, which were soldered together after assembling the shield system, the total length of wire from the tube to the ring being about 7 cm. A thermocouple junction on the tube just below the copper wire indicated the difference in temperature between this point and the shield. By means of this thermocouple and the tube heater the tube was kept about 0.01 degree warmer than the calorimeter to prevent condensation of butadiene in the tube.

The Dewar flask, *D*, contains a bath that supplies the refrigeration. Solid hydrogen was used for the lowest temperatures, which were obtained by closing the filler tube, T_4, and reducing the pressure over a bath of liquid hydrogen by pumping out the vapor through the tube, T_2, by means of a large vacuum pump. For successively higher temperatures the refrigerating materials were liquid hydrogen, liquid air, solid carbon dioxide, ice, and water. When liquid or solid hydrogen was used as the refrigerant, the brass case, *Ca*, surrounding the Dewar flask was immersed in liquid air, in a larger flask, to a level above the top plate, *P*.

The electric leads enter the vacuum space through the wax seal at *L* and pass down through the tube, T_3. They are brought to the temperature of the bath by being wound twice around the brass ring, R_1, and are cemented to it with Glyptal lacquer. Leaving the ring, the leads pass down outside the shield and are brought to the temperature of the shield by means of the heater, H_2, wound on the leads. This preheating of the leads before they come into contact

with the shield is done to avoid a cold spot on the shield. The leads are then wound in a single layer as a helix passing up the side of the shield under the shield heater and making four turns around the shield. At point K some of the leads are separated from the bundle and are connected to the heaters and thermocouples. The remaining leads enter the shield and make a turn around ring R_2, which is soldered to the top of the shield. They then pass to the calorimeter, making a turn around ring R_3, which is soldered to the top of the calorimeter. The leads are cemented to the rings with Glyptal lacquer and are bound down tightly with thread. Leaving ring R_3 the leads pass down the side of the calorimeter and are connected to the thermometer and heater. All the leads are No. 34 AWG copper wire insulated with enamel and silk.

The filling tube, T_1, communicates through the valves with the flasks, F_1 and F_2, or with the vacuum system. The amount of butadiene involved in an experiment was determined by transferring the butadiene from the calorimeter to the brass container, F_1, and weighing F_1 before and after the transfer. A union not shown permitted the removal of F_1 so that it could be weighed on an analytical balance. In the Pyrex flask, F_2, the approximate volume of the butadiene was visually estimated before transferring it to the calorimeter. This flask was also used as an auxiliary reservoir in experiments on the heat of vaporization.

(b) ELECTRIC CONTROL CIRCUITS

The thermocouple circuits and the locations of the junctions on the apparatus are shown in figure 4. The numbered arrows on the diagram of the calorimeter and shield show the locations of the junctions and refer also to the corresponding junctions shown in the circuit diagrams, A and B. Multiple-junction thermocouples were used between the shield and the calorimeter, as it is here that the most accurate control is necessary. The three-junction couple between the calorimeter and the side and bottom of the shield was wired so that the galvanometer, G_2, could be connected through the plug contacts, P, to any adjacent pair of leads from junctions 1, 2, 3, and 4. This allowed the operator to explore the temperature distribution over the shield so that the ratio of the heat supplied to the side and bottom could be adjusted to minimize the temperature differences. While measurements were being made the contacts, P, were connected to leads 1 and 4, thus using the total emf generated by the three-junction thermocouple. The six-junction thermocouple, between the top of the shield, 8, and the top of the calorimeter, 9, permits the detection of very small temperature differences between these two points. Very accurate control was desirable here to prevent heat conduction between the shield and the calorimeter along the leads and the filler tube. The elements of the multiple-junction thermocouples were constantan and Chromel-P. The combination of these alloys has a greater thermoelectric power than constantan-copper, and Chromel-P possesses the additional advantage that its thermal conductivity is much less than that of copper. Copper-constantan junctions at 11 and 12 with the reference junction at 10 were used in maintaining temperature equality between these points. Single junctions were used at 11 and 12 as high accuracy is not necessary in controlling the temperature

of these points. The constantan and Chromel-P thermocouple wires were No. 32 AWG, double silk insulated. All the junctions except 11 and 12 were enclosed in flat sheaths about 3 mm wide and 8 mm long, made of sheet copper 0.2 mm thick. Strips of mica were used to insulate the wires from the copper sheaths. A cross section of this arrangement is shown at *C*, figure 4. After inserting the junctions and the mica insulating strips into the copper sheath, the copper was crimped tightly on the mica by pressing in a vise. Junction 11 was insulated with silk floss and inserted into the bundle of leads, which were then bound together with thread and impregnated with Glyptal lacquer. Junction 12 was insulated with silk floss and bound to the

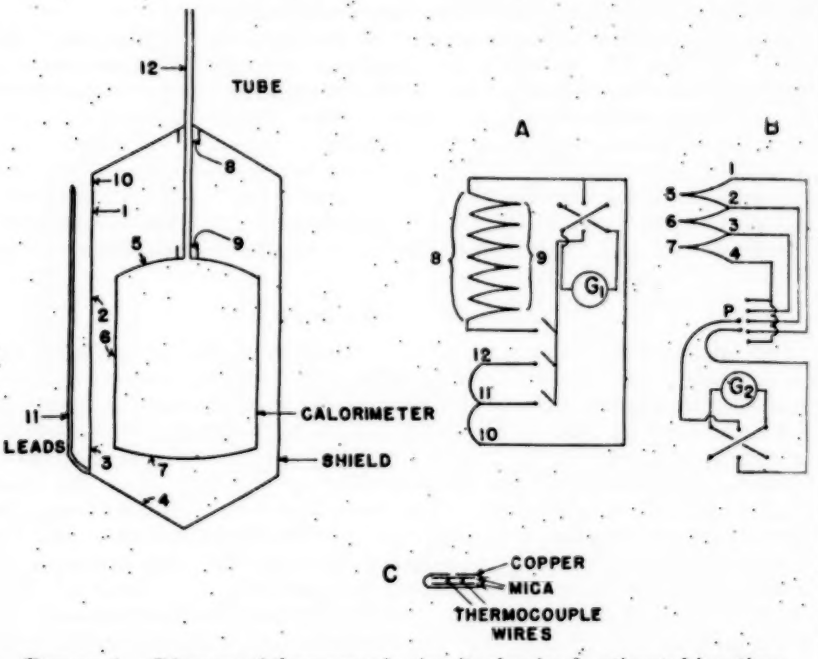

FIGURE 4.—*Diagram of thermocouple circuits showing locations of junctions.*

A, circuits for top, cable, and tube; *B*, circuits for side and bottom; *C*, enlarged diagram of thermojunction.

tube with thread, Glyptal lacquer again being used as a cement for improving thermal contact. The sheathed junctions were held in place on the surfaces of the calorimeter and shield by wedging them under small bridges of copper which were soldered to the surfaces. The junctions of the six-junction thermocouple were held against the inner surfaces of the rings, R_2 and R_3, by short pieces of watch spring coiled inside the rings. The sensitivity of the thermocouple circuits at 90° K were as follows: Top (six junction) 1.6 mm per millidegree; side (three junction) 0.8 mm per millidegree; ring and tube (single junction) 0.2 mm per millidegree.

The control circuit for the shield system is shown in figure 5. The resistances marked side, bottom, top, ring, and tube represent the electric heaters on the respective parts of the adiabatic shield system.

A_1, A_2, A_3, and A_4 are milliameters for measuring the current in each circuit. The currents supplied to the heaters are controlled by the 1-amp Variac transformers, V_1 and V_2, and the 500-ohm 50-w potential-divider rheostats, R_1, R_2, R_3, and R_4. When measurements are being made, the Variacs and rheostats are first adjusted so that the thermocouples on the shield system indicate approximately constant adiabatic conditions and then minor variations are compensated by the use of keys K_1 and K_2 in each circuit. K_1 shorts out a resistor of 100 ohms, thus momentarily increasing the current in the circuit, and K_2 opens the circuit momentarily. This operation is more convenient than changing the rheostat settings to compensate small variations in temperature. The 3,200-ohm potential divider is used

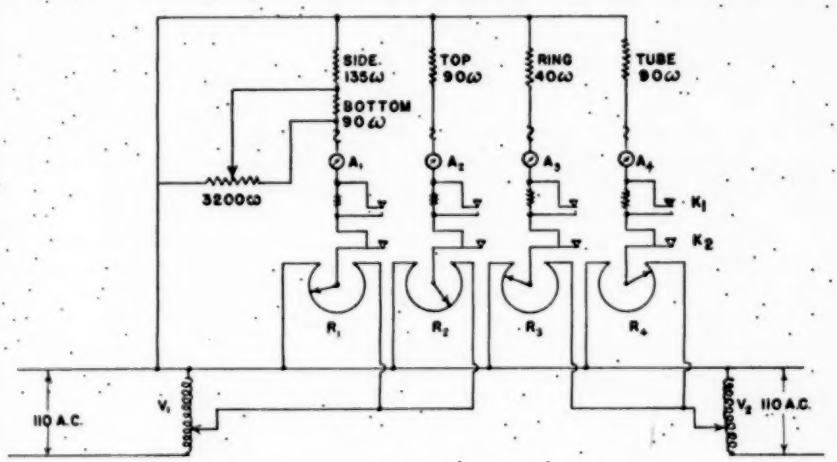

FIGURE 5.—*Diagram of electrical control circuits.*

A_1, A_2, A_3, and A_4, ammeters; K_1 and K_2, contact keys; R_1, R_2, R_3, and R_4, rheostats; V_1 and V_2, Variac transformers.

to adjust the ratio of the heat supplied to the side and bottom parts of the shield. After once adjusting this ratio, it was not found necessary to change it.

(c) MEASURING CIRCUITS

The circuits for measuring the electric energy supplied to the calorimeter and for measuring its temperature before and after heating are shown in figure 6. The current through the heater is determined by measuring the potential drop across a 1-ohm standard in series with the heater. The potential across the heater is determined by measuring a part of this potential by means of the volt box, which has a nominal ratio of 1 to 150. The leads from the volt box to the heater are actually part of the total volt-box resistance, so it is necessary to include their resistance when calculating the potential across the heater. Also part of the current that flows through the 1-ohm standard flows through the volt box; so this correction must be also made in calculating the current through the heater. One of the potential leads is connected to a current lead at its point of thermal

contact with the shield just before crossing the space between the calorimeter and shield. The other potential lead is connected to the other current lead at its first point of thermal contact with the calorimeter. Thus the measured electric energy is the energy developed in the heater plus the energy developed in that part of one current lead which traverses the space between the shield and the calorimeter. As the two sections of the current leads crossing from the shield to the calorimeter are equivalent, the same amount of heat will be developed in each. If it is assumed that this heat divides equally between the calorimeter and shield, then the heat supplied to the calorimeter will be that which is measured by this arrangement of the potential leads.

The time of heating was controlled and measured by making use of time signals supplied by the Riefler clock in the Time Section of this

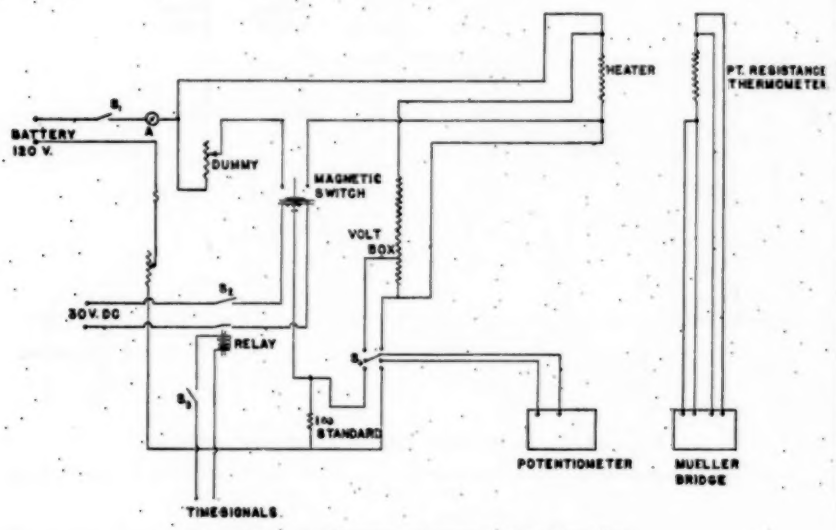

FIGURE 6.—*Diagram of measuring circuits.*

Bureau. The signals consist of electric impulses at 1-second intervals, except for a 2-second interval at the end of each minute. With switch S_3 closed, the operator notes the impulses actuating the relay. When the 2-second interval appears, the switch S_2 is closed, and the next impulse will close the 30-v circuit that actuates the magnetic switch. This switch is so constructed that it may be preset to snap either from left to right or from right to left when it receives the 30-v impulse. Thus the time of heating is an integral number of minutes. When the current is not flowing through the calorimeter heater, it flows through a dummy of equal resistance so that the battery current is constant.

Some tests were made in which the magnetic switch was used to operate the clutch of a synchronous interval timer driven by an accurately controlled 60-cycle supply. The reading of the interval timer were found to be within 0.01 second of the interval indicated by the clock-controlled circuit.

The temperature of the calorimeter was determined by measuring the resistance of the four-lead platinum resistance thermometer by means of the Mueller resistance bridge. The temperature rise during a heat was determined with an accuracy of about 0.001 degree except at temperatures below 20° K, where the sensitivity was of the order of 0.01 degree.

2. SPECIFIC HEAT

(a) METHOD OF MEASUREMENT

The specific heat of butadiene was obtained from measurements of the heat capacity of the calorimeter and contents. Two sets of heat-capacity measurements were required, one with a large amount of material in the calorimeter and one with a small amount. This procedure, which entails measurements with a small amount of material in the calorimeter rather than with the calorimeter empty, has been described by Osborne [9]. It not only takes into account the tare heat capacity of the calorimeter but makes possible an accurate correction for the effect of the vapor in the space above the solid or liquid in the calorimeter and connecting tube. In making the correction it is not necessary to know the volume of the vapor space nor the temperature of the filler tube, provided the temperature is the same during both sets of measurements.

The data from which heat capacities were calculated consisted of values of the temperature of the calorimeter and contents before and after a measured amount of electric energy had been added. The temperature rise during a heating period was usually about 10 degrees, although it was sometimes as small as 4 degrees or as large as 30 degrees. The rate of temperature rise was varied from about 0.5 degree per minute to 7 degrees per minute. The rate of 7 degrees per minute was taken between 20° and 30° K, where the heat capacity was small. This high rate could not safely be reached at temperatures above 100° K because the electric leads were too small for the required current. About 3 degrees per minute was the highest rate attained at temperatures above 100° K. One to two degrees per minute was the normal rate of rise. No consistent differences were observed between the data obtained from long heating intervals and those from short intervals, or between the data obtained from rapid heating and those from slow heating.

(b) METHOD OF CALCULATION

If a quantity of energy, ΔQ, is required to raise the temperature of the calorimeter and contents an amount, ΔT, the average heat capacity over this temperature interval is $\Delta Q/\Delta T$. The true heat capacity, dQ/dT, is the limit of this fraction as ΔT approaches zero. This limit, $dQ/dT=[G]_{T_a}$, may be calculated from the finite measured quantities by means of a relation given by Osborne, Stimson, Sligh, and Cragoe [10].

$$[G]_{T_a}=\left[\frac{dQ}{dT}\right]_{T_a}=\frac{\Delta Q}{\Delta T}-\left[\frac{\partial^2 G}{\partial T^2}\right]_{T_a}\frac{(\Delta T)^2}{24}-\left[\frac{\partial^4 G}{\partial T^4}\right]_{T_a}\frac{(\Delta T)^4}{1920}, \qquad (1)$$

where ΔQ is the heat added, ΔT is the temperature rise, and T_a is the average temperature of the heating. In making the calculations, the

derivatives of G with respect to T were replaced by derivatives of $\Delta Q/\Delta T$ with respect to T. This is permissible because $\Delta Q/\Delta T$ is approximately equal to G. Values of the derivatives were determined from graphs of $\Delta Q/\Delta T$ versus T. The last term involving the fourth derivative of G was found to be negligible for all the data for which this method was used. In fact, the term in which the second derivative of G appears was usually less than 0.1 percent of G.

The heat-capacity data were correlated and values obtained at intervals of 5 degrees by finding approximate analytical representations and plotting the deviations of the observed values from these formulas. At low temperatures the heat capacity was represented approximately by a modified Debye function $D[\Theta/(T+B)]$ suggested by Harold J. Hoge. The Debye function was evaluated from the tables prepared by Beattie [11]. By determining appropriate values of Θ and B, this function could be made to fit the heat-capacity data of the full calorimeter from 15° to 100° K. When the calorimeter contained only a small amount of butadiene it was possible to use this function from 15° to 150° K, the maximum deviation being about 2.5 percent of the heat capacity at 100° K. The conventional Debye function $D(\Theta/T)$ could not be used over such large ranges of temperature. At temperatures above 100° K for the full calorimeter and above 150° for the almost empty calorimeter, the heat-capacity data were represented approximately by equations of the form $G=a+bT+cT^2$. Tables were constructed giving G_b, the gross heat capacity when the calorimeter contained a large amount of butadiene, and G_a, the gross heat capacity when it contained a small amount.

The specific heat along the saturation line, $C_{sat.}$, was calculated by means of the equation

$$C_{sat.}=\frac{G_b-G_a}{M_b-M_a}+T\frac{d}{dT}\left(v\frac{dP}{dT}\right), \tag{2}$$

where v is the specific volume of the condensed phase and P is the vapor pressure. This equation was derived from relations given by Osborne [9]. The term $T\frac{d}{dT}\left(v\frac{dP}{dT}\right)$ allows for the fact that the gross heat capacity G includes some heat of vaporization. That is, sufficient butadiene evaporates to maintain saturation pressure in the space above the condensed phase in the calorimeter. The last term of equation 2 is negligible for solid butadiene because the vapor pressure of the solid is low.

Values of $v(dP/dT)$ for the liquid were obtained from vapor-pressure equation 4 (section IV–1, c) and values of v from table 13.

(c) RESULTS

The results of the specific-heat determinations are shown in figure 7 and in tables 1 and 2. The symbol $C_{sat.}$ is used to denote the specific heat at saturation. The graph at the bottom of figure 7 shows the differences between the specific-heat values obtained for the different

samples in the temperature range 60° to 215° K. In the liquid range there is excellent agreement, the differences usually being less than 0.1 percent. However, in the solid state the differences between the specific heats of the different samples is considerably larger. At 70° K the specific heat of sample 1 is about 1.8 percent larger than that of sample 4. It is unlikely that this difference can be accounted for by experimental error as different measurements on the same sample agreed within about 0.1 percent, and in the liquid state the agreement between the measurements on different samples was equally good. It was thought at first that the discrepancies might

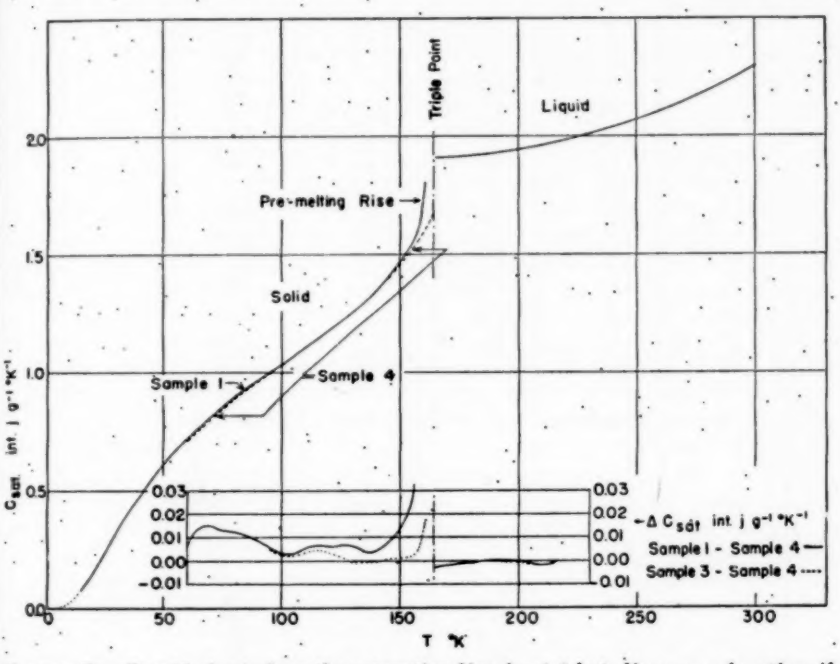

FIGURE 7.—*Specific heat along the saturation line for 1,3-butadiene as a function of temperature*

have resulted from different rates of cooling of the different samples, but a test made to detect such an effect gave a negative result. The most reasonable conclusion is that the differences were caused by different amounts of impurity in the different samples. This explanation requires that the impurity affect the specific heat to a much greater extent than would be expected from the additive law of specific heats. The large differences just below the triple point are caused by the premelting of samples 1 and 3. Sample 4, the specific heat of which is used as the reference in the deviation graph, contained so little impurity that there was no apparent premelting until the temperature was within 0.2 degree of the triple point.

TABLE 1.—*Specific heat of solid 1,3-butadiene*

T	$C_{sat.}$		
	Sample 1	Sample 3	Sample 4
° K	*Int. j g⁻¹°K⁻¹*	*Int. j g⁻¹°K⁻¹*	*Int. j g⁻¹°K⁻¹*
15	0.0747	----------	----------
20	.1492	----------	----------
25	.2341	----------	----------
30	.3193	----------	----------
35	.4012	----------	----------
40	.4762	----------	----------
45	.5447	----------	----------
50	.6081	----------	----------
55	.6654	----------	----------
60	.7186	----------	0.7136
65	.7670	----------	.7532
70	.8112	----------	.7964
75	.8522	----------	.8393
80	.8923	----------	.8800
85	.9307	----------	.9202
90	.9674	----------	.9585
95	1.0006	0.9999	.9954
100	1.0333	1.0328	1.0302
105	1.0668	1.0656	1.0636
110	1.1017	1.1000	1.0963
115	1.1376	1.1358	1.1312
120	1.1745	1.1718	1.1685
125	1.2136	1.2089	1.2071
130	1.2524	1.2474	1.2481
135	1.2963	1.2930	1.2926
140	1.3454	1.3408	1.3412
145	1.4019	1.3951	1.3942
150	1.4651	1.4533	1.4521
155	1.5450	1.5200	1.5186
160	1.7356	1.6007	1.5968

TABLE 2.—*Specific heat of liquid 1,3-butadiene*

T	$(G_b-G_a)/(M_b-M_a)$			$\frac{d}{dt}\left(\rho\frac{dp}{dt}\right)$	$C_{sat.}$
	Sample 1	Sample 3	Sample 4		Mean
° K	*Int. j g⁻¹°K⁻¹*	*Int. j g⁻¹°K⁻¹*	*Int. j g⁻¹°K⁻¹*	*Int. j g⁻¹°K⁻¹*	*Int. j g⁻¹°K⁻¹*
165	1.9104	1.9099	1.9130	0.000	1.911
170	1.9116	1.9116	1.9136	.000	1.912
175	1.9139	1.9141	1.9151	.001	1.915
180	1.9172	1.9172	1.9177	.001	1.918
185	1.9214	1.9211	1.9213	.001	1.922
190	1.9262	1.9257	1.9258	.002	1.928
195	1.9319	1.9311	1.9317	.002	1.934
200	1.9387	1.9379	1.9387	.003	1.941
205	1.9459	1.9454	1.9467	.004	1.950
210	1.9542	1.9539	1.9557	.006	1.961
215	1.9650	1.9657	1.9657	.008	1.973
220	1.9735	1.9744	----------	.009	1.983
225	1.9837	1.9854	----------	.012	1.997
230	1.9943	1.9964	----------	.015	2.010
235	2.0055	2.0078	----------	.018	2.025
240	2.0168	2.0192	----------	.021	2.039
245	2.0284	2.0308	----------	.025	2.055
250	2.0414	2.0440	----------	.030	2.073
255	2.0529	2.0551	----------	.035	2.089
260	2.0661	----------	----------	.041	2.107
265	2.0794	----------	----------	.047	2.126
270	2.0934	----------	----------	.054	2.147
275	2.1079	----------	----------	.062	2.170
280	2.1227	----------	----------	.070	2.193
285	2.1377	----------	----------	.080	2.218
290	2.1530	----------	----------	.090	2.243
295	2.1684	----------	----------	.101	2.269
300	2.1840	----------	----------	.112	2.296

In table 1 values of specific heat at 5-degree intervals at saturation are given for the different samples of butadiene in the solid state. Table 2 gives values at 5-degree intervals of $(G_b-G_a)/(M_b-M_a)$ for the three samples in the liquid state together with values of $T\frac{d}{dT}\left(v\frac{dP}{dT}\right)$. The values of $C_{sat.}$ in table 2 were obtained by averaging the values of $(G_b-G_a)/(M_b-M_a)$ at each temperature and adding the value of $T\frac{d}{dT}\left(v\frac{dP}{dT}\right)$.

3. HEAT OF FUSION

(a) METHOD OF MEASUREMENT

The heat of fusion of butadiene was determined by measuring the energy required to heat the calorimeter and contents from a temperature somewhat below the triple point to a temperature above the triple point. The initial temperature was chosen so as to be below the premelting region. The heat of fusion was obtained by subtracting from the total energy (1) the energy required to heat the calorimeter plus its solid contents from the initial temperature to the melting temperature, and (2) the energy required to heat the calorimeter plus its liquid contents from the melting temperature to the final temperature. In computing quantity (1), the specific heat of pure butadiene was used in obtaining the heat capacity of the calorimeter and contents so as to avoid errors that may be caused by the premelting of impure samples. In this way the heat of premelting is included in the value obtained for the heat of fusion. The heat of fusion was from 60 to 90 percent of the total energy added in the measurements on the different samples.

(b) RESULTS

The results of the determinations of the heats of fusion are as follows: Sample 1, 147.53; sample 3, 147.59; sample 4, 147.65 int. j g^{-1}. The mean of these values is 147.59 int. j g^{-1}. It may be noted that there is little difference in the heats of fusion of the samples, although they contain different amounts of impurity. The scattering of the results is no more than would be expected from ordinary errors of observation. Assigning a reasonable probable error, the heat of fusion of butadiene may be given as $147.6+0.1$ int. j g^{-1}, or 1908.4 ± 1.3 cal $mole^{-1}$.

4. HEAT OF VAPORIZATION

(a) METHOD OF MEASUREMENT

The measurement of the heat of vaporization consisted of determining the amount of electric energy required to vaporize a measured quantity of butadiene. This was accomplished in the following manner:

Referring to figure 3, the reservoirs, F_1 and F_2, were cooled by surrounding them with solid CO_2. The calorimeter was brought to the desired temperature and the shields adjusted to adiabatic conditions. Then the switch was closed, sending current through the calorimeter heater. The valve leading to F_2 was opened, and the valve leading to the calorimeter was used as a throttle and adjusted until the temperature of the calorimeter was almost constant. A final adjustment of the current through the calorimeter was necessary to obtain a steady temperature. After equilibrium had been established, the

valve leading to F_2 was closed and the valve to F_1 was opened without disturbing the adjustment of the throttling valve. After a measured interval of time, the valve to F_1 was closed and the calorimeter heater turned off. The amount of butadiene vapor removed from the calorimeter during the measured time was determined by weighing F_1 before and after each run. The temperature of the calorimeter was kept constant during a run by making small adjustments of the heating current at measured times, so that the total energy input could be measured by measuring the current and potential drop through the heater during each interval of time between these adjustments. The adjustments of heating current were of the order of 1 percent, and usually several minutes would elapse between adjustments. The platinum resistance thermometer was assumed to be at the temperature of the vaporizing liquid. This may not be strictly true, but if errors arise from this source they should be dependent on the power input, and no such dependence was observed. As the time of withdrawal of the measured sample is determined by manual operation of the valves, the error in timing may be as large as one-half second. The time of withdrawal ranged from 15 to 40 minutes.

(b) RESULTS

If Q is the energy input during the withdrawal of M grams of vapor, the heat of vaporization L_v is

$$L_v=\frac{Q}{M}\left(1-\frac{v}{V}\right), \tag{3}$$

where v is the specific volume of the liquid, and V is the specific volume of the vapor. Q/M is not the true heat of vaporization as part of the material vaporized does not leave the calorimeter but fills the space vacated by the vaporized liquid.

Table 3 gives the data and results on the heats of vaporization. The energy input, Q, and the mass withdrawn, M, are given for each individual vaporization at a given temperature, and the quantity Q/M is computed. In order to obtain the mean value of Q/M for each temperature the sum of the energy input was divided by the total amount withdrawn. This is shown in the bottom line of each group of measurements. This mean value is equivalent to that which would have been obtained by weighting the individual observations in proportion to the amount of butadiene vaporized. In calculating the latent heat, $L_v=\frac{Q}{M}\left(1-\frac{v}{V}\right)$, values of v and V were taken from table 13. The average deviations of the observations from the mean value of Q/M are given in the next to last column of table 3. These range from 0.04 to 0.06 percent, and the maximum deviation of a single observation is 0.20 percent.

TABLE. 3.—*Data and results of heat-of-vaporization experiments*

T	Q	M	Q/M	Power input	$1-\frac{v}{V}$	$L_v=Q/M\left(1-\frac{v}{V}\right)$	Average deviation of observations	L_v calculated from table 13
°K	*Int. j*	*g*	*Int. j g*$^{-1}$	*w*		*Int. j g*$^{-1}$	*Int. j g*$^{-1}$	*Int. j g*$^{-1}$
247.07	2043.3	4.6846	436.17	1.17				
	1282.2	2.9307	437.50	1.19				
	884.9	2.0257	436.62	0.74				
	915.1	2.0970	436.39	0.76				
	1708.4	3.9128	436.62	1.78				
	2324.6	5.3246	436.58	2.58				
Total	9158.5	20.9764	436.61		0.99843	435.92	0.27	435.21
268.60	1552.2	3.7147	417.85	0.86				
	3616.3	8.6651	417.34	2.08				
	2405.2	5.7582	417.70	0.93				
	1801.8	4.3165	417.42	2.00				
	1878.8	4.4975	417.74	1.01				
Total	11254.3	26.9520	417.57		0.99610	415.99	0.19	415.47
295.67	2594.4	6.6222	391.77	1.05				
	2286.0	5.8263	392.36	2.54				
	1128.4	2.8801	391.79	0.99				
	2324.2	5.9312	391.86	2.15				
	2709.6	6.9174	391.71	2.66				
Total	11042.6	28.1772	391.90		0.99012	388.03	0.20	388.17

The formulated values of L (see section VI–2) at temperatures of even degree centigrade (table 13) lead through interpolation to the values given in the last column of table 3. The agreement at 295.67° K is excellent, the calculated value being slightly higher than the observed. The calculated values at 268.60° and 247.07° K are only 0.13 and 0.16 percent lower than the respective observed values.

5. ACCURACY OF CALORIMETRIC MEASUREMENTS

Some tests were made with the calorimeter to determine the accuracy with which measurements could be made. Water was chosen as the test material as very reliable data [12] are available. The specific heat of water was measured in the calorimeter between 1° and 22° C. Three heats were made in this range of temperatures, and the maximum difference between the values obtained and those given by Osborne, Stimson, and Ginnings was 0.03 percent. Three determinations of the heat of vaporization of water at 20° C yielded a maximum difference of 0.17 percent, although the mean of the three measurements agreed with Osborne's values to 0.03 percent. The measurements on the specific heat of water are probably somewhat more reliable than those obtained on substances having lower specific heats, as the heat capacity of the water sample is a larger fraction of the total heat capacity of the calorimeter plus contents than it is for other substances. The measurements of the heat of vaporization of water, however, are probably comparable with the measurements on butadiene. The heating rates and total energy input during heats were about the same for the two substances.

Taking into consideration these tests, and the scattering of the observations previously mentioned, the estimates of the probable errors of the calorimetric measurements described in this paper are as follows: Specific heat, 0.1 percent between 40° and 300° K, becoming possibly as large as 1 percent below 20° K; heat of fusion, 0.07 percent; heat of vaporization, 0.15 percent.

IV. PRESSURE-VOLUME-TEMPERATURE MEASUREMENTS

1. VAPOR PRESSURE

The vapor-pressure measurements comprised two groups of observations made with two independent sets of apparatus. The first group of observations covered a temperature range from 195° to 288° K or a corresponding pressure range up to about 2 atm. The second group covered the temperature range 0° C to the critical temperature. Above 110° C, however, the accuracy was reduced considerably by rapid polymerization of the sample. The method used in both series of measurements was that in which static equilibrium was approached between the liquid and the vapor portions of the sample. At the higher temperatures the approach was always by condensation of some of the sample rather than by evaporation, as the former procedure had been found to be more rapid with other substances.

(a) MEASUREMENTS FROM 195° TO 288° K

The apparatus used for these observations consisted of a mercury manometer of 10-mm bore, which was read by means of a mirror-

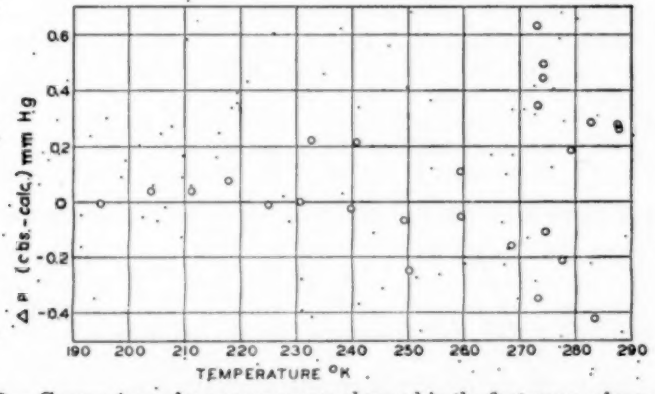

FIGURE 8.—*Comparison of vapor pressures observed in the first group of measurements with calculated values.*

backed glass scale graduated in millimeters and supported against the manometer tubes. One arm of the manometer was connected to the filler tube of the calorimeter, in which there was a quantity of butadiene from sample 4. When making measurements of vapor pressures below 1 atm the other arm of the manometer was evacuated. For measurements above 1 atm this arm was open to the atmosphere. In the latter case, one measurement of the atmospheric pressure was made with a precision barometer for each set of three readings of the manometer at a given temperature.

Figure 8 shows the deviations of the observations from the values calculated from equation 4. It was thought that the pressure measurements were reproducible to about ± 0.2 mm Hg. The deviations below 270° K confirm this. However, above this temperature there is considerably greater scattering, which has been attributed to the presence of some impurity, causing the vapor pressure to depend on the amount condensed, as described in the section on purity.

(b) MEASUREMENTS FROM 0° TO 152° C

The apparatus used in these measurements was entirely independent of that used in the group (a) measurements made in connection with the calorimetric experiments.

It is shown diagrammatically in figure 9. The vapor pressure of the butadiene in the closed end of one manometer is transmitted through the mercury and oil to either an open-ended auxiliary mercury manometer for the low-pressure measurements or to a dead-weight piston gage for the high-pressure measurements [14].

As static vapor-pressure measurements are susceptible to errors due to more volatile impurities, provision was made to vary the butadiene vapor space so that the vapor-pressure measurements could be extrapolated to large vapor volumes. The vapor space was varied

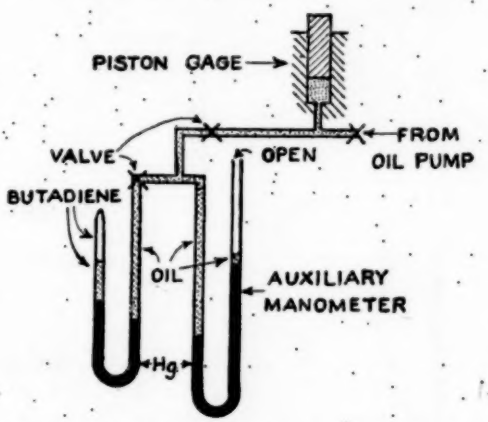

FIGURE 9.—*Connecting lines for vapor pressure measurements.*

by changing the amount of oil between the mercury manometers by means of the piston-gage oil pump.

Two types of manometers containing the butadiene were used and are shown in figure 10. Each consisted of a U-shaped glass tube with a metal valve soldered [13] to one arm. In the manometer shown in figure 10, *A*, the butadiene was distilled into a space above the mercury meniscus and sealed at *C*. In figure 10, *B*, the butadiene was distilled through a small third arm and sealed at *D*. By closing the main portion of the manometer with a mercury seal before sealing the glass, any gases freed during the sealing off and not removed by the vacuum pump were trapped at *D*. In the sealing of both types of manometers the butadiene was cooled with liquid air. The manometer shown in figure 10, *B*, was made with calibrated volumes as shown, and could also be used later in the measurement of vapor density.

The small size of the samples used in this group of observations necessitated great care in regard to the cleanliness of the apparatus. The glass manometers were washed with nitric acid, soaked several hours with freshly prepared chromic acid, and rinsed several times with

distilled water. The last rinse water, which remained in the manometers several hours, had substantially the same electric conductivity as the distilled water used. The manometers were outgassed by heating with a torch during evacuation, and the mercury was introduced by distillation. A small quantity of butadiene was admitted and then pumped out before condensing a sample into a manometer.

For the measurement at 0° C, the butadiene was completely im-

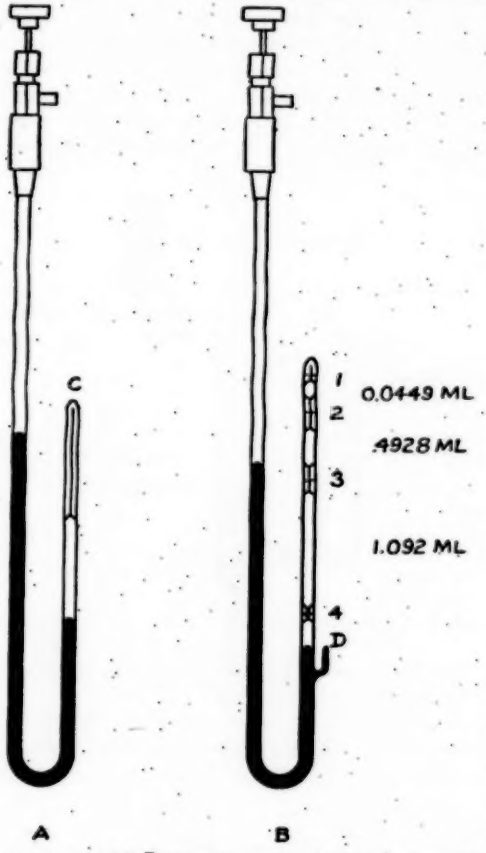

FIGURE 10.—*Manometers used in measurements of vapor pressure and of density of vapor.*

mersed in an ice bath. At higher temperatures, a stirred thermoregulated oil bath was used. Temperatures were measured with a four-lead, potential-terminal, platinum resistance thermometer of the coiled-filament type, calibrated according to specifications of the International Temperature Scale [15]. The elevations of the mercury surfaces were referred to steel scales graduated in millimeters and suspended between the arms of the manometers.

Seven samples were at various times distilled into manometers for these vapor-pressure measurements. The first five were subsamples taken from sample 3, already described in the section on preparation of samples, and were numbered 3a, 3b, 3c, 3d, and 3e, respectively. The other two (4a and 4b) were taken from sample 4.

The results of the measurements on samples 3b, 3e, and 4b are presented in figures 11, 12, and 13, respectively, in which the abscissas represent the volume occupied per gram of sample, whereas the ordinates represent pressures in centimeters of mercury corrected to 0° C and to standard gravity. In order to represent several isotherms with the same coordinates, a constant of appropriate amount for each isotherm is subtracted from the pressures. Observed values are represented in the three figures by various symbols, the same symbol being used uniformly for any one isotherm, calculated values are represented by black squares, the vapor pressure being calculated from vapor-pressure equation 4, and the corresponding volume being calculated from the equation of state 6. At 0° C the specific volume of the vapor (336 ml/g) is considerably off the scale.

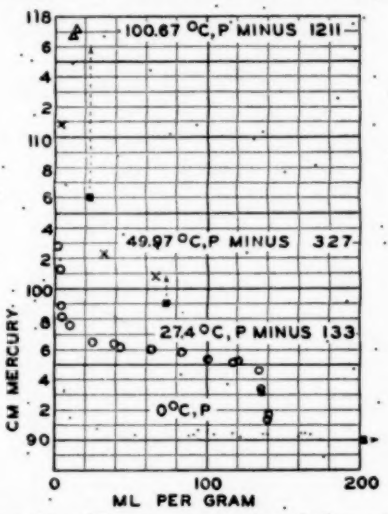

FIGURE 11.—*Vapor-pressure data for sample 3b.*

■=Values of pressure calculated from vapor pressure equation 11 and values of specific volume of saturated vapor calculated from equation of state 13. Specific volume at 0° C=335 ml/g. Dotted line and arrow indicate temperature to which ■ symbol belongs. Other symbols represent observed values.

The data at 0° C consist of numerous observations made initially on each sample, followed by observations at higher temperatures, with occasional repeated observations at 0° C. Such repeated observations after 62° C for samples 3e and 4b and after 112° C for sample 3e are represented in figures 12 and 13 by the same symbols as earlier measurements at 0° C. As their positions in the figures do not distinguish them from earlier measurements, it is believed that polymerization was thus far negligible. The agreement between the vapor pressures of the purer samples also indicates that at temperatures up to and including 112° C polymerization caused no appreciable effect.

Of the first four samples, which were not as pure as the others, only the data on sample 3b are presented. Besides comprising most of the data above 100° C, they are of special interest, as this sample was the only one in a manometer of sufficient capacity to permit the complete evaporation of the sample at room temperature, thus furnishing a better illustration of the variation of pressure with volume. The observed values for the vapor pressure of this sample (fig. 11) are

noticeably higher than the calculated. These differences are attributed to volatile impurities. On the other hand, the observed vapor pressure, 31,945 mm, at 152° C (not shown in fig. 11) is low by 484 mm, at least partially due to the extremely rapid rate of polymerization at this temperature.

Two observed values of vapor pressure at 62.05° C for sample 3e (see fig. 12) are notable for being considerably below the calculated pressure, even though the volume of sample was in one case slightly less than that calculated for saturated vapor. This is probably due to an impurity less volatile than butadiene, which appears to be absent in sample 4b (see fig. 13).

In addition to these data the vapor pressure of sample 4a was measured at 0°, 99.88° C, and at the critical temperature (discussed

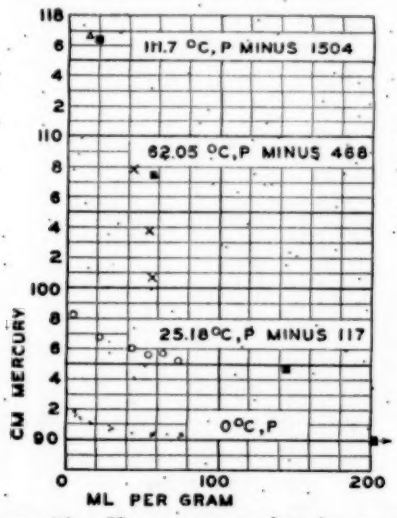

FIGURE 12.—*Vapor-pressure data for sample 3e.*

■=Values of pressure calculated from vapor-pressure equation 11 and values of specific volume of saturated vapor calculated from equation of state 13. Specific volume at 0°=335 ml/g. Other symbols represent observed values.

later). The observed values corresponding to the first two temperatures, 902.0 mm and 12,973 mm, are in very good agreement with the respective values calculated from the vapor-pressure equation, namely 899.7 and 12,971 mm, especially when one considers that observations with this sample at 0° C were possible only with a small portion evaporated on account of the relatively large mass of sample.

The results of these measurements show that the observed vapor pressures depended somewhat on the relative amounts of the sample that were in the liquid and vapor phases. This indicates the presence of an impurity. The data show that the first four samples, 3a, 3b, 3c, and 3d, contained approximately equal percentages of impurity, that sample 3e contained somewhat less impurity (probably due to the improved method of sealing the sample), and that samples 4a and 4b contained still less impurity (in consequence of a purer sup-

ply). The accuracy of reading at 0° C would lead one to expect results reproducible to within 0.5 mm, but the variation obtained was about three or four times that amount, as may be seen in figure 14, in which the observed pressures for samples 3e and 4b are represented at 0° C with a more open scale than in figures 12 and 13. It would

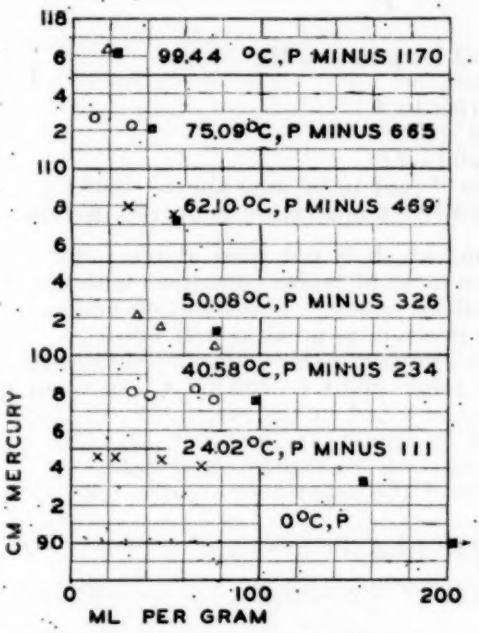

FIGURE 13.—*Vapor pressure data for sample 4b.*

Symbols are same as in figure 12.

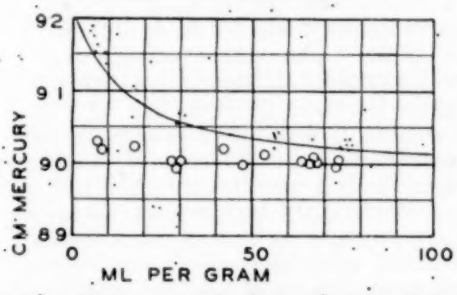

FIGURE 14.—*Vapor pressure of samples 3e and 4b at 0° C.*

appear that the excessive variation was due to a rather large lag in approaching equilibrium. The time required to remove the heat of condensation may have been supplemented by the time required for diffusion of an impurity between the butadiene liquid surface and the remainder of the liquid, especially in the earlier and less pure samples.

649238—45——5

(c) VAPOR-PRESSURE EQUATION

The vapor pressure of 1,3-butadiene is represented over the temperature range from the triple point to the critical temperature by the empirical equation [2]

$$\log p = A - \frac{1}{T}[B + CX(10^{DX^2} - 1)] - E(T - 243.16)^6, \quad (4)$$

where

$A = 7.2363$ for p in mm Hg
$B = 1165.21$
$C = 1.5875 \times 10^{-4}$
$D = 0.766 \times 10^{-10}$
$X = 125{,}000 - T^2$
$E = 2 \times 10^{-14}$ (not to be used above $-30°$ C)
$T = t + 273.16$ = temperature in degrees Kelvin.

The last term, which is not used above $-30°$ C, was added in order to produce a set of tables consistent with specific-heat data in the low-temperature region. This addition makes no change in the values of vapor pressure as great as 0.01 mm.

The equation represents the vapor-pressure measurements in the range from the triple point ($-108.92°$ C) to room temperature, as illustrated in figure 8 and in the range 0° C to the critical temperature, as shown in figures 11, 12, and 13. The representation is within the precision of the experimental data.

Differentiation of the vapor-pressure equation gives

$$\frac{d \ln p}{dT} = \frac{1}{T^2}[B + CX(10^{DX^2} - 1)] + 2C[10^{DX^2}(4.6052DX^2 + 1) - 1] - 6E(T - 243.16)^5. \quad (5)$$

(d) COMPARISON WITH DATA OF OTHER OBSERVERS

The values for vapor pressure calculated from equation 4 are compared in table 4 with those obtained by previous observers. Some preliminary measurements made by R. S. Jessup of this Bureau are included in this table. These measurements were made with a Bourdon gage and samples of butadiene that were not as pure as those used to obtain the data presented in figures 8, 11, 12, and 13. The results of Vaughan [16] differ considerably from the present results both in pressure and in the rate of change of pressure with temperature. Heisig's [17] results are in much better agreement, although they are consistently higher than those obtained in this investigation. There appears to be a slight difference between Heisig's observations obtained with the platinum resistance thermometer below the freezing temperature of mercury and the observations with a mercury thermometer at higher temperatures. The data obtained

[2] A vapor-pressure equation of the form

$$\text{Log } p = A - \frac{1}{T}[B + CX(10^{DX^2} - 1)]$$

was first used to represent the observed vapor pressures of CO_2 within about 3 parts in 10,000. See BS J. Research **10**, 381 (1933) RP538. It has also been used to represent the vapor pressures for several other substances. The value of X is usually approximately 0.7 $T_c^2 - T^2$, except for those substances having a low critical temperature, in which case the coefficient of T_c^2 is smaller. The value of C for substances previously tried has been between 1.1×10^{-4} and 1.22×10^{-4}. The exceptionally high value obtained for C for butadiene may be a consequence of the lack of accurate vapor-pressure data above 112° C.

by Moore and Kanep [18] deviate in an irregular manner, which suggests lack of equilibrium when their observations were made. The normal boiling temperature observed by Lamb and Roper [19] is only slightly lower than that calculated from equation 4 and agrees with that obtained for some of the less pure samples of the present investigation.

TABLE 4.—*Comparison of data of other observers with vapor pressures calculated from equation 4*

Temperature	$p_{obs.}$	$p_{obs.}-p_{calc.}$	Temperature	$p_{obs.}$	$p_{obs.}-p_{calc.}$	Temperature	$p_{obs.}$	$p_{obs.}-p_{calc.}$
R. S. Jessup. Sample 1			G. B. Heisig			Wm. E. Vaughan		
°C	mm	mm	°C	mm	mm	°C	mm	mm
0	917	.17	−75.5	14.6	0.2	−81.9	9.2	0.8
25	2,142	.37	−63.4	35.4	.1	−79.1	11.0	.3
50	4,340	.76	−51.6	77.1	1.0	−38.5	156.9	−3.8
65	6,250	.77	−39.4	153.4	0.2	−24.0	327.5	−3.2
			−38.6	161.7	1.8	−17.0	442.7	−10.0
			−32.7	219.0	1.9	−3.1	772.4	−27.2
			−26.1	301.4	1.8	+0.5	862.6	−54.1
			−19.9	400.5	1.6			
R. S. Jessup. Sample 2			−15.5	484.2	1.2	G. Moore and E. K. Kanep		
			−10.4	599.9	1.6			
			−5.6	729.7	4.2	−4.5	763	6
0	904	4	−1.5	854.0	3.8	3.0	957	−49
25	2,124	19	A. B. Lamb and E. E. Roper			10	1,266	−24
50	4,290	26				16	1,627	47
65	6,210	37				22	1,926	9
			−4.51	760	2.9			

2. DENSITY OF SUPERHEATED VAPOR

(a) METHOD AND APPARATUS

The density of the superheated vapor was measured for three samples of butadiene 3d, 3e, and 4b, the first of these being in the manometer illustrated in figure 10 *A*, and the other two in the manometer illustrated in figure 10 *B*. The volumes of these manometers were determined by weighing the mercury which filled the right-hand arms to various depths when in an inverted position.

A measured length of capillary in figure 10 *A*, and the space between marks 1 and 2 in figure 10 *B*, were used to measure the sample when nearly all condensed. A small vapor space was retained above the liquid to prevent sticking of the liquid in the top of the manometer. It had been previously observed that, after the sample was entirely condensed, the liquid broke away from the top of the manometer only after the pressure had been reduced considerably below the vapor pressure, and the violence of the separation was sufficient to scatter mercury droplets into undesirable places. In addition to this method of measuring the volume of the liquid and estimating the mass of sample from the known density, volume (about 120 ml), pressure, and temperature of the vapor were observed before the sample was condensed into the manometer. A correction was applied for the deviation from the ideal-gas law. This correction amounted to 1.5 parts in 1,000 for sample 3d, and 2.4 parts in 1,000 for samples 3e and 4b, which were filled with a charge at higher pressures than was sample 3d.

The measurements of vapor density may be divided into two classes. In the first class are a few measurements in which the vapor occupied the space down to either mark 3 or 4 (see fig. 10 and accompanying discussion in the text). In the second class are a larger number of measurements in which the vapor extends to unmarked parts of the manometers. This latter class of measurements is less accurate than the first. For sample 3d the position of only the dome of the meniscus was observed, whereas for samples 3e and 4b, both the dome and the edge of the meniscus were located with consequent improvement in accuracy.

(b) RESULTS OF MEASUREMENTS AND THEIR FORMULATION

The results of the measurements on samples 3d, 3e, and 4b are presented in tables 5, 6, and 7, respectively, together with a comparison of the observed values of pV/RT with those calculated from the empirical equation of state [3]

$$\frac{pV}{RT}=1-\frac{68.4[1-10^{-.045(Tc/T)^2}]-1.48}{V}+\frac{6\left(\frac{T_c}{T}\right)^4+3.5}{V^2}, \tag{6}$$

where v is in milliliters per gram, and the other variables are in consistent units. When p is in millimeters of mercury, and T is in degrees Kelvin ($T=273.16+°C$), the value of R is 1152.95 mm Hg (ml)/g mole° C. Only a few of the differences in tables 5, 6, and 7 exceed an amount appropriate to the accuracy of reading the position of the mercury-butadiene interface (see fig. 10, *A* and *B*). The consistent difference between data for samples 3d and 3e does not exceed the uncertainty in determining the mass of sample.

TABLE 5.—*Measurements of vapor density for sample 3d*

Mass of sample by measurement of vapor	0.01591
Mass of sample by measurement of liquid	.01591
Weighted mean value	0.01591 gram

Date	Class of observation	Temperature	Pressure	Specific volume	pv/RT observed	pv/RT calculated	$10^4\frac{\text{col. 6}-\text{col. 7}}{\text{col. 7}}$
1943		°C	mm Hg	ml/g			
Mar. 2	2	30.78	2206.0	147.39	0.9279	0.9260	21
	2	30.80	2271.9	142.86	.9261	.9237	26
	2	30.81	2337.8	138.34	.9228	.9213	16
	2	30.80	2470.8	130.04	.9169	.9165	4
	2	36.41	2674.8	122.31	.9166	.9145	23
	2	36.41	2742.7	119.11	.9153	.9121	33
	2	36.41	2844.6	114.20	.9101	.9086	17
	2	36.41	2945.2	109.43	.9030	.9050	−22
Mar. 3	2	49.90	2680.2	129.04	.9285	.9256	33
	2	49.90	3365.6	100.64	.9094	.9049	50
	2	49.90	4062.5	81.14	.8850	.8831	22
	2	100.04	7,509	71.28	.9127	.9041	95
	2	99.99	9,119	39.09	.8277	.8268	10
	2	99.95	12,739	24.89	.7372	.7352	27
Average deviation							29

[3] Equation 6 expresses p at a given T as a cubic equation in V, necessitating the use of successive approximations for calculating the specific volume of the saturated vapor. For the first approximation it was convenient to obtain values of v [27] from the simpler equation

$$\left(1-\frac{pV}{RT}\right)_g=\frac{(p/2.718\ p_c)^{0.702}}{\left(1-\frac{pV}{RT}\right)_l},$$

where the subscripts g and l refer to gas and liquid, respectively, and p_c is the critical pressure.

TABLE 6.—*Measurement of vapor density for sample 3e*

Mass of sample by measurement of vapor	0.02749
Mass of sample by measurement of liquid	.02741
Weighted mean value	0.02746 gram

Date	Class of observation	Temperature	Pressure	Specific volume	$p\sigma/RT$ observed	$p\sigma/RT$ calculated	$10^4\frac{\text{col. 6}-\text{col. 7}}{\text{col. 7}}$
1943		°C	mm Hg	ml/g			
April 1	2	59.64	4283.7	79.24	0.8847	0.8881	−39
	2	59.65	4561.6	73.78	.8771	.8800	−33
	2	59.66	5117.6	64.79	.8641	.8635	+7
	2	62.03	4287.1	80.12	.8888	.8908	−22
	2	62.03	4562.7	74.58	.8806	.8830	−27
	2	62.03	4840.9	69.77	.8740	.8750	−12
	2	62.03	5120.1	65.44	.8670	.8669	+1
	1	62.03	5544.9	59.47	.8533	.8541	−9
April 3	2	111.71	5588.3	72.25	.9099	.9106	−8
	1	111.71	6665.5	59.43	.8928	.8917	+12
	2	111.70	9143.2	40.93	.8434	.8455	−25
	2	111.71	12,755	26.91	.7735	.7693	+55
	1	111.71	15,649	19.70	.6948	.6937	+16
Average deviation class 1							10
Average deviation class 2							23

TABLE 7.—*Measurement of vapor density for sample 4b*

Mass of sample by measurement of vapor	0.02757
Mass of sample by measurement of liquid	.02746
Weighted mean value	0.02750 gram

Date	Class of observation	Temperature	Pressure	Specific volume	$p\sigma/RT$ observed	$p\sigma/RT$ calculated	$10^4\frac{\text{col. 6}-\text{col. 7}}{\text{col. 7}}$
1943		°C	mm Hg	ml/g			
May 5	2	50.08	4,060	80.87	0.8811	0.8831	−23
	2	50.08	4,264	76.15	.8713	.8765	−60
	2	62.10	4,288	80.43	.8922	.8910	+13
	1	62.10	5,557	59.37	.8536	.8540	+5
May 7	2	75.09	4,350	83.23	.9017	.9029	−13
	1	75.08	5,854	59.37	.8657	.8647	+12
	2	75.08	6,983	48.43	.8423	.8341	+98
	2	99.44	4,717	83.27	.9144	.9163	−21
	1	99.44	6,406	59.37	.8854	.8833	+24
	2	99.44	9,111	39.27	.8329	.8257	−34
	2	99.44	12,724	25.09	.7432	.7344	+120
	2	149.00	5,589	81.16	.9315	.9359	−47
	1	149.00	7,479	59.38	.9125	.9128	−3
	2	149.00	12,745	32.40	.8484	.8437	+56
	1	149.00	18,621	19.67	.7526	.7539	−17
	2	148.98	22,189	15.09	.6880	.6887	−10
	2	148.98	23,637	13.78	.6693	.6587	+160
	2	148.98	25,092	11.96	.6166	.6247	−133
	2	148.98	25,820	11.38	.6037	.6068	−52
	2	148.98	26,548	10.80	.5891	.5872	+33
	2	148.98	27,278	10.15	.5689	.5657	+39
	2	148.98	28,008	9.53	.5484	.5416	+125
	2	148.98	28,736	8.69	.5131	.5124	+14
	2	148.98	29,464	7.78	.4710	.4783	−155
Average deviation class 1							12
Average deviation class 2							63

3. DENSITY OF SATURATED LIQUID

(a) METHOD AND APPARATUS

The density of liquid butadiene was measured in the pyrex glass picnometer illustrated in figure 15. The picnometer was calibrated by weighing the amounts of mercury or water that filled the various parts of the picnometer. The results of these calibrations are given

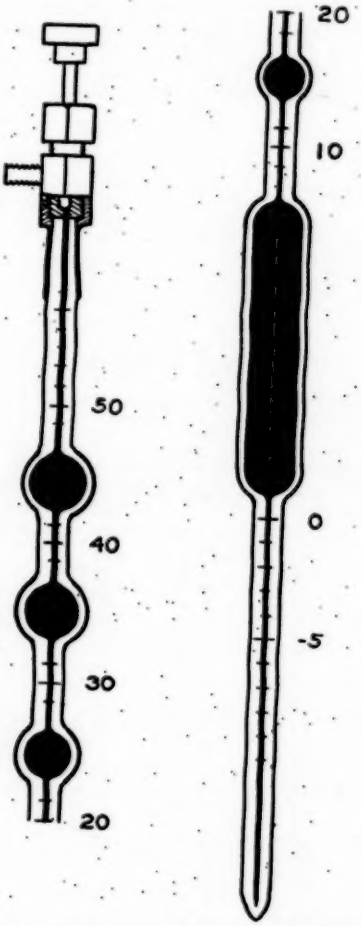

FIGURE 15.—*Semisectional view of picnometer.*

in table 8. The worst discrepancy between the two calibrations is at mark 40, which amounts to about 1 part in 7,000. The mean value, which is less than 1 part in 10,000 from either calibration, was used in calculating the results. The cross section of the capillary used in the picnometer was measured as an aid in correcting for readings not directly at a mark. The cross section of the capillary portions between the valve and the large bulb is 1.00 mm^2, that for the capillary below the large bulb is 1.38 mm^2. Both capillaries were calibrated by weighing mercury threads of measured length.

TABLE 8.—*Data from calibration of picnometer*

Space included	Capacity at 0°C			
	Water calibration (Sept. 15–16, 1943)	Mercury calibration (Oct. 1–12, 1943)	Mean	Total volume
	ml	*ml*	*ml*	*ml*
Valve to mark 50	0.0731		0.0731	15.6955
Mark 50 to mark 40	1.8348	1.8365	1.8356	15.6224
Mark 40 to mark 30	1.3442	1.3423	1.3433	13.7868
Mark 30 to mark 20	.8922	.8921	.8922	12.4435
Mark 20 to mark 10	.5667	.5665	.5666	11.5513
Mark 10 to mark 0	10.8448	10.8446	10.8447	10.9847
Mark 0 to bottom	.1400		.1400	.1400

The coefficient of volumetric expansion of the picnometer was assumed to be 1.00×10^{-5} per degree centigrade. The stretch of the picnometer with pressure, calculated from the dimensions of the large picnometer bulb (18-mm outside diameter and 1.8-mm wall thickness) and the elastic properties of Pyrex, was 1.61×10^{-5}/atm.

The measurement of the density of liquid butadiene was subject to error from polymerization, especially at the higher temperatures. On this account, the densities at low temperatures were observed first and a correction applied to the measurements at higher tempertures. This correction was determined by repeating the measurement at 0° C and noting the change in volume at 0° C resulting from polymerization at the higher temperature. Two subsamples, 4c and 4d, were taken from the larger sample 4 for the measurements of liquid density. Except at −78.72° C and at 0° C, the temperature was measured with the same platinum resistance thermometer used for measuring temperatures during the vapor-pressure investigation (IV–1 b).

Several different baths were used for measuring the density of these samples at various temperatures. At −78.72° C the picnometer was packed in finely divided dry ice up to the level of the meniscus. Precautions were taken to purge air from the space above the solid, and to pack the dry ice thoroughly enough to avoid radiation from the surroundings between the particles of solid CO_2. At 95.67° C the picnometer was totally immersed in a steam bath operated at a pressure below atmospheric. The data indicated that the temperature of this bath changed too rapidly with time, and in consequence of prolonged efforts to attain equilibrium, the correction for polymerization was unduly large, so that the corrected result is not as reliable as at the other temperatures. At 0° C an ice bath of shaved ice packed with enough water to fill the crevices but not to float the ice was used. In order to maintain the butadiene meniscus also at 0° C during the observations, a glass sight tube was placed between the picnometer and the bath container and ice was piled over the tube. At the remaining temperatures thermally controlled stirred liquid baths were used.

(b) RESULTS OF MEASUREMENTS AND THEIR FORMULATION

The data obtained are presented in tables 9 and 10. In these tables the "volumes occupied" include corrections to the volume of the picnometer at 0° C and 1 atm. It is to be noted that the density

of the vapor given in these tables is not necessarily that of the saturated vapor but that of the vapor existing in the picnometer. The "apparent liquid density" is the quotient obtained by dividing the mass of liquid by the volume occupied. The corrected density was obtained by adding to the apparent density (columns 8 of the tables 9 and 10) the correction for polymerization already discussed.

TABLE 9.—*Measurements of liquid density for sample 4c*

Mass of sample by weighing in..... 8.0392
Mass of sample by weighing out..... 8.0390

Mean value..... 8.0391 grams.

Date (1943)	Temperature t	Volume		Vapor density	Vapor mass	Liquid mass by difference	Liquid density		Col. 5+col. 9 +0.001067
		Liquid	Vapor				Apparent	Corrected [a]	
	°C	ml	ml	g/ml	g	g	g/ml	g/ml	g/ml
Oct. 15	−78.72	10.9808	4.711	0.00005	0.0002	8.0389	0.73209	0.73209	0.6481
Oct. 15	−44.92	11.5486	4.144	.00043	.0018	8.0373	.69595	.69595	.6469
Oct. 15	0	12.4463	3.252	.00277	.0089	8.0303	.64519	.64519	.6483
Oct. 20	+53.04	[b] 13.7909	1.833	.01456	.0267	[b] 7.9656	.5776	.5776	.6482
Oct. 21	+53.23	[c] 13.8016	1.824	.01423	.0260	[c] 7.9677	.5773	.5772	.6482
Oct. 27	95.67	15.704	.010	.036	.0004	8.0387	.5119	.5089	.6484

[a] Corrected for compressibility of liquid and for polymerization.
[b] Not including 0.0475 gram of liquid in top capillary next to valve.
[c] Not including 0.0454 gram of liquid in top capillary next to valve.

TABLE 10.—*Measurements of liquid density for sample 4d*

Mass of sample by weighing in..... 7.4635
Mass of sample by weighing out..... 7.4642

Mean value..... 7.4638 grams.

Date (1943)	Temperature t	Volume		Vapor density	Vapor mass	Liquid mass by difference	Liquid density		Col. 5+col. 9 +0.001067
		Liquid	Vapor				Apparent	Corrected [a]	
	°C	ml	ml	g/ml	g	g	g/ml	g/ml	g/ml
Nov. 3	−29.79	10.9814	4.71	0.00081	0.0038	7.4600	0.67933	0.67933	0.6486
Nov. 2	0	11.5494	4.146	.00277	.0115	7.4523	.64525	.64525	.6482
Nov. 8	+38.73	12.4487	3.253	.00961	.0313	7.4325	.59705	.59702	.6480
Nov. 9	79.62	13.794	1.914	.02613	.0500	7.4138	.53746	.53709	.6484

[a] Corrected for compressibility of liquid and for polymerization.

The rule of the rectilinear diameter by Cailletet and Mathias states that the sum of the densities of the liquid and the vapor is a linear function of temperature. A graph plotted for numerous substances shows that this rule gives a very close approximation if the rate of change with temperature of the sum of the densities is less than −1, when both variables are expressed in reduced units. The constants given for butadiene by Cragoe [20] lead to the equation

$$\rho_l+\rho_g=0.64817-0.0010674t, \tag{7}$$

where ρ_l and ρ_g are the densities of saturated liquid and vapor, respectively, in grams per milliliter and t is the temperature in degrees centigrade.

It will be seen that the sum of ρ_l, ρ_s, and $0.0010674t$ should be very nearly constant. Such sums are given in column 10 of tables 9 and 10 and are shown graphically as ordinate with temperature as abscissas in figure 16. The densities of the vapor used for this purpose are calculated from equations 4 and 6 in the same manner as the values in table 15 (discussed in section VII).

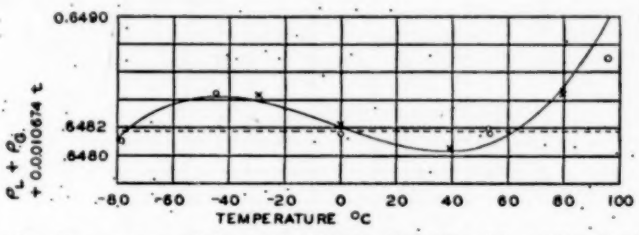

FIGURE 16.—*Comparison of observed with calculated densities of liquid 1,3-butadiene.*

⊙=ρ_l from sample 4c.
×=ρ_l from sample 4d.
----, ρ_l from equation 7.
——, ρ_l from equation 8.

The values calculated from equation 7 are represented by the dotted line in figure 16. The differences between the observed values and these calculated values are somewhat greater than the precision of the observed data, which are better represented by the continuous curve. This curve is calculated from the equation

$$\rho_l+\rho_s=0.64820-0.0010748t+1.6t^2 10^{-8}+1.5t^3 10^{-9}, \qquad (8)$$

in which the notation is the same as in equation 7. The constant 0.64820 in this cubic equation corresponds to a liquid density of 0.64523 g/ml at 0° C. This is nearly the mean of the observations on the two samples at 0° C, and is believed to be correct within a few units in the fifth decimal place. As may be seen from figure 16, equation 8 is in agreement with the observed values within five units in the fifth decimal place in the temperature range −80° to +40° C. Below −60° C the uncertainty in the expansion of the picnometer is relatively large, and above +50° C the observations are less accurate, in consequence of which the data in that temperature range are not considered accurate beyond the fourth decimal place, and above 100° C beyond the third decimal place. Values calculated from equation 8 are given in table 6 (discussed in section VI).

(c) COMPARISON WITH OTHER DATA

The densities measured by other observers are compared with the values calculated from the present formulation in figure 17. Prevost's [21] value for the density near the boiling point is notably low. The low normal boiling point (−4.75° C) for his sample suggests the presence of lighter hydrocarbons as impurities, which would explain the low density. The data given in Landolt-Bornstein [22] appear to be smoothed and have been represented by a dotted curve. The present data are intermediate between those from Pennsylvania State College [23] and those by Dean and Legatski [24]. The latter observers heated the surface of their sample above the average tem-

perature of the sample. In consequence, the liquid was subjected to a pressure exceeding the saturation pressure, and at the higher temperatures, where the liquid is more compressible, the observed densities may be appreciably too high.

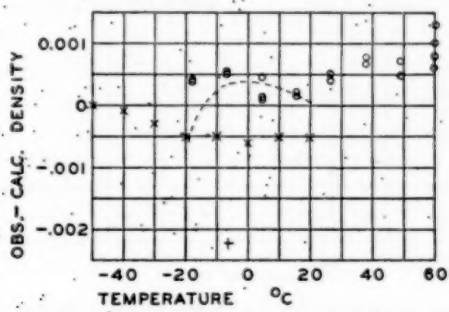

FIGURE 17.—*Comparison of values calculated from equation 16 with data of other observers.*

+=C. Prevost [19]
– – –=I. G. Farbenindustrie [20]
×=Pennsylvania State College [21]
O=M. R. Dean and T. W. Legatski [22]

4. RATE OF POLYMERIZATION

The observations taken during the measurement of liquid density at 79.6° C, together with the assumption that the volumes of 1,3-butadiene and its dimer are additive upon mixing, lead to a rate of dimerization for pure butadiene of 0.12 percent/hr at 79.6° C. This is in very good agreement with the value 0.11 percent at 82° C found by Robey, Wiese, and Morrell [25], who have made a thorough investigation of the rates of polymerization for pure butadiene and butadiene containing peroxides. It should be noted that in the present work the lower end of the column of butadiene was in contact with mercury, which has been reported to be a catalyst for polymerization [26].

5. CRITICAL CONSTANTS

Due to the rapid polymerization of the butadiene samples near the critical state, accurate direct measurement of critical constants was not possible. The procedure near the critical temperature was to start with the sample in the vapor phase and to compress it by steps, observing the pressure after each step and watching for the butadiene meniscus to appear. When sample 3b was thus treated at 152.0° C the meniscus suddenly appeared in the middle of the sample. At first it was very faint but soon became much more noticeable. Sudden expansion of the sample was accompanied by a transient opalescence, and as the sample was thus evaporated the meniscus took on the appearance of being considerably below the critical temperature. This effect is believed to be due to polymerization. The initial appearance only should be considered, on which basis 152° C is very near the critical temperature.

Sample 4b was observed at 149.0° C. The meniscus, very faint at first, appeared near the mercury at a volume considerably greater

than expected. Although "rain" and "fog" appeared during expansion (a phenomenon characteristic of the region near the critical), the volume at which the meniscus appeared indicated that the specific volume of the saturated vapor was considerably greater than the critical volume, and it was concluded that 149° C is below the critical temperature.

Sample 4a was observed at 157.36° C. The mass of the sample was unknown, hence only relative volumes were observed, but the pressure measurements are probably the best obtained near the critical state. These data are illustrated in figure 18, in which the upper portion

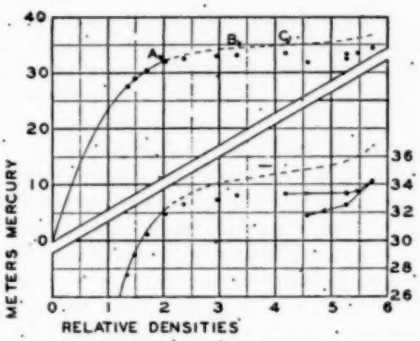

FIGURE 18.—*Isotherm at 157.36° C for sample No. 4a.*

Upper part—General view of whole isotherm.
Lower part—Magnified pressure scale near critical region.
Continuous curve represents calculated values from equation 13, with the assumption that the lowest observed point is unaffected by polymerization. Connected straight lines with arrows indicate chronological order of experiments.
A meniscus appears near mercury.
B meniscus disappears near middle of sample leaving opalescent band 1 or 2 mm wide.
C opalescent band disappears.

illustrates the whole isotherm and the lower portion illustrates the field covered by the observations with an enlarged pressure scale. After being compressed step by step until the highest density observed was reached, the sample was expanded. To avoid ambiguity, part of the points in figure 18 are connected with straight lines and the chronological order is indicated with arrows. The decrease in pressure indicated by the last two observations is obviously the result of polymerization. The continuous curve represents values calculated from the equation of state 6, which is believed to be valid up to about half the critical density, the relative volume scale being adjusted to fit the observed pressure at the lowest density. Assuming the value 0.245g ml^{-1} given in table 13 for the critical density, this adjustment places the critical density on the relative scale at approximately 3.7. The dotted curve was then drawn in to illustrate the path that would be expected had there been no polymerization. The course that this dotted curve should follow is uncertain for two reasons: (1) the rate of polymerization varies with the density, and (2) the data do not furnish an estimate of the effect on pressure of this rate except where pressures were observed with the densities varied in both directions. The short horizontal line in figure 18 represents a calculated pressure obtained from equations 4 and 5, together with the assumption that at the critical density, $(dp/dt)_v$ has a constant value above the critical temperature (152° C), an assumption

made by inference from the behavior of CO_2 and other substances with well-known properties.

The point A (fig. 18) represents the relative volume at which a liquid butadiene meniscus appeared near the mercury. At B this meniscus had approached the middle of the sample and vanished, leaving an opalescent band 1 or 2 mm wide. At C even this band had vanished without reaching the top of the sample. It may be inferred that the polymer at first condensed to form a solution relatively rich in polymers, the solution becoming diluted with more and more of the monomer until the critical temperature of the solution fell below 157° C, and the meniscus, and even the opalescent band, vanished. Thus the phenomenon just discussed, as well as the slope of the isotherm in figure 18, indicates that 157° C is above the critical temperature of pure butadiene. The discrepancy of about 1 atm between the isotherm as drawn and the pressure calculated from the vapor-pressure equation can be attributed to one or more of several causes, namely: (1) polymerization existing already at the first observation, (2) an underestimation of the rate of polymerization during experiments, and (3) a failure of the vapor-pressure equation to represent the facts.

The vapor pressure calculated from equation 4 for the critical temperature (152° C) is 32.42 meters of mercury. This value has been adopted for the critical pressure in producing a consistent set of tables, although the data in figure 18 suggest that the true critical pressure may be slightly lower.

The critical density is best determined from the mean of the data on the density of the liquid and the vapor. Two equations for the mean of these data are given. The linear equation 7 leads to 0.243 g/ml, whereas the cubic equation 8 leads to 0.245 g/ml. As the cubic equation represents the observed values of liquid densities better than the linear equation in the range −80° to +100° C. the larger value 0.245 g/ml is preferred.

The values P_c=32.42 meters of mercury, T_c=152+273.16° Kelvin, and P_c=0.245 g/ml give

$$\frac{p_c V_c}{RT_c}=0.270 \text{ or } \frac{RT_c}{P_c V_c}=3.70.$$

V. PURITY OF SAMPLES AND MELTING POINT OF PURE BUTADIENE

The melting curve of a material provides a sensitive method of determining the amount of impurity that is soluble in the liquid phase and insoluble in the solid phase. Such a curve is shown in figure 19 and was obtained as follows:

Starting with the calorimeter containing the sample (in the solid state) at the temperature A, measured amounts of electric energy were added and the temperature of the calorimeter observed after thermal equilibrium had been established following each heating. The resultant curve, A, E, B, C, gives the temperature of the calorimeter and contents as a function of the energy added. In order to obtain the more useful relation, fraction melted versus temperature,

the line *AD* is drawn. This is an extrapolation of the part of the curve representing the energy-temperature relation when the material is all solid. The horizontal distance *EF* from any observed point to the line *AD* represents the energy that has been used to melt part of the sample, as *F* represents the temperature energy condition which would have existed if no material had melted. Accordingly the distance *DB* represents the total heat of melting. Therefore, if the

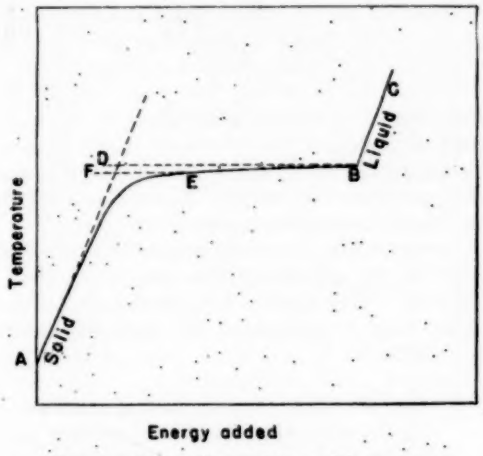

FIGURE 19.—*Illustrative melting curve.*

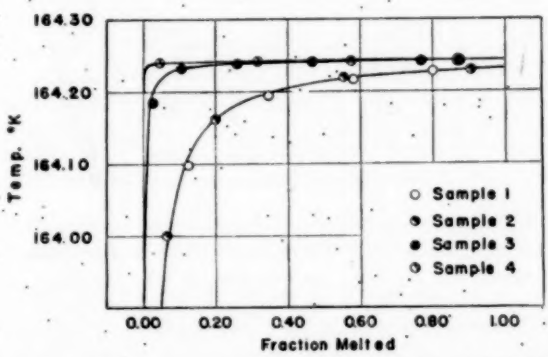

FIGURE 20.—*Melting curves for the four samples of 1,3-butadiene.*

heat of fusion is assumed to be constant, the fraction melted at point *E* is (*EF*/*DB*).

Figure 20 shows the melting curves of the four samples, giving the temperature as a function of the fraction melted. The data represented in these curves were used to obtain values for the purity of the samples and for the melting temperature of pure butadiene. If it is assumed that the impurity is soluble in the liquid and insoluble in the solid, then the curves shown in figure 20 will have approximately the form

$$T_m - T = (a/F), \tag{9}$$

where

T=temperature at a point on the curve
T_m=melting temperature of pure butadiene
F=fraction melted
a=constant=T_m-T (when $F=1$).

This equation is derived from the formula relating the depression of the freezing point of a material with the mole fraction of impurity

$$x=\frac{L_f(T_m-T_f)}{RT_m^2}, \tag{10}$$

where

x=the mole fraction of impurity
L_f=the heat of fusion
T_m=the freezing (melting) temperature of the pure substance
T_f=the temperature at which the liquid containing x mole fraction of impurity starts freezing.

The constants in equation 9 were determined for the melting curve of sample 3, figure 20, by selecting a value of T_m that gave the most constant values for a. The results are shown in table 11. The data on this sample were best represented by equation 9 when 164.244° K was chosen as the value of T_m.

TABLE 11.— *Data from the melt of sample 3*

T_m-T	F	$a=F(T_m-T)$
° K		
0.059	0.027	0.00159
.011	.107	.00118
.005	.269	.00130
.0021	.466	.00098
.0017	.768	.00131
.0013	.872	.00113
	a (mean)	0.00125

The amount of liquid soluble, solid insoluble impurity may now be computed from equation 10. It is seen that the constant a in equation 9 is the same as T_m-T_f in equation 10. Using T_m=164.244° K, $T_m-T_f=a$=0.00125° K, L_f=7980 int. j mole^{-1}, the mole fraction impurity, x, in sample 3 is 0.000045, or 45 moles per million. Calculations of the amounts of impurity in samples 1 and 2 gave 552 moles per million and 516 moles per million, respectively. The treatment of the melting data of samples 1 and 2 yielded a value for T_m 0.006 degrees Kelvin higher than that obtained from the melt of sample 1. These two samples were so nearly alike that the melting data on both samples were well represented by a single curve.

The curve for sample 4, figure 20, shows that this was the purest sample obtained. In fact, the melting curve is so flat that only the point at 4.7 percent melted exhibited any measurable depression of the melting point, and even here it amounted to only 0.001 degree Kelvin. The temperature obtained for the other points on the melting curve was 164.242° K. The liquid soluble, solid insoluble impurity in sample 4 was calculated to be 2 moles per million.

The difference between the values of the melting point of pure butadiene, 164.244 degree Kelvin, obtained from the data on sample 3, and 164.242 degree Kelvin from the data on sample 4, may have been caused by small errors in the calibrations of the resistance bridges used. Two different Mueller bridges were used for these measurements. This difference of 0.002 degree Kelvin is considerably smaller than the absolute accuracy of temperature measurements, as platinum resistance thermometers, calibrated in the same way, can deviate from each other by as much as 0.01 degree centigrade at −110° C. The most probable value of the melting point of pure butadiene, as determined from the data on samples 3 and 4, is 164.243° ±0.010° K or −108.917° ±0.010° C.

The vapor-pressure measurements at the ice point and above indicated the presence of an impurity that did not appear to affect the melting curves. The vapor pressures of samples 1, 2, and 3 were found to depend somewhat on the fraction condensed, being higher when 95 to 98 percent was condensed than when 75 percent or less was condensed. This indicated the presence of an impurity that was more volatile than butadiene. With sample 3, which was relatively pure according to the melting curve test, the increase in vapor pressure upon condensing most of the sample amounted to about 6 mm at 0° C. The impurity of 45 parts per million, indicated by the melting curve, was not great enough to have caused this increase in vapor pressure. The more elaborate procedure in preparing sample 4 was carried out primarily for the purpose of improving the vapor-pressure data. When 96 percent of this sample was condensed at 0° C the pressure was only 0.3 mm Hg higher than when 40 percent was condensed.

In figure 14 the continuous curve represents values calculated for a hypothetical liquid having a vapor pressure of 899 mm with 0.001 mole fraction of an ideal-gas impurity that is soluble in the hypothetical liquid to the extent of 5.5×10^{-7} moles/cm^3 of liquid for a partial pressure of 1 mm. These assumptions, together with the mass of the sample (0.0275 g), lead to the equation

$$P=899+\frac{1{,}000}{3.04v+45.4}, \qquad (11)$$

where P is the total pressure in millimeters of mercury and v is the volume occupied per gram of sample. Although the curve represents the data for sample 3e very well, the spread in the data permits some variation in the assumed values; moreover, the impurity may not form an ideal solution as assumed.

No specific estimate of the impurity in sample 4b can be made because the spread of the data permits a considerable variation in the value assumed for the solubility of the impurity with a corresponding variation in the estimated amount present. It is evident, however, that the amount of more volatile impurity in sample 4b was considerably less than that in sample 3e.

VI. DERIVED PROPERTIES AND FORMULATED TABLES OF THE THERMODYNAMIC PROPERTIES OF 1,3-BUTADIENE

1. ENTROPY AND ENTHALPY OF SOLID AND LIQUID 1,3-BUTADIENE FROM 15° TO 300° K

The tables of specific heat, together with the value of the heat of fusion, were used to calculate the entropy and enthalpy of solid and liquid butadiene. It was first necessary to obtain values of $C_{sat.}$ between 0° and 15° K, the latter temperature being the lower limit of the observed data. This was accomplished by using the equation

$$C_{sat.}=0.7188D\left(\frac{134}{T}\right), \tag{12}$$

where $C_{sat.}$ is the specific heat in int. j $g^{-1}°K^{-1}$ and $D(\ )$ is the Debye function [11]. This function was selected to represent the data from 15° to 30° K, inclusive. The agreement between the observed values of $C_{sat.}$ and those calculated from equation 12 was not entirely satisfactory, but the function was considered adequate for the purpose of extrapolating the specific heat function to 0° K. The increases in entropy and enthalpy between 0° and 15° K are small compared with the total changes of these quantities between 15° and 300° K, so an error in the function used between 0° and 15° K would have little effect on the values obtained at 300° K.

The calculated values of entropy and enthalpy of the solid and liquid are given at 5-degree intervals in table 12. As different sets of measurements of $C_{sat.}$ were available it was necessary to make a selection in order to use the most reliable values for the calculation of entropy and enthalpy. From 15° to 55° K, inclusive, the data on sample 1 were used, as no other data were available in this temperature range. From 60° K to the triple point (164.24° K) the data of sample 4 were used because this was the purest sample measured. Above the triple point there was no choice between the data obtained for the different samples so the values of $C_{sat.}$ were simply averaged. Column 2 of table 12 gives these values of $C_{sat.}$

TABLE 12.—*Entropy and enthalpy of solid and liquid 1, 3-butadiene*

T	$C_{sat.}$	$S_{sat.}$	$\int_0^T C_{sat.}dT$	$\int_0^T V_{sat.}\frac{dP}{dT}dT$	$H_{sat.}-E_0^s$
			SOLID		
°K	*Int. j g*$^{-1}$°K^{-1}	*Int. j g*$^{-1}$°K^{-1}	*Int. j g*$^{-1}$	*Int. j g*$^{-1}$	*Int. j g*$^{-1}$
0	0	0	0		0
5	.00291	.0010	.0036		.0036
10	.02322	.0078	.0581		.0581
15	.0747	.0257	.289		.289
20	.1492	.0568	.844		.844
25	.2341	.0991	1.798		1.798
30	.3193	.1493	3.183		3.183
35	.4012	.2047	4.985		4.985
40	.4762	.2633	7.182		7.182
45	.5447	.3234	9.737		9.737
50	.6081	.3841	12.621		12.621
55	.6654	.4448	15.807		15.807
60	.7136	.5050	19.258		19.258
65	.7532	.5637	22.929		22.929
70	.7964	.6210	26.803		26.803
75	.8393	.6775	30.892		30.892
80	.8800	.7329	35.191		35.191
85	.9202	.7875	39.692		39.692
90	.9585	.8412	44.389		44.389
95	.9954	.8940	49.274		49.274
100	1.0302	.9460	54.339		54.339
105	1.0636	.9970	59.574		59.574
110	1.0963	1.0473	64.973		64.973
115	1.1312	1.0968	70.541		70.541
120	1.1685	1.1457	76.289		76.289
125	1.2071	1.1942	82.228		82.228
130	1.2481	1.2423	88.364		88.364
135	1.2926	1.2902	94.715		94.715
140	1.3412	1.3381	101.297		101.297
145	1.3942	1.3861	108.134		108.134
150	1.4521	1.4343	115.246		115.246
155	1.5186	1.4830	122.669		122.669
160	1.5968	1.5324	130.453		130.453
164.24	1.6742	1.5752	137.384		137.384
			LIQUID		
164.24	1.9110	2.4739	284.98	•0	284.98
165	1.911	2.4827	286.44		286.44
170	1.912	2.5398	295.99		295.99
175	1.915	2.5952	305.56		305.56
180	1.918	2.6492	315.14		315.14
185	1.922	2.7018	324.74		324.74
190	1.928	2.7531	334.37		334.37
195	1.934	2.8033	344.02		344.02
200	1.941	2.8524	353.71		353.71
205	1.950	2.9004	363.43	.00	363.43
210	1.961	2.9475	373.21	.01	373.22
215	1.973	2.9938	383.05	.01	383.06
220	1.983	3.0393	392.93	.01	392.94
225	1.997	3.0840	402.88	.02	402.90
230	2.010	3.1280	412.90	.02	412.92
235	2.025	3.1714	422.99	.03	423.02
240	2.039	3.2142	433.15	.04	433.19
245	2.055	3.2564	443.38	.05	443.43
250	2.073	3.2981	453.70	.07	453.77
255	2.089	3.3393	464.11	.08	464.19
260	2.107	3.3800	474.60	.10	474.70
265	2.126	3.4203	485.18	.13	485.31
270	2.147	3.4603	495.86	.16	496.02
275	2.170	3.4999	506.65	.19	506.84
280	2.193	3.5392	517.56	.23	517.79
285	2.218	3.5782	528.58	.28	528.86
290	2.242	3.6170	539.74	.33	540.07
295	2.269	3.6556	551.02	.39	551.41
298.16	*2.286*	*3.6799*	*558.22*	.44	*558.66*
300	2.296	3.6940	562.44	.46	562.90

• Column 5, zero from 0°K to 205°K.

The entropy, S, was calculated by integrating $(C_{sat.}/T)\,dT$ by means of Simpson's rule, and the results were checked by a graphical integration. The increase in enthalpy referred to the solid at absolute zero, $H-E_0'$, is

$$H-E_0'=\int_0^T C_{sat.}\,dT+\int_0^T v\frac{dp}{dT}dT, \tag{13}$$

where v is the specific volume of the liquid and p is the vapor pressure. The integrals were evaluated by Simpson's rule. Values of dp/dT were obtained from equation 5 and values of v from table 13. The calculated values of H were checked by performing the integration $\int_0^T SdT$ and comparing the values so obtained with the quantity $(TS-\mathrm{H}+E_0')$, which should equal $\int_0^T SdT$. This provides a check on the internal consistency of the calculations.

TABLE 13.— *Thermodynamic properties of 1,3-butadiene saturated vapor and liquid*

Temperature	log p_{mm}	Pressure	Liquid			Vapor		
			Volume	Density	pv/RT	Volume	Density	pv/RT
°C		mm Hg	ml/g	g/ml		ml/g	g/liter	
−108.92	1.7157	0.520	1.3092	0.7638	0	364,200	0.00275	0.998
−100	0.1638	1.46	1.3258	.7545	0	136,890	.0073	.998
−90	.6064	4.04	1.3440	.7440	0	52,230	.0192	.998
−80	.9960	9.91	1.3633	.7335	0	22,450	.0445	.998
−70	1.3410	21.93	1.3833	.7229	.0001	10,660	.0938	.997
−60	1.6482	44.49	1.4041	.7122	.0003	5,503	.1817	.996
−50	1.92334	83.8	1.4257	.70140	.0005	3,050	.3279	.993
−40	2.17098	148.2	1.4483	.69048	.0008	1,795	.5572	.989
−30	2.39492	248.3	1.4718	.67945	.0013	1,112	.8993	.985
−20	2.59836	396.6	1.4964	.66826	.0020	719.8	1.3892	.979
−10	2.78399	608.1	1.5224	.65685	.0030	483.8	2.0668	.969
0	2.95410	899.7	1.5499	.64522	.0044	335.9	2.977	.956
10	3.11060	1,290	1.5790	.63331	.0062	239.8	4.171	.943
20	3.25510	1,799	1.6102	.62106	.0086	175.3	5.706	.930
25	3.32332	2,105	1.6265	.61480	.0100	151.0	6.621	.923
30	3.38906	2,449	1.6436	.60842	.0115	130.8	7.647	.916
40	3.51363	3,263	1.6797	.59533	.0152	99.3	10.069	.901
50	3.62984	4,264	1.7191	.58169	.0197	76.6	13.060	.876
60	3.73862	5,478	1.7624	.5674	.0251	59.8	16.73	.852
70	3.84074	6,930	1.8104	.5524	.0317	47.2	21.20	.829
80	3.93692	8,648	1.8643	.5364	.0396	37.5	26.66	.797
90	4.02780	10,661	1.9259	.5192	.0490	30.0	33.33	.756
100	4.11397	13,001	1.9975	.5006	.0604	24.1	41.54	.725
110	4.19604	15,705	2.0833	.480	.0741	19.3	51.82	.666
120	4.27459	18,820	2.1909	.456	.0910	15.4	65.08	.638
130	4.35029	22,400	2.3351	.428	.113	12.0	83.17	.579
140	4.42389	26,540	2.5652	.390	.143	9.0	111.41	.500
150	4.49639	31,360						
152	4.51087	32,420	4.08	0.245	0.270	4.08	245	0.270

TABLE 13.—*Thermodynamic properties of 1, 3-butadiene saturated vapor and liquid*—Continued

Temperature	Enthalpy			Entropy			C_{sat}	
	$H-E_0^\circ$ liquid	Evaporation	$H-E_0^\circ$ vapor	Liquid	Evaporation	Vapor	Liquid	Vapor
°C	*Int. j/g*	*Int. j/g*	*Int. j/g*	*Int. j/g° C*	*Int. j/g° C*	*Int. j/g° C*	*Int. j/g° C*	*Int. j/g° C*
−108.92	(284.98)	509.7	794.87	(2.4739)	3.1035	5.5782	(1.911)	−2.18
−100	(302.05)	501.2	803.30	(2.5749)	2.8944	5.4695	(1.914)	−1.934
−90	321.22	491.8	813.06	2.6826	2.6853	5.3679	1.922	−1.689
−80	340.50	482.7	823.18	2.7850	2.4989	5.2839	1.933	−1.471
−70	359.90	473.7	833.63	2.8829	2.3318	5.2147	1.947	−1.271
−60	379.45	464.9	844.38	2.9769	2.1811	5.1580	1.965	−1.090
−50	399.24	456.2	855.45	3.0675	2.0443	5.1118	1.990	−.926
−40	419.29	447.5	866.78	3.1555	1.9192	5.0748	2.019	−.776
−30	439.63	438.7	878.33	3.2408	1.8041	5.0449	2.048	−.641
−20	460.33	429.7	890.08	3.3241	1.6975	5.0216	2.083	−.518
−10	481.40	420.6	901.98	3.4055	1.5982	5.0037	2.122	−.407
0	502.88	411.1	913.99	3.4854	1.5050	4.9904	2.163	−.308
10	524.80	401.2	926.04	3.5640	1.4170	4.9810	2.207	−.220
20	547.24	390.9	938.11	3.6414	1.3333	4.9747	2.258	−.141
25	558.66	385.5	944.12	3.6798	1.2928	4.9726	2.286	−.108
30	570.23	379.9	950.11	3.7180	1.2531	4.9711	2.313	−.073
40	593.82	368.2	962.01	3.7940	1.1757	4.9697	2.367	−.014
50	618.01	355.7	973.72	3.8694	1.1007	4.9701	2.427	+.033
60	642.87	342.3	985.17	3.9442	1.0274	4.9716	2.489	+.070
70	668.41	327.8	996.25	4.0187	.9554	4.9741	2.551	+.093
80	694.67	312.2	1006.84	4.0930	.8839	4.9769	2.617	+.099
90	721.71	295.1	1016.77	4.1671	.8125	4.9796	2.688	+.084
100	749.59	276.2	1025.79	4.2411	.7402	4.9813	2.769	.038
110	778.5	255	1033.5	4.316	.665	4.981	2.87	−.06
120	808.9	230	1039.2	4.392	.586	4.978	3.02	−.24
130	841.4	200	1041.6	4.471	.496	4.967	3.34	−.63
140	878.8	158	1036.9	4.558	.383	4.941		
150								
152	(978)	0	(978)	(4.79)	0	(4.79)		

2. THERMODYNAMIC PROPERTIES OF LIQUID AND VAPOR 1,3-BUTADIENE FROM −109° TO +150° C

The experimental data previously described, together with data on the specific heat of the vapor [4], have been used as a basis for the formulation of a consistent set of values for the thermodynamic properties given in tables 13 and 14. The values given in these tables were calculated from the following empirical equations: vapor pressure (eq 4), vapor density (eq 6), liquid density (eq 8), and

$$C_p^\circ = 1.3660 + 0.00445t - 1.88 \times 10^{-5}(t-30)^3, \qquad (14)$$

where C_p° is the specific heat of the vapor at zero pressure in international joules per gram degree centigrade, and t is in degrees centigrade.

TABLE 14.—*Thermodynamic properties of 1,3-butadiene superheated vapor*

Temperature	C_p°	$C_{p\ sat.}-C_p^\circ$	$H^\circ-E_0^\circ$	$H^\circ-H_{sat.}$	S°	$S^\circ-S_{sat.}$	$H^\circ-H_{1\ atm}$	$S^\circ-S_{1\ atm}$	$(pV/RT)_{1\ atm}$	$(1/V)_{1\ atm}$
°C	*Int. j/g °C*	*Int. j/g °C*	*Int. j/g °C*	*Int. j/g °C*	*Int. j/g °C*	*Int. j/g °C*	*Int. j/g*	*Int. j/g °C*		*g/liter*
−108.92	0.932	0.0000	794.9	0.00	4.4580	−1.1201	.....	.....	.....	.....
−100	.962	.0001	803.31	.01	4.5081	−0.9614	.....	.....	.....	.....
−90	.998	.0003	813.10	.04	4.5632	−.8047	.....	.....	.....	.....
−80	1.035	.0006	823.27	.09	4.6172	−.6667	.....	.....	.....	.....
−70	1.073	.0011	833.81	.18	4.6704	−.5443	.....	.....	.....	.....
−60	1.113	.0023	844.74	.36	4.7229	−.4351	.....	.....	.....	.....
−50	1.153	.0040	856.07	.62	4.7748	−.3370	.....	.....	.....	.....
−40	1.194	.0067	867.81	1.03	4.8263	−.2483	.....	.....	.....	.....
−30	1.237	.0106	879.96	1.63	4.8773	−.1676	.....	.....	.....	.....
−20	1.279	.0158	892.54	2.46	4.9280	−.0936	.....	.....	.....	.....
−10	1.323	.0229	905.55	3.57	4.9784	−.0253	.....	.....	.....	.....
0	1.366	.032	919.00	5.01	5.0286	+.0382	4.21	0.0102	0.9660	2.496
10	1.410	.044	932.88	6.84	5.0785	.0975	3.95	.0093	.9696	2.400
20	1.455	.059	947.21	9.10	5.1282	.1535	3.72	.0085	.9726	2.311
25	1.477	.068	954.54	10.42	5.1530	+.1804	3.60	.0081	.9740	2.268
30	1.499	.078	961.98	11.87	5.1777	+.2066	3.48	.0078	.9753	2.228
40	1.544	.101	977.20	15.19	5.2271	.2574	3.30	.0071	.9777	2.152
50	1.588	.130	992.86	19.14	5.2764	.3063	3.11	.0066	.9798	2.081
60	1.632	.167	1008.97	23.80	5.3254	+.3538	2.94	.0060	.9817	2.014
70	1.676	.214	1025.51	29.26	5.3744	.4003	2.78	.0056	.9833	1.952
80	1.720	.275	1042.49	35.65	5.4231	.4462	2.64	.0051	.9848	1.894
90	1.762	.356	1059.90	43.13	5.4718	.4922	2.50	.0048	.9861	1.840
100	1.805	.470	1077.74	51.95	5.5202	.5389	2.38	.0044	.9873	1.789
110	1.846	.641	1095.99	62.51	5.5684	+.5874	2.26	.0041	.9884	1.740
120	1.886	.925	1114.65	75.42	5.6166	.6391	2.15	.0038	.9893	1.694
130	1.926	1.508	1133.71	92.10	5.6644	.6973	2.04	.0036	.9902	1.651
140	1.964	.....	1153.16	116.29	5.7121	.7706	1.95	.0033	.9910	1.610
150	2.001	.....	1172.99	.....	5.7594	.....	1.85	.0031	.9917	1.571
200	.....	.....	.....	.....	.....	.....	*1.5	*.002	*.994	*1.400
300	.....	.....	.....	.....	.....	.....	*1.0	*.001	*.997	*1.152
400	.....	.....	.....	.....	.....	.....	*0.7	*.001	*.999	*0.980
500	.....	.....	.....	.....	.....	.....	*.5	*.000	*.999	*.852
600	.....	.....	.....	.....	.....	.....	*.3	*.000	*1.000	*.755

*These values are obtained by extrapolation of the equation of state beyond the temperature range in which there are experimental data.

Equation 14 is in reasonable agreement with results recently reported [28, 29] and represents the results reported by Scott and Mellors [4] as follows:

Temperature	Specific heat, C_p° int. J/g °C	
	Reported	Calculated, eq 14
°C		
−35	1.217	1.215
0	1.366	1.366
40	1.549	1.544
80	1.721	1.720

Values of the tabulated quantities $H^\circ - E_0^*$ and S° for the vapor were calculated from equations obtained by substituting the definitions $dH = C_p dT$ and $dS = (C_p/T)dT$ in equation 14 and performing the integration. These equations are

$$H^\circ - E_0^* = 919.00 + 1.3660t + 0.002225t^2 - 0.47 \times 10^{-8} (t-30)^4 \quad (15)$$

and

$$S^\circ = 0.93615 + 1.55252 \log T - 0.0007335T + 8.549(10)^{-6}T^2 - 6.2667(10)^{-9}T^3, \quad (16)$$

where E_0^* is the internal energy of the solid at absolute zero, H° in international joules per gram, and S° in international joules per gram degree centigrade represent the ideal gas state at 1-atm pressure, t is in degrees centigrade, and $T = t + 273.16$. The constants of integration were chosen to make the calculated values for the liquid agree as closely as possible with the values in table 12.

The tabulated values for the specific heat of the liquid were calculated from the specific heat of the vapor with the aid of the following exact thermodynamic relations:

$$(C_s)_g = (C_s)_l + T\frac{d(L/T)}{dT} \quad (17)$$

$$(C_p)_{sat.} = (C_s)_g + T\left(\frac{\partial V}{\partial T}\right)_p \left(\frac{dp}{dT}\right)_{sat.} \quad (18)$$

$$C_v = C_p - T\left[\left(\frac{\partial V}{\partial T}\right)_p \left(\frac{\partial p}{\partial T}\right)_v\right] \quad (19)$$

$$C_v^* = C_v - \int_\infty^V T\left(\frac{\partial^2 p}{\partial T^2}\right)_V dV \quad (20)$$

$$C_p^* = C_v^* + R, \quad (21)$$

where $(C_s)_g$ and $(C_s)_l$ are the specific heats of saturated vapor and liquid, respectively, C_p and C_v are the specific heats of the vapor at constant pressure and volume, respectively, and C_p^* and C_v^* are the corresponding values at zero pressure. The procedure just described may appear to be reversed from the normal, as the experimental values of specific heat of the liquid are the more accurate and had already been tabulated in table 12. These values did not extend above

20° C, however, and at least a tentative formulation for the vapor would have been necessary to obtain values for the liquid above that temperature. Moreover, formulation for the liquid is necessarily limited to temperatures below the critical, whereas the limitations for the procedure used depend only upon the accuracy with which the chosen formula can be extrapolated.

The tabulated valus of L and L/T were calculated from the Clapeyron equation written in the dimensionless form

$$\frac{L}{RT}=\left[\left(\frac{pV}{RT}\right)_v-\left(\frac{pV}{RT}\right)_l\right]\left(T\frac{d\ ln\ p}{dT}\right), \tag{22}$$

values of pV/RT from table 13 being used. The quantity $T(d\ ln\ p)/dT$ was calculated from equation 5. Values of the quantity $d(L/T)/dT$ were calculated from the values of L/T by the Rutledge method. The various other derivatives were obtained through differentiation of equation 8.

The tabulated values of enthalpy and entropy were calculated from the equations

$$\frac{H^0-H}{RT}=\frac{14.1747\,(T_c/T)^2 10^{-0.045(Tc/T)^2}+68.4(1-10^{-0.045(Tc/T)^2})-148}{V}-\frac{36(T_c/T)^4+7}{2V^2} \tag{23}$$

$$\frac{S^0-S}{R}=\ln\frac{1.5171T}{V}+\frac{14.1747\,(T_c/T)^2 10^{-0.045(Tc/T)^2}-68.4(1-10^{-0.045(Tc/T)^2})+1.48}{V}-\frac{18(T_c/T)^4-3.5}{2V^2}, \tag{24}$$

where V is in milliliters per gram, H° and S° are given by equations 14 and 15, and R is 0.15369 int. j/g°C. Equations 23 and 24 were derived from equation 8. The values in table 13 are in excellent agreement with values interpolated from table 12. Except for the values shown in parentheses in table 13, which were obtained from table 12, the largest differences are 0.05 int. j/g in the enthalpy at −70° C, 0.0002 int. j/g°C in the entropy at several temperatures, and 0.002 int. j/g°C in the specific heat of the saturated liquid.

In order to retain accuracy on differences, most of the items in table 13 and some in table 14 are given to more places than the accuracy of the individual values would warrant. Although in some cases the values in the tables may be in error by a somewhat greater amount, the following are considered reasonable tolerances:

1. Vapor pressures: 0.1 mm or slightly better at low temperatures, 0.05 to 0.1 percent for −20° to +110° C, and about 1 percent at the critical temperature.
2. Liquid densities: 0.00005 g/ml near zero,
   0.0001 between −30 and +30° C,
   0.001 below 100° C.
3. Vapor densities: 0.1 or 0.2 percent,
   1 or 2 percent near the critical temperature.

4. Enthalpy of evaporation: Same as vapor densities.
5. Specific heats: Liquid below 20° C about 0.1 percent, the uncertainty increasing at higher temperatures, becoming very large near the critical temperature: vapor between −35° and +80° C about 0.5 percent, the uncertainty increasing greatly as the critical temperature is approached.
6. Enthalpy and entropy differences: Same as for specific heats.

The assistance of L. A. Matheson, of the Research Laboratory, Dow Chemical Co., in providing pure 1,3-butadiene for this investigation is gratefully acknowledged. The authors express their thanks to Patricia Husbands, who performed a large part of the calculations involved in determining the constants of the equations in this formulation and in preparing tables 13 and 14.

VII. REFERENCES

[1] R. B. Scott, R. D. Rands, Jr., F. G. Brickwedde, Report to the Office of the Rubber Director (July 23, 1943).
[2] C. H. Meyers, R. B. Scott, F. G. Brickwedde, R. D. Rands, Jr., Report to the Office of the Rubber Director (June 30, 1943).
[3] L. A. Wood and C. F. Higgins, NBS Letter Circular LC710 (1942).
[4] Russell B. Scott and Jane W. Mellors, J. Research NBS **34,** 243 (1945) RP1640.
[5] Martin Shepherd, BS J. Research **12,** 185 (1934) RP643.
[6] J. C. Southard and F. G. Brickwedde, J. Am. Chem. Soc. **55,** 4378 (1933).
[7] J. C. Southard and R. T. Milner, J. Am. Chem. Soc. **55,** 4384 (1933).
[8] Harold J. Hoge and F. G. Brickwedde, J. Research NBS **22,** 351 (1939) RP1188; **22,** 217 (1942) RP1454.
[9] N. S. Osborne, BS J. Research **4,** 609 (1930) RP168.
[10] N. S. Osborne, H. F. Stimson, T. S. Sligh, and C. S. Cragoe, BS Sci. Pap. **20,** 65 (1925) S501.
[11] J. A. Beattie, J. Math. Phys. **6,** 1 (1926).
[12] N. S. Osborne, H. F. Stimson, and D. C. Ginnings, NBS J. Research **23,** 197 (1939) RP1228.
[13] C. H. Meyers, J. Am. Chem. Soc. **45,** 2135 (1923).
[14] C. H. Meyers and R. S. Jessup, BS J. Research **6,** 1061 (1931) RP324.
[15] G. K. Burgess, BS J. Research **1,** 635 (1928) RP22.
[16] Wm. E. Vaughan, J. Am. Chem. Soc. **54,** 3863 (1932).
[17] G. B. Heisig, J. Am. Chem. Soc. **55,** 2304 (1933).
[18] G. Moor and E. K. Kanep, Trans. Experimental Research Lab., Chemgas [III] Leningrad (1936).
[19] A. B. Lamb and E. E. Roper, J. Am. Chem. Soc. **62,** 806 (1940).
[20] C. S. Cragoe, NBS Letter Circular LC 736 (1943).
[21] C. Prevost, Comp. rend. **186,** 1209 (1928).
[22] I. G. Farbenindustrie Ludwigshafen (1929) Landolt-Bornstein Physical Chemical Tables, 5th edition, 2d supplement, part I, page 207.
[23] Some physical constants of seven four-carbon-atom hydrocarbons and neopentane, Petroleum Refining Laboratory, Pennsylvania State College, Thesis (1941).
[24] M. R. Dean and T. W. Legatski, Ind. Eng. Chem. **36,** 7 (1944).
[25] R. F. Robey, H. K. Wiese, and C. E. Morrell, Ind. Eng. Chem. **36,** 3 (1944).
[26] The storage of 1,3-butadiene, Research Bul. 7.381–B, Mellon Inst. Ind. Research.
[27] C. H. Meyers, BS J. Research **11,** 691 (1933) RP616.
[28] J. G. Aston, G. W. Moessen, H. C. Hardy, and G. J. Szasz, J. Chem. Phys. **12,** 458 (1944).
[29] D. H. Templeton, D. D. Davies, and W. A. Felsing, J. Am. Chem. Soc. **66,** 2033 (1944).

WASHINGTON, April 30, 1945.

U. S. Department of Commerce National Bureau of Standards

RESEARCH PAPER RP1662

Part of Journal of Research of the National Bureau of Standards, Volume 35, July 1945

EFFECTS OF SOME OXIDE ADDITIONS ON THE THERMAL LENGTH CHANGES OF ZIRCONIA

By R. F. Geller and Paul J. Yavorsky

ABSTRACT

The oxides of cerium, yttrium, silicon, magnesium, and calcium were added in various proportions to zirconia of 99-percent purity, and the effects of these additions, combined with preheating at various temperatures ranging from 1,450° to 1,950° C, on thermal length changes of the zirconia during heating and cooling between room temperature and a maximum of 1,700° C were observed. The results are compared with similar observations on zirconia of 96-, of 98-, and of 99-percent purity without oxide additions.

The results show that the irregular thermal length changes accompanying phase transformations in zirconia may be prevented by changing the crystal to the stable cubic form. This was accomplished by (a) 11.5- and 15-percent additions of Y_2O_3 and heating at 1,700° C or higher; (b) 8- and 15-percent additions of MgO and heating at 1,550° C or higher, but only for the range from room temperature to 1,200° C; and (c) 5-, 6-, 8-, and 15-percent additions of CaO and heating at 1,550° C or higher, but additions of more than 6 percent caused the specimens to be very porous and proportionately weak. In all cases, however, the expansion during heating and contraction during cooling was relatively high. The coefficients of linear thermal expansion of the specimens that were all, or nearly all, cubic ranged from 8.8 to 11.8×10^{-6}. Also, zirconia has a low thermal conductivity relative to such materials of high thermal expansion as alumina, magnesia, and beryllia (unpublished data). Consequently, a high resistance to thermal shock cannot be expected of the stabilized product, even though it is not subject to the structural disintegration characteristic of the commercially pure material.

CONTENTS

	Page
I. Introduction	87
II. Materials	89
III. Apparatus and test methods	90
IV. Results	93
1. Zirconia	93
2. Zirconia with additions	97
(a) Effect of CeO_2	97
(b) Effect of Y_2O_3	97
(c) Effect of SiO_2	99
(d) Effect of MgO	101
(e) Effect of CaO	105
V. Discussion and conclusions	107

I. INTRODUCTION

The large number of articles in the literature on the general subject of zirconia and its possibilities and limitations, as shown by

Kreidl's excellent bibliography,[1] evidence the interest in this material. As early as 1916, articles appeared in England[2] and in Germany[3] describing ZrO_2 and its uses in refractory ware. Zirconia has a number of excellent qualities as a ceramic body ingredient. Principally, these are its hardness, chemical stability at both ordinary and elevated temperatures, and the wide temperature range over which it may be used.[4]

Most of the earlier investigations were concerned with studies of oxide additions that would promote reduction in porosity and increase the mechanical strength of ZrO_2 shapes. It was found that ware made of zirconia would undergo rapid weakening and structural disintegration in service, even though the initial strength was quite satisfactory. It had been made evident during the course of another investigation[5] that refractory shapes of ZrO_2 have a discouragingly short life in service. Some thermal-expansion curves for ZrO_2 had been published,[6] but these did not contain information upon which an explanation for the structural weakening could be based. It is known from the literature[7] that zirconia has several crystalline forms, of which the monoclinic is stable at ordinary temperatures and occurs as the mineral baddeleyite. Optical data for the various forms are incomplete, as shown by the following summary:

Form	Birefringence	Mean index	Interference figure	Unit cell size, in angstroms
Monoclinic (baddeleyite).	High	2.15	Biaxial (−)	$a=5.21$, $b=5.26$, $c=5.37$, $\beta=80°32'$
Tetragonal	Low	>2.15	Uniaxial (−)	$a=5.07$, $c=5.16$
Trigonal	Medium (?)	?	Uniaxial (+)	$a=3.598$, $c=5.875$

That changes from one form to another, specifically the monoclinic ⇄ tetragonal inversion, might be accompanied by destructive volume changes was indicated by Ruff and Ebert,[8] who published considerable data on ZrO_2 with oxide additions. They reported a fourth, or cubic, crystalline modification, which is actually a solid solution of some oxide in zirconia. The effect of this solid solution is a distortion of the tetragonal lattice to a "stabilized" cubic crystal, which is not subject to further inversions. Ruff and Ebert[8] demonstrated, by examinations with a heated X-ray camera, that the monoclinic-tetragonal inversion takes place somewhere between 800° and 1,200° C in relatively pure zirconia, and that CaO, MgO, Sc_2O_3, Y_2O_3, and CeO_2 additions brought about the formation of the stable cubic form. They did not, however, present thermal-expansion curves to prove that this stabilized zirconia was free from undesirable volume changes, but ample evidence[9] has been published that unstabilized

[1] Norbert J. Kreidl, J. Am. Ceram. Soc. **25**, 129 (1942).
[2] J. A. Audley, Trans. Ceram. Soc. (England) **16**, 121 (1916).
[3] O. Ruff and G. Lauschke, Z. anorg. Chem. **97**, 73 (1916).
[4] D. Kirby, Metallurgia **30**, 65 (1944), states that ZrO_2 can be used up to 2, 400° C.
[5] R. F. Geller, J. Research NBS **27**, 555 (1941) RP1443.
[6] G. E. Merritt, Trans. Am. Electrochem. Soc. **50**, 165 (1926). F. H. Norton; J. Am. Ceram. Soc. **8**, 799 (1925).
[7] Willi M. Cohn and S. Tolksdorf, Z. physik. Chem. [B] **8**, 331 (1930); Willi M. Cohn, Trans. Electrochem. Soc. **68**, 65 (1935).
[8] Otto Ruff and Fritz Ebert, Z. anorg. Chem. **180**, 19 (1929); see also U. S. Patent 1,969,099.
[9] Willi M. Cohn, Keram. Rundschau **38**, 721, 753, 777, 781, (1930); R. F. Mather, J. Am. Ceram. Soc. **25**, 93 (1942).

ZrO_2 is subject to erratic length changes between room temperature and 1,400° C.

Because of the incomplete evidence on the thermal length changes of zirconia and the favorable properties of the oxide, a study was undertaken to determine the oxide additions and heat treatments that would most efficiently form the cubic zirconia, and thereby presumably overcome the erratic thermal length changes. The results of the study, covering the effect of CeO_2, Y_2O_3, SiO_2, MgO, and CaO additions, and preheating at various temperatures ranging from 1,450° to 1,950° C., on the thermal length changes of ZrO_2 from room temperature to 1,700° C. are reported in this paper. During the course of the investigation there were several developments which it would have been interesting to study in detail, but the scope of the work was restricted to determining if the several oxides, as minor additions, would produce ceramic bodies with industrial possibilities.

II. MATERIALS

Zirconia of three grades was used in the tests. All of the zirconia was washed through a No. 325 U. S. Standard Sieve before being formed into specimens. The chemical compositions [10] are as follows:

Zirconia (grades)	ZrO_2	SiO_2	Al_2O_3	Fe_2O_3	CaO
	%	%	%	%	%
A, fused	96.0	2.05	0.67	0.14	0.19
B, fused	98.0	1.21	.34	.08	.17
C, calcined	99.0	.27	.08	.02	.24

The materials used as additions to the zirconia are described as follows:

CeO_2 (two grades were used): (a) Purified cerous oxalate, which was calcined at 1,425° C and hand-ground to pass dry through a No. 325 sieve. The color of the ground sample was a reddish brown; (b) pure ammonium hexanitrato cerate $(NH_4)_2Ce(NO_3)_6$, which was calcined, hand-ground, and sieved the same as grade (a). The color of the ground sample was a light buff.

Y_2O_3: Commercially pure material, which was repurified by twice dissolving it in hydrochloric acid and precipitating it as the hydroxide, followed by a third solution, precipitation as the oxalate, and calcination at 1,425° C. It was then hand-ground to pass wet through a No. 325 sieve. Color of the powder was cream.

SiO_2: Pulverized quartz, which had been passed wet through a No. 325 sieve, and which, by chemical analysis, contained 99.6 percent of SiO_2.

MgO (two types were available): (a) Periclase of nominal 97-percent purity and passing the No. 200 sieve. The material used was that portion of the sample that passed dry through a No. 325 sieve; (b) commercial $MgCO_3$, which had been calcined at 816° C, and which was of very fine particle size. Described by the producer as containing 2.3 percent of CaO, 0.2 percent of soluble salts, and having a 5.0 percent ignition loss.

CaO: Reagent quality $CaCO_3$, hand-ground to pass dry through a No. 325 sieve.

[10] The chemical compositions were supplied by Eugene Wainer, of the Titanium Alloy Mfg. Co.

For calibration and comparison, the following materials were tested also:

A water-clear single crystal of MgO, from which an expansion specimen was obtained by cutting with a diamond saw and grinding. The measured expansion was parallel with the octahedral axis.

Beryllia, claimed by the producer to contain at least 99.9 percent of BeO, and which, by spectrographic analysis, contained less than 0.01 percent each of Cu, Fe, Mg, and Si. The material was fused in an electric arc supplied with oxygen through the electrodes to prevent formation of the carbide;[11] ground in an iron mill to pass, wet, a No. 325 sieve; and acid-treated to remove iron contamination.

Thoria of nominal 99-percent purity, which was fused and ground by the same method used for the beryllia, passed dry through a No. 325 sieve, and acid-treated. A spectrogram of the unfused sample indicated over 0.01 percent each of Al, Si, and Ca, and less than 0.01 percent each of Cu and Mg.

Zirconium silicate of two types: (a) the mineral zircon, containing by chemical analysis (see footnote 10) 64.82 percent of ZrO_2 and 34.78 percent of SiO_2, (which, by calculation, equals 96.5 percent of $ZrSiO_4$); and (b) zirconium silicate prepared by intimately mixing zirconia C and silica in the proper proportions, pressing into specimens, and heating at 1,500° and at 1,700° C.

III. APPARATUS AND TEST METHODS

Specimens consisting of one oxide were made by thoroughly mixing the oxide with about 10 percent of a 5-percent solution of soluble starch, and pressing the mixture in a hardened steel mold under a pressure of 9,300 lb/in.^{2} to form rods 1.6 cm in diameter by about 5 cm long. After drying, these rods were ground to equilateral triangular prisms approximately 0.5 cm^2 in cross-sectional area.

The specimens consisting of ZrO_2 and an admixture were made by first mechanically blunging a 40-g batch of the body with 40 percent of water, drying, pulverizing, and then following the same procedure used for the single-oxide specimens.

A few of the specimens were matured in a gas-heated kiln at 1,550° or 1,600° C. The others were matured either in an electrically heated platinum-wound furnace, when the temperatures did not exceed 1,450° C, or in the resistor furnace shown in figure 1. This furnace is the same in principle as the one previously described[12] but is larger, having a heating chamber 3¼-in. inside diameter by 4 in. high and requiring eight resistors.

For the thermal-expansion tests, this furnace was modified slightly to accommodate the dilatometer shown in figure 1. This dilatometer is practically the same in design as the one used in an investigation of clays,[13] except for one important detail. The three members supporting the gage, and the center member extending from the specimen to the gage stem, were single-crystal artificial-corundum rods, approximately ⅛ in. in diameter by 18 in. long. The three rods supporting the gage were cemented into a base made of beryllia.[14] The

[11] U. S. Patent 1,545,951.
[12] R. F. Geller, J. Research NBS **27**, 555 (1941) RP1443.
[13] R. F. Geller and E. N. Bunting, J. Research NBS **25**, 15 (1940) RP1311.
[14] Reaction between the rods and the beryllia, particularly at temperatures above about 1,700° C, warrants the recommendation that the base be made of Al_2O_3 instead of BeO.

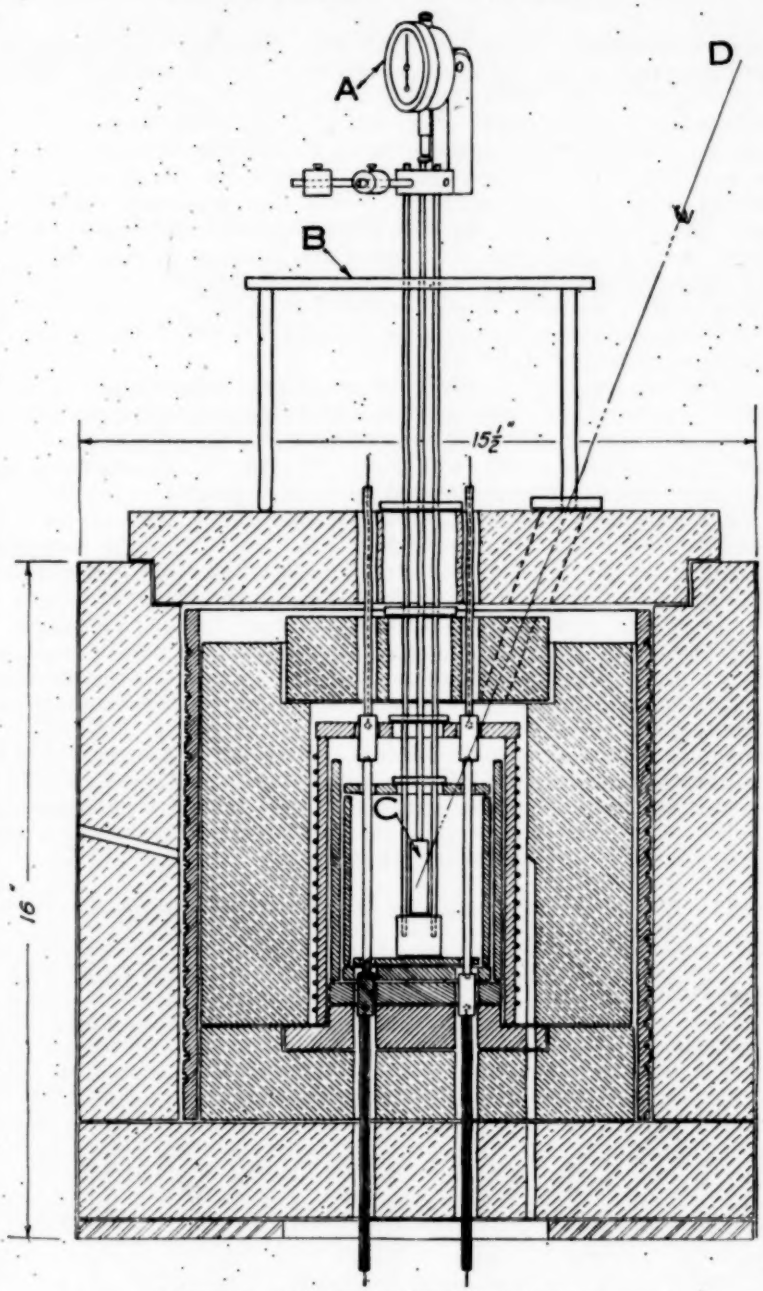

FIGURE 1.—*Dilatometer installed in furnace.*

A, Gage, 0.01-mm divisions; *B*, Bakelite shield; *C*, specimen; the center line *D*, is the axis of the openings in the furnace parts, through which the Pt–10-percent Rh thermocouple was inserted for temperature measurements up to 1,200° C. At about this temperature, the thermocouple was removed and higher temperature measurements were made with an optical pyrometer sighted on the specimen through the same openings. Only two of the eight ThO_2–Y_2O_3 resistors used for heating the furnace are shown in place. The ¼- by 18-in. rods supporting the gage and the rod extending from the specimen to the gage stem are artificial corundum.

rods were furnished by the Linde Air Products Co. The longitudinal axis of each rod was at the same crystal orientation (parallel with the rhombohedral axis). The thermal expansion parallel with this axis was determined, from room temperature to 1,000° C, by the interferometer method, and the expansion curve then extrapolated to 1,800° C. The resultant values were used to correct the expansion values obtained from the gage readings. This was necessary because the length changes indicated by the gage were the difference between the true thermal dilatation of the specimen and the thermal dilatation of a length of corundum rod equivalent to the length of the specimen. Consequently, all the thermal-expansion data presented in this paper for temperature ranges above 1,000° C are based on extrapolated values for corundum (table 1).

Temperature measurements between room temperature and about 1,200° C were made with a platinum–10-percent-rhodium thermocouple, the junction of which was adjacent to the specimen. Above 1,200° C the thermocouple was removed, and the observations were then made with a calibrated optical pyrometer sighted on the specimen.

Preliminary tests with MgO, BeO, and ThO_2 showed that the corundum rods had ample strength at 1,800° C to resist deformation, but results above 1,600° C were not always satisfactory because of the reaction between the beryllia base and the corundum rods mentioned in footnote 14, and possibly also because of further shrinkage, or reactions at the surface of the specimens. Surface reactions, if any, must have occurred with vapors in the furnace because the specimens were separated from the base, and from the center corundum rod, by platinum-rhodium plates.

The substantial agreement (table 1) between the values obtained in this investigation for MgO, BeO, and ThO_2 and values obtained by the interferometer method, and also those for MgO published by Heindl [15], show that the method and apparatus may be relied upon to give values good to at least ±0.05 percent.

TABLE 1.—*Comparison of thermal-expansion values obtained with the dilatometer used in this investigation and results obtained by other methods*

From room temperature to—	Interferometer method [a]						Dilatometer method			Heindl
	ThO_2 [b]	BeO [b]	MgO [c]	Al_2O_3 [d]	Al_2O_3 [e]	Al_2O_3 [f]	ThO_2 [g]	BeO [h]	MgO [i]	MgO [j]
°C	%	%	%	%	%	%	%	%	%	%
200	0.14	0.10	0.19	0.10	0.12	0.11	0.14	0.12	0.16	0.13
400	.31	.26	.45	.26	.29	.26	.32	.28	.43	.41
600	.51	.45	.73	.43	.47	.43	.52	.48	.71	.70
800	.70	.65	1.04	.60	.....	.61	.73	.69	1.01	1.02
1,000	.....	.....	.....	.....	.....	.81	.94	.92	1.32	1.32
1,200	.....	.....	.....	.....	.....	(1.01)	1.15	1.16	1.64	1.65
1,400	.....	.....	.....	.....	.....	(1.22)	1.37	1.40	1.98	1.99
1,600	.....	.....	.....	.....	.....	(1.45)	1.59	1.66	2.34	2.37
1,700	.....	.....	.....	.....	.....	(1.57)	1.71	1.78	2.46	2.49

[a] Determinations made by A. S. Creamer.
[b] Preheated at 2,000° C.
[c] Preheated at 1,900° C.
[d] Corundum crystal, perpendicular to "C" axis.
[e] Corundum crystal, parallel to "C" axis.
[f] Expansion was measured parallel with the rhombohedral axis, or 57° 34′ from the "C" axis. These values were used to correct the gauge readings. The values in parentheses are extrapolated.
[g] Preheated at 1,850° C.
[h] Several preheatings with a total of 15 above 1,800° C.
[i] Cut from a single crystal of periclase.
[j] R. A. Heindl, BS J. Research **10**, 715 (1933) RP562.

[15] R. A. Heindl, BS J. Research **10**, 715 (1933) RP562.

The heating and the cooling rates in all of the tests did not exceed 3½ degrees centigrade per minute.

The absorptions were determined by boiling the test prisms in CCl_4 for 5 hours and dividing the increase in weight by the density of the CCl_4. The resultant values are comparable with data for absorption obtained conventionally by boiling in water.

IV. RESULTS

Because of the very irregular thermal length changes of most of the compositions tested, the results are usually presented as graphs rather than as coefficients.

1. ZIRCONIA

The first series of graphs is shown in figures 2 and 3 and illustrates the thermal length change behavior of the three zirconias (A, B, and C) without oxide additions. One specimen of each zirconia had been preheated within the range of temperatures to which refractories are subjected in present-day commercial practice, and another specimen had been preheated at a relatively much higher temperature:

Zirconia A.—The specimen preheated at 1,450° C (fig. 2) was heated in the expansion test to 1,200°, 1,300°, 1,400°, and 1,100° C consecutively, with intermediate cooling to about 800° C. The following points of interest are illustrated by the graph: (a) The contraction during heating and the expansion during cooling will apparently take place an indefinite number of times during repeated heating and cooling cycles; (b) the beginning of contraction during heating is not clearly defined but the beginning of expansion during cooling occurs sharply (and actually was duplicated within 2 degrees); (c) the length changes will have no irregularities if the maximum temperature to which the zirconia is subjected remains below 1,100° C, as shown by the curve for the first heating and for the last heating and cooling cycle; and (d) an appreciable permanent shrinkage (0.65 percent) occurred while holding the specimen for 2½ hours at 1,400° C, even though it had been preheated at 1,450° C.

The zirconia preheated at 1,850° C (fig. 2) had acquired several cracks during the preheating, and it is conceivable that the minor irregularities in the curve between 1,200° and 1,700° C reflect further cracking and deforming of the specimen. This cracking was characteristic of all the zirconia pieces heated at or above 1,850° C. In fact, it was only after repeated trials that specimens were obtained sufficiently intact to be placed in the dilatometer. One specimen of zirconia A, preheated at 1,950° C, failed completely in the expansion test while the rapid expansion (during cooling) was taking place. For this specimen, as well as for the one preheated at 1,850° C, this "cooling-expansion" started at 1,004° C.

Zirconia B.—The two tests for which curves are presented in figure 2 represent specimens preheated at 1,415° and at 1,950° C. The latter was cracked, similar to the specimen of zirconia A heated at 1,850° C, and again the expansion during cooling started sharply at 1,004° C. The most noticeable difference between the two specimens of zirconia B is the very large permanent shrinkage of the one preheated at

1,415° C as compared to the other, which showed a net expansion or "growth." Similar growth had been noted also by Mather.[16]

Zirconia C.—The difficulties encountered in making usable test prisms, mentioned in connection with zirconia A, were seemingly

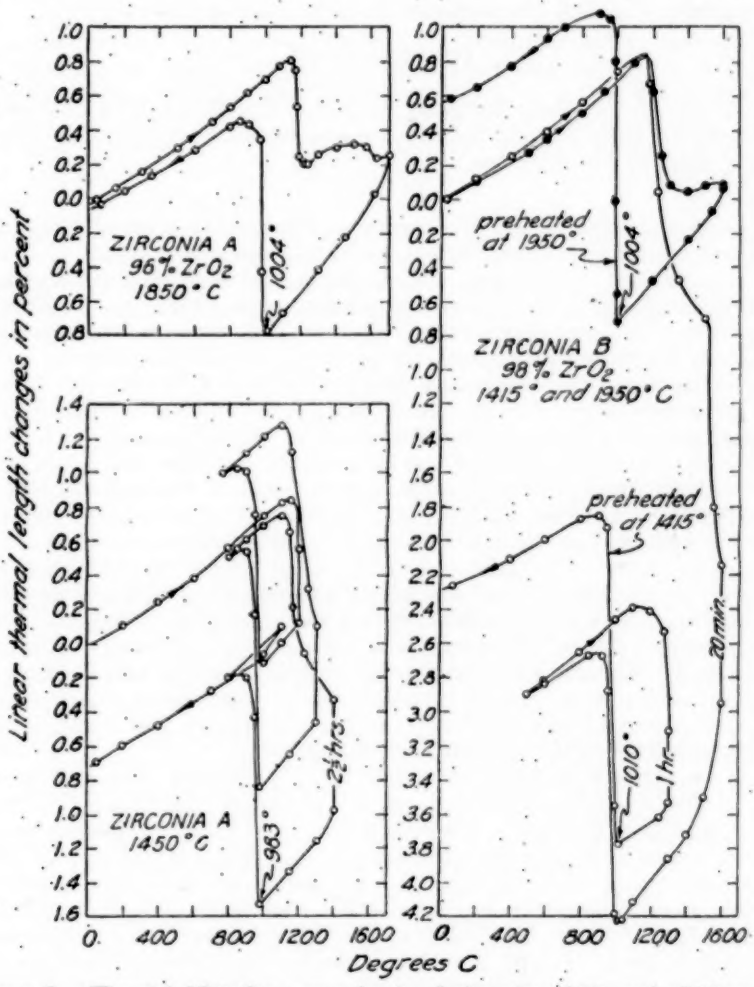

FIGURE 2.—*Thermal dilatation curves for fused zirconias of 96- and of 98-percent purity.*

The temperatures in the legends indicate the heat treatment the specimens had received prior to the testing. The time notations on the curves indicate the interval of holding at the maximum temperature.

insurmountable with the C material. It was found necessary to admix some of the fused zirconia, and the curves shown in figure 3 were obtained with pieces made of 90 parts of zirconia C and 10 parts of zirconia B.

The expansion during cooling started at temperatures significantly higher than for either of the less pure zirconias, A and B, and the

[16] R. F. Mather, J. Am. Ceram. Soc. **25**, 93 (1942).

resultant length change was at least as great. In the case of zirconia C heated at 1,950° C, the length changes during both the "heating-contraction" and the "cooling-expansion" were greater than for any other specimen tested. Consequently, this material was selected for

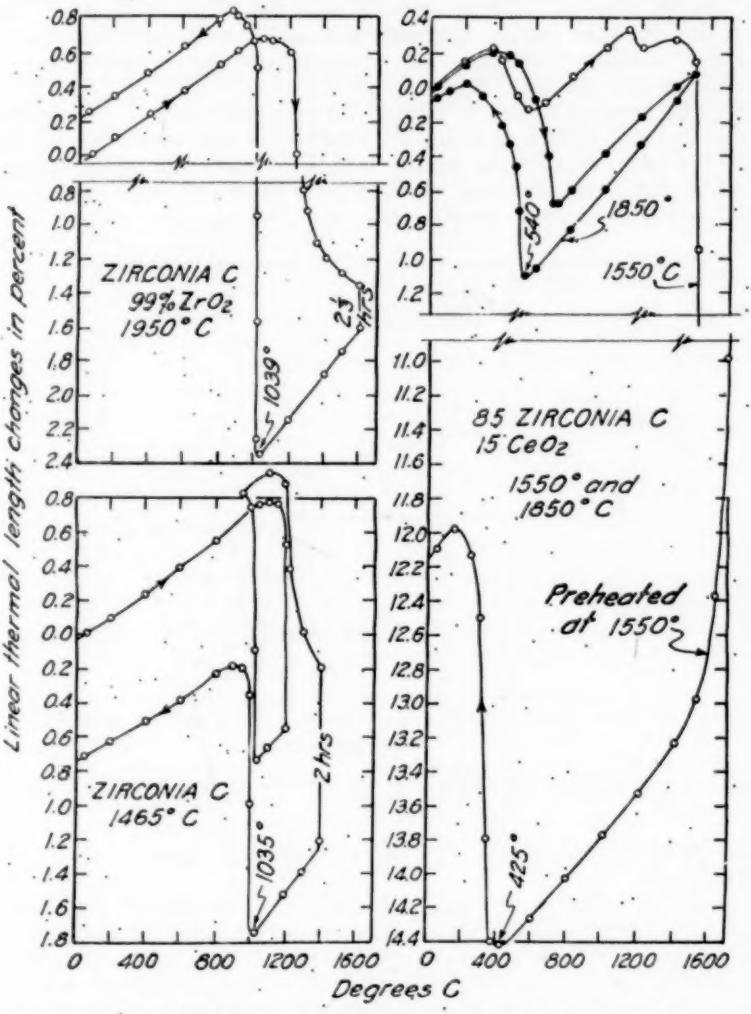

FIGURE 3.—*Thermal-dilatation curves for calcined zirconia of 99-percent purity and calcined zirconia with* CeO_2 *additions.*

The temperatures in the legends indicate the heat treatment the specimens had received prior to the testing. The time notations on the curves indicate the interval of holding at the maximum temperature.

differential thermal analysis,[17] the result of which is shown in figure 4.

In general, it may be concluded, with respect to zirconia, that (a) preheating to temperatures in the range from 1,450° to 1,950° C will not change, significantly, the amount of length change accompany-

[17] This analysis was made by E. N. Bunting, using a platinum-to-platinum–10-percent-rhodium differential thermocouple, a K-type potentiometer, and corundum as the reference material.

ing the rapid contraction during heating, or the expansion during cooling; (b) the trend is for these length changes to be greater, and for the "cooling-expansion" to begin at a relatively higher temperature, with increase in purity of the zirconia; (c) for any one material the length changes during cooling can be duplicated more closely than the changes during heating; and (d) the "heating-contraction" and the "cooling-expansion" are accompanied by an endothermic and an exothermic reaction, respectively.

For the present at least, it may be assumed that the irregularities in the thermal length changes are caused by the reversible inversions of the low-temperature monoclinic and the high-temperature tetragonal forms of ZrO_2, as reported by Ruff and Ebert.[15] Several samples of ZrO_2 were examined petrographically during the course of this

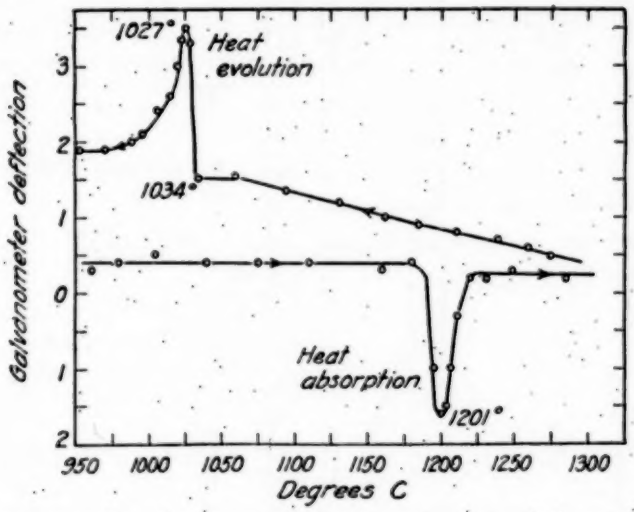

FIGURE 4.—*Heat effect curves for calcined zirconia of 99-percent purity preheated at 1,950° C.*

investigation, and the following report was submitted by B. L. Steierman:

"Some crystals in zirconia which had been heated in the range 1,000° to 1,900° showed a negative uniaxial interference figure and are presumed to be the tetragonal form. Another sample, used as a muffle in the furnace shown in figure 1, contained crystals 5 to 10 microns in size, with medium birefringence and apparently uniaxial positive in character, indicating the trigonal form. A third sample, which had been used as a pedestal for supporting test pieces in the furnace described in NBS Research Paper RP 1443 [see footnote 12] and which had been heated to a maximum temperature of 2,025°, was extremely weak, crushed easily to a fine powder, and was composed solely of ZrO_2 crystals ranging from 2 to 8 microns in size. These crystals were mostly monoclinic. Occasional grains were tetragonal and also present, but not common, were grains with internal bladed crystals indicative of the tetragonal-monoclinic inversion."

[15] Otto Ruff and Fritz Ebert, Z. anorg. allgem. Chem. **180**, 19 (1929).

The conclusion to be drawn from the petrographic data is, that the reversion from a high temperature to the low-temperature form is not necessarily complete, even with relatively slow cooling.

2. ZIRCONIA WITH ADDITIONS

(a) EFFECT OF CeO_2

Only one composition, containing 85 weight percent of zirconia C and 15 percent of CeO_2, was investigated. It is evident from the graphs in figure 3 that this addition of ceria would not prevent the irregular and rapid thermal length changes noted for zirconia alone. Similar results were obtained with ceria from both sources (section II, page 89).

The very large permanent shrinkage, beginning at about 1,400° C, of the specimen preheated at 1,550° C is of secondary interest only. Of primary interest is the low-temperature range in which the inversions take place as compared with the corresponding ranges for the three zirconias. That oxide additions may depress the inversion temperatures was shown by Mather's work with zirconia and spinel, see footnote 16, in which case the expansion during cooling started as low as about 600° C for a mixture containing 90 mole percent of spinel. As the data show, only 15 weight percent (11.2 mole percent) of CeO_2 was sufficient to lower the beginning of the expansion during cooling to 425° C. The small contraction between 1,150° and 1,200° C, for the specimen preheated at 1,550° C, may be caused by ZrO_2 unaffected by CeO_2, during the preheating. Petrographic examination of specimens containing CeO_2 obtained from the oxalate, and which had been heated at 1,550°, at 1,800°, and at 2,000° C also showed that all the zirconia was in the monoclinic form.

(b) EFFECT OF Y_2O_3

Typical results are shown by the graphs in figure 5. The addition of 8 percent of yttria to zirconia C and preheating at 1,850° C, produced length changes resembling in general those obtained with the 15-percent addition of CeO_2. In contrast to this, adding 11.5 percent of Y_2O_3, and preheating to only 1,700° C, had almost completely eliminated the irregularities indicative of the monoclinic-tetragonal transformation, but there was an appreciable permanent shrinkage at temperatures above about 1,400° C. The three other curves in figure 5 illustrate the effect of the preheating temperature on the composition containing 15 percent of Y_2O_3 and 85 percent of zirconia C. A correlation of the information furnished by the curves in figure 5 with the results of petrographic examinations, summarized in table 2, shows that the decrease in the irregularities of the thermal length changes during both heating and cooling is directly related to the presence of the "stabilized" cubic zirconia.

Increasing additions of Y_2O_3 to ZrO_2 tend to produce mechanically weaker and more porous bodies, as shown by the following values for absorption:

ZrO_2+ 8.0 percent of Y_2O_3 preheated at 1,850 C	3.6 percent.
ZrO_2+11.5 percent of Y_2O_3 preheated at 1,700 C	5.6 percent.
ZrO_2+15.0 percent of Y_2O_3 preheated at 1,700 C	12.5 percent.
ZrO_2+15.0 percent of Y_2O_3 preheated at 1,850 C	7.7 percent.

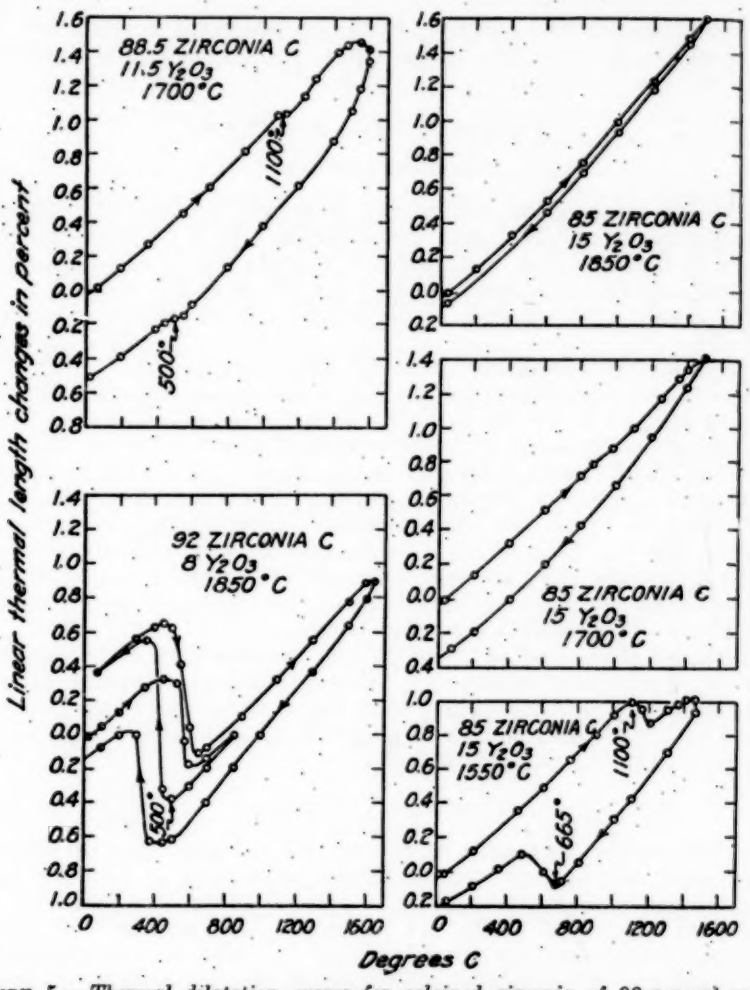

FIGURE 5.—*Thermal dilatation curves for calcined zirconia of 99-percent purity with Y_2O_3 additions.*

The temperatures in the legends indicate the heat treatment the specimens had received prior to the testing.

TABLE 2.—*Petrographic data on heated specimens of zirconia with yttria additions*

Test number	Composition		Maximum preheating temperature	Form of ZrO_2 determined microscopically
	ZrO_2	Y_2O_3		
	%	%	°C	
307-L	85	15	1,550	85 to 90 percent cubic.
304-L	85	15	1,650	At least 95 percent cubic.
305-L	85	15	1,700	95 percent cubic, 5 percent monoclinic.
301-L	85	15	1,750	About 99 percent cubic.
335-L	92	8	1,850	Monoclinic with possibly some tetragonal, but definitely no cubic.
295-L	85	15	1,850	All cubic.
299-L	85	15	1,850	Do.
441 [a]	92	8	1,900	15 percent cubic, and 85 percent monoclinic, of which about one-third appears to have inverted from the tetragonal.
441 [a]	85	15	1,900	All cubic.

[a] The X-ray patterns of the samples from this test contained the lines for cubic zirconia having a face-centered cubic cell with a_0=5.108 A. The pattern for the sample with 8 percent of yttria contained also lines for monoclinic zirconia.

(c) EFFECT OF SiO_2

It was thought of potential interest to investigate some ZrO_2-SiO_2 combinations because of the ready availability of silica and because of the well-established use in industry of zircon ($ZrSiO_4$).

Samples of the mineral zircon were heated for 1 hour at 1,700°, at 1,750°, and at 1,800° C, and samples of the zirconia-silica mixture in 1:1 mole ratio were heated for 1 hour at 1,700° and at 1,800° C. The macroscopic and petrographic appearance of the mineral before and after heating at 1,700° and at 1,750° C was identical, but after the 1,800° C treatment the orignially granular sample had sintered into a hard mass, and the X-ray pattern contained only lines for monoclinic zirconia. The X-ray pattern for the ZrO_2:SiO_2 mixture heated at 1,700° C contained strong lines for zircon and weak lines for monoclinic zirconia, and the pattern for the mixture heated at 1,800° C was identical with that for the mineral zircon heated at 1,800° C. This is good evidence that zircon breaks down between 1,750° and 1,800° C to form zirconia and liquid (as there were lines for only one crystalline phase). It is in agreement with the petrographic report in Heindl's paper[19] that zircon heated at 1,800° C was composed wholly of zirconium oxide and glass. Matignon[20] and Wartenburg and Gurr[21] also noted the decomposition of zircon above 1,800° C. In reference 21 a curve is published showing the amount of SiO_2 lost by volatilization. The data are based on chemical analyses of zircon samples after having been heated for 30 minutes at each of a series of temperatures. At 1,800° C, for example, the loss of silica was practically negligible, at 2,000° C it was about 18 percent, at 2,200° C it was about 65 percent, and at 2,300° C it was indicated to be complete. The observed decomposition of ZrO_2 is not in agreement with published diagrams for the system ZrO_2-SiO_2,[22] showing congruent melting of $ZrSiO_4$ above 2,400° C.

Thermal-expansion tests were made on the following specimens: (a) 85 percent of zirconia C and 15 percent of silica (by weight) preheated at 1,700° C; (b) zirconia and silica in equimolar proportions preheated at 1,500° and at 1,700° C; and (c) the mineral zircon preheated at 1,700° C. The results are plotted in figure 6.

Although the results of the two tests made on each of the two test pieces containing 15 percent of silica do not duplicate in detail, they are sufficiently alike to justify the conclusion that the expansion following the break during heating in the first test and the contraction following the break during heating in the second test are caused by an actual change in the structure of the body. The nature of the change was not discernible by either petrographic or X-ray examination, and the subject was not investigated further because, for the present at least, it was of academic interest only.

The relatively small length changes accompanying the inversions of the zirconia in the two specimens made of equimolar proportions of ZrO_2 and SiO_2 indicate that the ZrO_2 is present mostly as $ZrSiO_4$. This is in the accord with the X-ray pattern and, although only indicative, is the best information that could be obtained because the structure was so finely crystalline that quantitative estimates of the

[19] R. A. Heindl, BS. J. Research **10**, 715 (1933) RP562.
[20] M. Camille Matignon, Compt. rend. **177**, 1290 (1923).
[21] H. von Wartenburg and W. Gurr, Z. anorg. allgem. Chem. **196**, 374 (1931).
[22] E. W. Washburn and E. E. Libman, J. Am. Ceram. Soc. **3**, 634 (1920); N. Zirnowa, Z. anorg. allgem. Chem. **218**, 198 (1934).

crystalline phases present were not possible by optical examination.

The zircon specimen preheated at 1,700° C showed a slight decrease in expansion per degree above 1,500° C, but this was probably caused by permanent shrinkage. The length changes during heating and

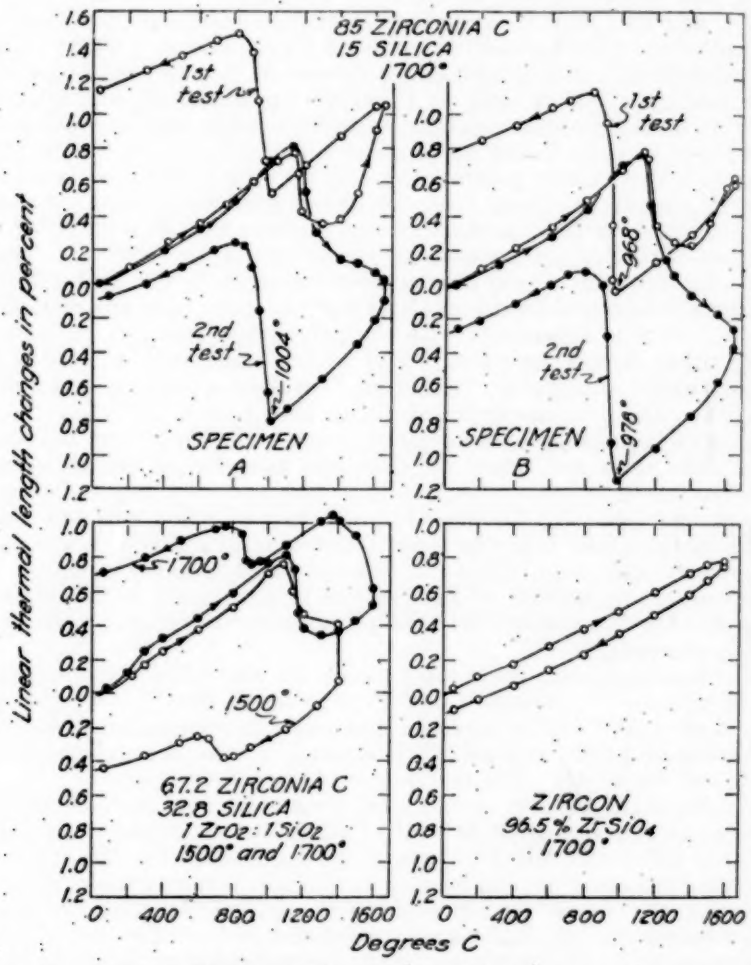

FIGURE 6.—*Thermal dilatation curves for calcined zirconia of 99-percent purity with SiO_2 additions, and for mineral zircon.*

The temperatures in the legends indicate the heat treatment the specimens had received prior to the testing.

during cooling between room temperature and 1,500° C were nearly uniform throughout this range. The average coefficient during heating is 5.1×10^{-6}, and during cooling it is 5.2×10^{-6}.

The two prisms containing 15 percent of SiO_2 had absorptions of 5.7 and 8.7 percent, respectively, and were relatively strong, as judged by observation. The ZrO:SiO_2 mixture preheated at 1,500° C was very

porous and mechanically weak, but the specimen preheated at 1,700° C was firm and had an absorption of 3.5 percent. The zircon test piece also was very firm and its absorption was 7.7 percent.

(d) EFFECT OF MgO

X-ray and petrographic evidence shows that additions of either 8 percent or 15 percent of MgO, and preheating at temperatures as low as 1,550° C, converted most of the zirconia to the stable cubic form. Attempts to determine the amounts of cubic zirconia quantitatively produced conflicting results between duplicate observations on the same specimens by different observers as well as between supposedly duplicate specimens by the same observer. The cubic crystal was face-centered with the unit cell size $a_0=5.063$ A in a sample heated at 1,600° C, and $a_0=5.07$ A in a sample heated at 1,800° C. The X-ray patterns contained also weak lines for monoclinic zirconia and very weak lines for MgO. Petrographic estimates (based on relative birefringence of the nonisotropic phases) indicated a small amount of tetragonal ZrO_2 in some samples.

The thermal length changes of the specimens containing magnesia (figs. 7 and 8), during both heating and cooling between room temperature and about 1,100°C, are very likely determined primarily by cubic zirconia. Comparison of coefficients for specimens containing 15 percent of MgO with the coefficients for the 85-percent-zirconia 15-percent-yttria test piece preheated at 1,850° C (fig. 5), which was reported to be 100-percent cubic ZrO_2 (table 2), shows good agreement (table 3). Above 1,100° C, however, the magnesia additions produced length changes that are unique among those observed in this investigation. They are characterized by (a) two small but well-defined irregularities or "breaks" during heating, but no corresponding break during cooling, such as observed for curves in preceding figures; and (b) a relatively very high average coefficient of length change during heating above 1,400° C and during cooling above about 1,100° C.

The first of the two breaks observed during heating is probably associated with the inversion of monoclinic to tetragonal zirconia. The second break, which occurred at about 1,500° C, is shown most clearly by the two curves for the duplicate tests of the 92-percent-zirconia 8-percent-periclase composition preheated at 1,850° C (fig. 7). These and the other curves for ZrO_2-MgO bodies provide ample evidence that the break at 1,500° C is significant. It may accompany the inversion of tetragonal to trigonal zirconia, although Cohn[23] states that the trigonal is formed only after prolonged heating at, or above, 1,900° C. The assumption that there has been a change in phase at 1,500° C is supported by the differences in the coefficients of thermal expansion (table 3) for the temperature ranges above and below the range of the second break. The gradual change in slope of the cooling curves, occurring between 1,200° and 1,000° C, probably means that a change in phase is taking place, but the absence of the expansion during cooling noted in preceding curves would seem to imply that the presence of MgO in the zirconia crystal lattice prevents

[23] Willi M. Cohn, Trans. Electrochem. Soc. 68, 65 (1935).

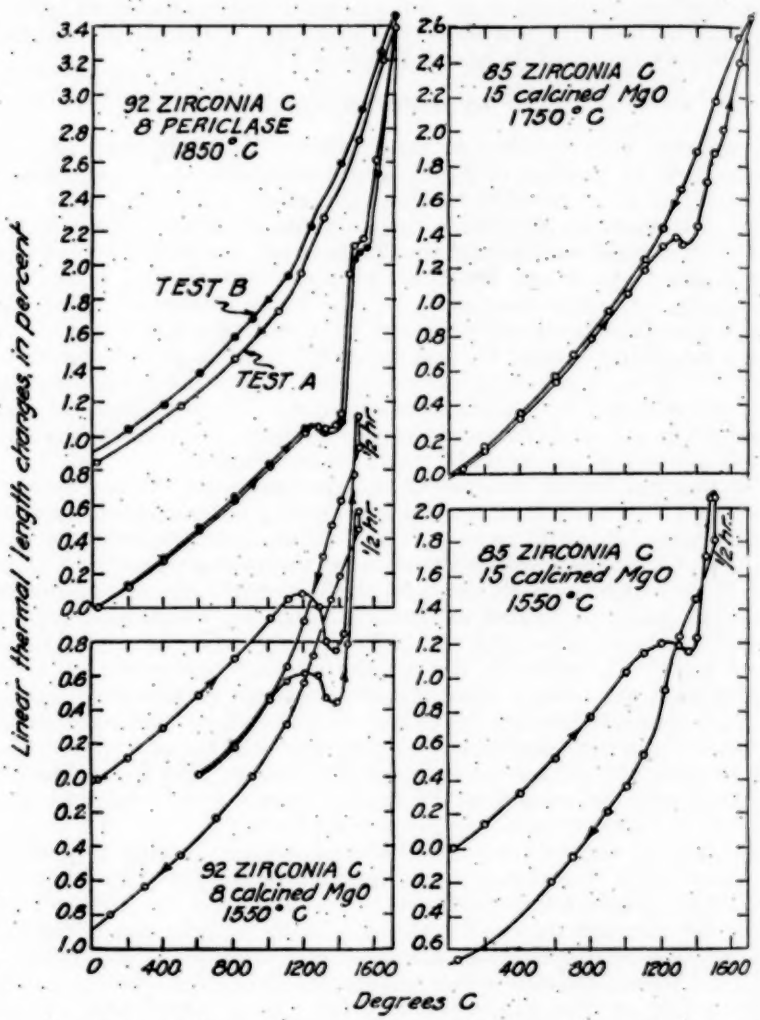

FIGURE 7.—*Thermal dilatation curves for calcined zirconia of 99-percent purity with* MgO *additions.*

The temperatures in the legends indicate the heat treatment the specimens had received prior to the testing. The time notations on the curves indicate the interval of holding at the maximum temperature.

the inversion taking place with sufficient rapidity to produce a measurable irregularity.

The thermal length changes above 1,400° C during heating, and above about 1,000° C during cooling (table 3, tests 363–E, 390–E, and 391–E), are much greater than can be explained with the average coefficients of linear thermal expansion for MgO and various crystal

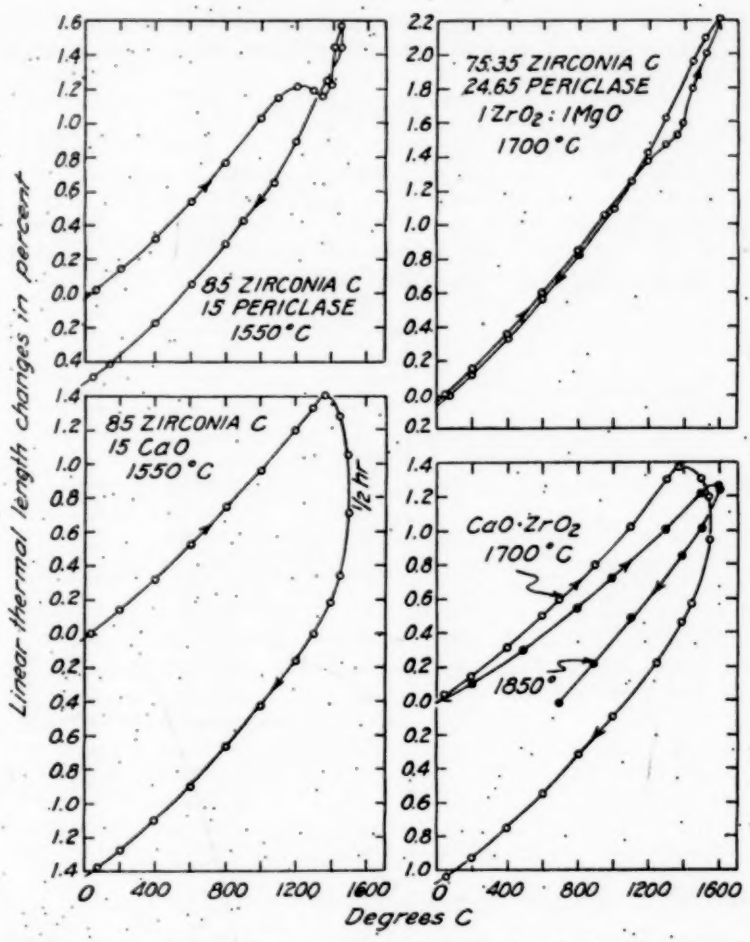

FIGURE 8.—*Thermal dilatation curves for calcined zirconia of 99-percent purity with* MgO *additions and with* CaO *additions, and curves for artificial* $CaO.ZrO_2$.

The temperatures in the legends indicate the heat treatment the specimens had received prior to the testing. The time notation on the curves indicates the interval of holding at the maximum temperature.

phases of ZrO_2 that may be present. These coefficients, given in table 3, are summarized as follows:

	Heating	Cooling
Periclase	15.3×10^{-6}	16.0×10^{-6}
Monoclinic zirconia	7.2 to 8.0×10^{-6}	5.4 to 7.3×10^{-6}
Tetragonal (?) zirconia	10.9 to 11.0×10^{-6}	11.4 to 13.5×10^{-6}
Cubic zirconia	10.5 to 11.1×10^{-6}	11.4 to 11.8×10^{-6}

TABLE 3.—*Coefficients of linear thermal expansion*

Test number	Specimen		Predominant crystal form [a]	Observations made during	Coefficient	
	Composition	Preheated 1 hr at			Temperature range	Value
		°C	ZrO_2		°C	×10⁶
332-E	Periclase (MgO)	(b)		Heating	100 to 1,600	13.
				Cooling	1,800 to 100	10.
340-E	Zirconia A (96% ZrO_2)	1,460	Monoclinic	Heating	50 to 1,050	6.
			do	Cooling	1,000 to 25	9.
			(Tetragonal)	do	1,200 to 1,000	12.
			do	do	1,300 to 1,000	11.
			do	do	1,300 to 1,000	11.
378-E	do	1,850	Monoclinic	Heating	40 to 940	7.
			do	Cooling	800 to 60	9.
			(Tetragonal)	do	1,600 to 1,050	12.
338-E	Zirconia B (98% ZrO_2)	1,415	Monoclinic	Heating	30 to 1,130	7.
			do	Cooling	800 to 100	8.
			(Tetragonal)	do	1,400 to 1,100	12.
384-E	do	1,950	Monoclinic	Heating	30 to 1,130	7.
			do	Cooling	800 to 100	9.
			(Tetragonal)	do	1,500 to 1,050	12.
339-E	Zirconia C (99% ZrO_2)	1,465	Monoclinic	Heating	70 to 1,000	7.
			do	Cooling	800 to 50	9.
			(Tetragonal)	do	1,350 to 1,050	12.
343-E	do	1,950	Monoclinic	Heating	80 to 900	7.
			do	Cooling	800 to 200	7.
			(Tetragonal)	do	1,600 to 1,050	12.
337-E	92% zirconia C, 8% Y_2O_3	1,850	(Tetragonal)	Heating	700 to 1,400	10.
				Cooling	1,500 to 600	12.
347-E	85% zirconia C, 15% Y_2O_3	1,850	Cubic	Heating	30 to 1,500	11.
				Cooling	1,500 to 50	11.
375-E	95% zirconia C, 5% CaO	1,700	do	Heating	30 to 1,230	10.
				Cooling	1,400 to 100	11.
377-E	do	1,850	do	Heating	25 to 1,300	11.
				Cooling	1,500 to 100	11.
361-E	92% zirconia C, 8% CaO	1,550	do	Heating	25 to 1,325	10.
				Cooling	1,300 to 100	11.
391-E	92% zirconia C, 8% periclase	1,850	Cubic (and monoclinic)	Heating	25 to 1,200	9.
			do	Cooling	1,000 to 100	9.
			?	Heating	1,400 to 1,450	132.
			?	do	1,550 to 1,700	77.
			?	Cooling	1,700 to 1,110	23.
381-E	85% zirconia C, 15% periclase	1,550	Cubic (and monoclinic)	Heating	40 to 1,140	10.
				Cooling	1,100 to 100	11.
363-E	85% zirconia C, 15% calcined MgO	1,750	Cubic (and monoclinic)	Heating	40 to 1,140	11.
			do	Cooling	1,000 to 100	11.
			?	Heating	1,400 to 1,450	84.
			?	do	1,550 to 1,700	37.
			?	Cooling	1,700 to 1,100	23.
390-E	MgO:ZrO_2 (molar)	1,700	Cubic	Heating	40 to 1,140	11.
			do	Cooling	1,100 to 100	12.
			?	Heating	1,400 to 1,600	31.
			?	Cooling	1,600 to 1,100	18.
397-E	Zircon	1,700		Heating	25 to 1,500	5.
				Cooling	1,500 to 100	5.

[a] Phases given in parentheses are believed to be present in appreciable amounts, but this was not established.

[b] Specimen cut from a single crystal of water-clear periclase and the expansion determined is parallel with the octahedral axis. This is the same specimen for which values are given in table 1.

It can be said, in general, that (a) the thermal length changes of zirconia with magnesia additions of from 8 to 24.65 percent are high but regular between room temperature and 1,100°, and that these bodies should have a fairly good resistance to thermal shock in this temperature range; and (b) these bodies will have a poor resistance to thermal shock in temperature ranges above 1,200° C because of inversions, or crystalline formations, the identity of which have not been established.

It is of interest that all these bodies were mechanically hard and strong, and that specimens of MgO and ZrO_2 in 1:1 molar ratio,

hen heated at 1,700° C, were the only ones encountered in this investigation that were completely vitrified (water absorption less han 0.1 percent).

(e) EFFECT OF CaO

Curves illustrating the length changes observed for zirconia with me additions are shown in figures 8, 9, and 10. The formation of he compound $CaO.ZrO_2$ having been reported in the literature,[24] it as thought that a determination of the thermal-expansion behavior ould be of interest. A mixture containing CaO and ZrO_2 in equiolar ratio (31.3 weight percent of CaO) heated at 1,700° C was over 0 percent one phase, and heating at 1,850° C produced over 99 ercent one phase. This phase was described as having medium irefringence, with index of refraction of about 2.05 maximum and .035 minimum. The X-ray pattern corresponds to the cubic form ut, since the optical properties are not those of a cubic substance, it s probable that the symmetry is of lower degree. This is in agreeent with Ruff, Ebert, and Stephan (footnote 24). There was istinct cleavage in one direction with polysynthetic twinning parallel o the cleavage.

The thermal-expansion and contraction curves for specimens of $CaO.ZrO_2$, preheated at 1,850° and at 1,700° C, are shown in figure 8. The average coefficient of linear thermal expansion for the composiion preheated at 1,850° C, in the range from room temperature to ,500° C, is 8.3×10^{-6}. (Specimens of this composition were very orous and friable, and the results obtained during cooling below 00° C are not believed to be significant.) The average coefficient f linear thermal change in the range from room temperature to ,300° C is 10.1×10^{-6} during heating, and 10.6×10^{-6} during cooling, or the composition heated at 1,700° C. These values approximate hose for the composition 85 ZrO_2—15CaO (fig. 8), which are 10.4×10^{-6} during heating and 11.2×10^{-6} during cooling. An X-ray pattern or the latter composition contained lines for only cubic zirconia and $CaZrO_3$.

Curves for zirconia with 6- and 8-percent CaO additions are shown n figure 9. The 6-percent addition and preheating at 1,450° C converted about two-thirds of the sample to cubic zirconia. The emaining one-third consisted of $CaZrO_3$ and (probably) monoclinic ZrO_2. The presence of an appreciable amount of noncubic zirconia s indicated by the breaks in the curve. Preheating the same composition at 1,565° C had converted all the uncombined ZrO_2 to the ubic form. It also had almost eliminated the permanent shrinkage, amounting to 2.0 percent for the test piece preheated at 1,450° C. Both of the specimens containing 8 percent of CaO, for which curves are shown in figure 9, contained only cubic zirconia and calcium irconate, and, in the range from room temperature to 1,400° C, heir curves are practically identical with the curve for the 6-percent-CaO composition preheated at 1,565° C. The average coefficient of linear thermal expansion for this group (fig. 9), in the range 25° to 1,400° C, is 11.0×10^{-6} during heating and 11.5×10^{-6} during cooling. All the specimens containing 6 or 8 percent of CaO were porous. The

[24] Otto Ruff, Fritz Ebert, and Edward Stephan, Z. anorg. Chem. **180** 215 (1929), who presented identifica tion data based on X-ray examinations.

lowest recorded water absorption was 9 percent for the 8-percent-CaO expansion piece preheated at 1,750° C.

The results for mixtures of zirconia with 4 and 5 percent of CaO are recorded in figure 10. The curves show what is the most striking

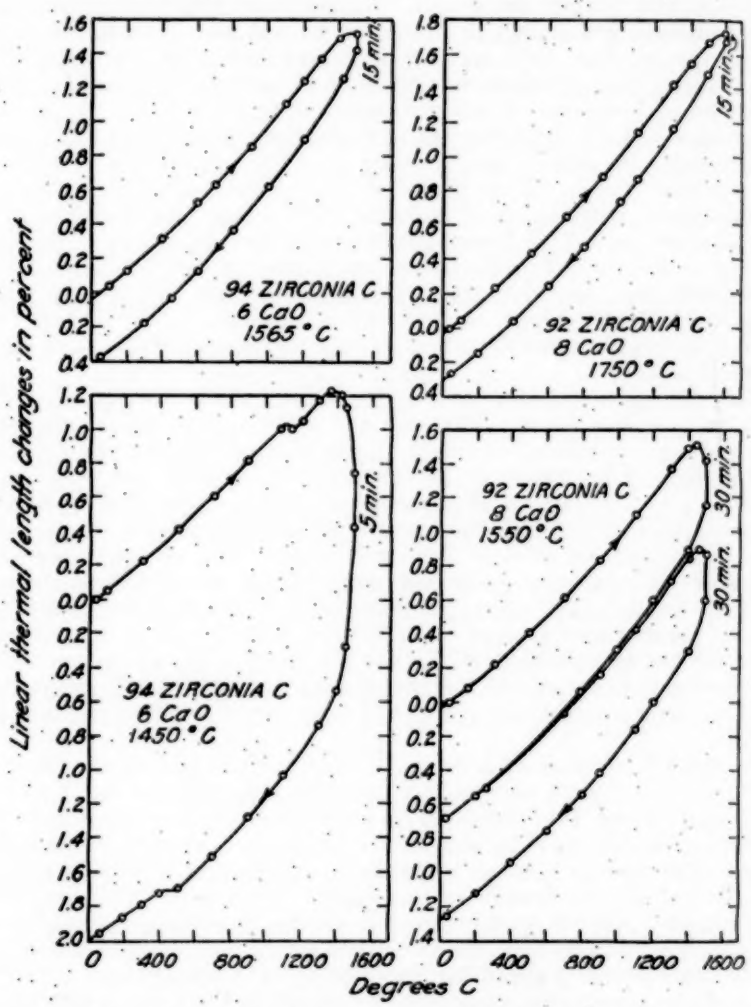

FIGURE 9.—*Thermal dilatation curves for calcined zirconia of 99-percent purity with* CaO *additions.*

The temperatures in the legends indicate the heat treatment the specimens had received prior to the testing. The time notation on the curves indicates the interval of holding at the maximum temperature.

development of the entire investigation—namely, that a 4-percent addition of CaO has little effect on the thermal expansion of zirconia, whereas a 5-percent addition eliminates the irregularities in the thermal length changes and causes an apparently complete conversion of the uncombined ZrO_2 to the stabilized cubic form. The average coefficients of linear thermal expansion for the 5-percent-CaO speci-

mens preheated at 1,700° and at 1,850° C are 10.8×10^{-6} during heating and 11.3×10^{-6} during cooling, in the range 25° to 1,400° C. All the specimens in this group (fig. 10) heated at 1,600° C or higher were fairly hard and dense, the absorption ranging from 3.08 to 6.15 percent.

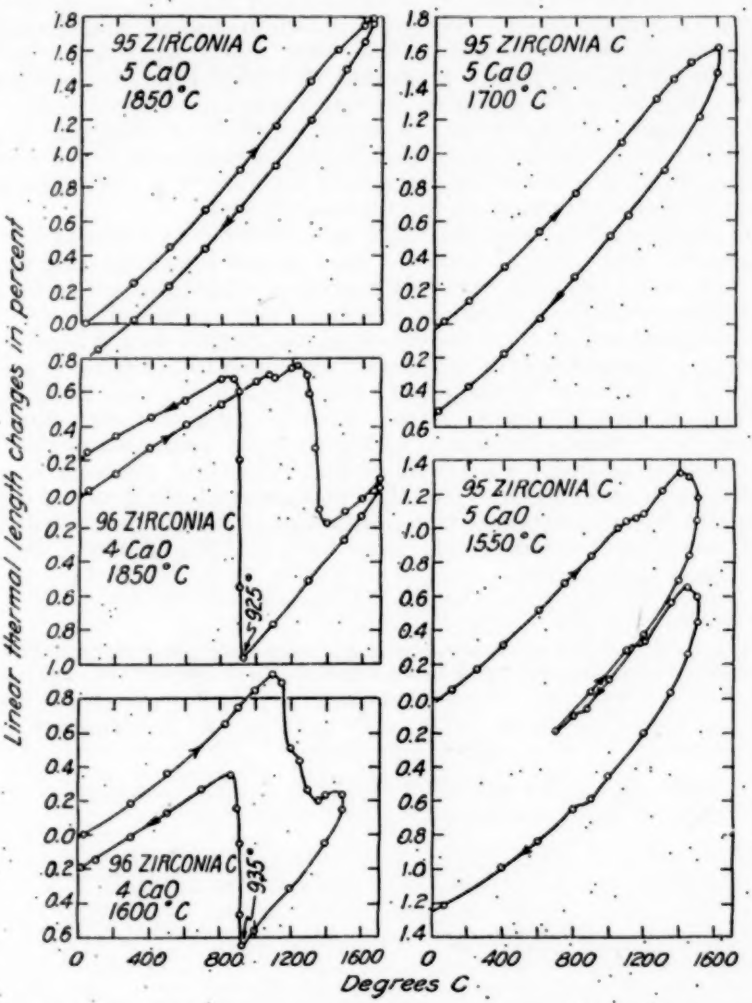

FIGURE 10.—*Thermal-dilatation curves for calcined zirconia of 99-percent purity with* CaO *additions.*

The temperatures in the legends indicate the heat treatment the specimens had received prior to the testing.

V. DISCUSSION AND CONCLUSIONS

It seems evident from the data presented in figures 2 and 3 that zirconia (96 to 99 percent pure), whether calcined or fused, and whether preheated in a test piece at a relatively low temperature (1,450° C) or as high as 1,950° C, will undergo large and rapid length changes

during both heating and cooling in the temperature ranges to which it would normally be subjected as a refractory in service. The temperature ranges through which these length changes occur, the sharply defined temperatures at which expansion begins during cooling, and the amounts of length change, will duplicate very closely in repeated tests for any one specimen, but are affected by the purity of the zirconia and the thermal history. The greatest length changes, and the highest temperature ranges in which these took place, were noted for the zirconia of highest purity preheated at 1,950° C. The contraction during heating is accompanied by heat absorption (endothermic), and the expansion during cooling is accompanied by a liberation of heat (exothermic). The former is presumably a manifestation of a phase change from monoclinic to tetragonal zirconia, and the latter a reversion of the tetragonal to the monoclinic form.

In their study of zirconia, Ruff and Ebert (see footnote 18) had concluded that a metal with an ionic radius approximating that of Zr^{++++}, and having an oxide with a cubic structure, would be most likely to enter the zirconia lattice and form the so-called stabilized cubic crystal, which is not subject to phase changes during heating and cooling. A correlation of pertinent values is given in table 4, and according to this one would expect the addition of CeO_2 to affect the ZrO_2 in a manner similar to the effect of Y_2O_3 or CaO. Ruff and Ebert (see footnote 18) did in fact report the formation of the cubic zirconia by adding 10 mole percent (13.4 weight percent) of CeO_2 and heating at 1,750° C. The information available does not explain why, in this investigation, the addition of 15 weight percent of CeO_2 and heating at various temperatures from 1,550° to 2,000° C failed to duplicate their result.

TABLE 4.—*Correlation of the atomic radius of some metals, and the crystalline form of their oxides, with their effect on the crystalline form and unit cell size of* ZrO_2

Metal			Zirconia plus oxide	
Ion	Ionic radius	Crystalline form of oxide	Crystalline form of ZrO_2 at room temperature	Unit cell size a
	A			*A*
Si^{++++}	0.40	(a)	Monoclinic	
Al^{+++}	.55	Trigonal	do [b]	
Mg^{++}	.75	Cubic	Cubic	5.05
Zr^{++++}	.80	(c)	(c)	[d] 5.05
Y^{+++}	.95	Cubic	Cubic	5.10
Ce^{++++}	1.01	do	Monoclinic [e]	
Ca^{++}	1.05	do	Cubic	5.10
Th^{++++}	1.10	do	(f)	(f)

[a] Quartz is trigonal, cristobalite is pseudoisometric, and tridymite is orthorhombic.
[b] Data from R. F. Geller, J. Research NBS **27**, 555 (1941) RP1443.
[c] Zirconia of high purity is normally monoclinic at room temperature.
[d] L. Passerini, Value for cubic zirconia, extrapolated to pure ZrO_2, Gazz. chim. ital. **60**, 762 (1930); in Phys. Rev. [2] **27**, 798 (1926), Wheeler P. Davey proposes a face-centered cubic structure with $a=5.098$ A.
[e] Otto Ruff and Fritz Ebert (Z. anorg. allgem. Chem. **180**, 19 (1929) obtained cubic ZrO_2 by adding 10 mole percent of CeO_2 and heating at 1,750° C.
[f] By heating a 1:1 (mole) composition of ThO_2 and ZrO_2 at 2,600° C, Otto Ruff, Fritz Ebert, and Hans Woitinek (Z. anorg. allgem. Chem. **180**, 252, 1929) prevented the reversion to monoclinic ZrO_2 and obtained two mixed crystals with fluorite (cubic) type lattice and unit cell sizes of 5.32 A and 5.51 A, respectively. After heating at 2,400° C, the zirconia retained its monoclinic structure.

The addition of at least 11.5 percent of Y_2O_3 and heating at 1,700° C was required to transform most of the zirconia to the stabilized condition, and complete conversion was obtained by adding 15 percent and heating at 1,850° C. However, because of the comparative rarity and high cost of yttria, this would be at present a commercially impracticable method for producing usable zirconia ware except in special applications.

Silica (added as quartz) reacted partially with zirconia at 1,500° and at 1,700° C to form zircon ($ZrSiO_4$), but zirconia which had not combined retained the monoclinic structure. As a result, the length changes of these compositions retained the irregularities of the unstabilized ZrO_2. The amount of length change at the monoclinic⇄tetragonal inversions was, however, much smaller for the ZrO_2-SiO_2

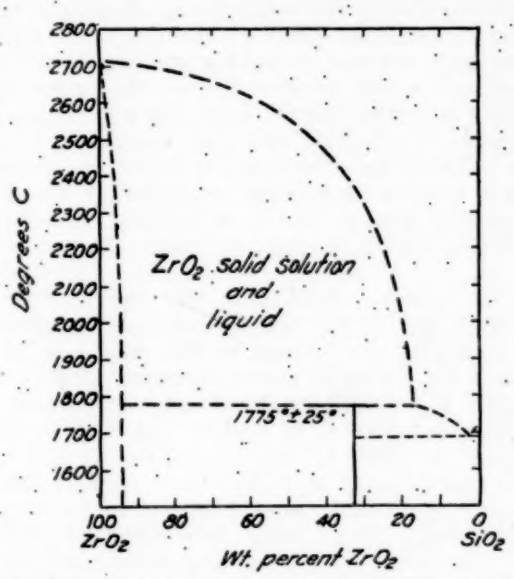

FIGURE 11.—*Proposed equilibrium diagram for the system* ZrO_2-SiO_2, *based on the observed incongruent melting of zircon at about 1,775° C.*

mixture in 1:1 mole proportions than for the zirconias without additions. The thermal length changes of mineral zircon preheated at 1,700° C were very uniform throughout the range from room temperature to 1,500° C during both heating and cooling, and the coefficient averaged 5.15×10^{-6}. This mineral would be an excellent refractory material for high temperature work if it did not break down between 1,750° and 1,800° C to form zirconia and liquid. Assuming complete breakdown, about one-third by weight, or one-half by volume, of the resultant body would be silica-rich glass. In view of the evidence presented for incongruent melting of ZrO_2, one must conclude that the published diagrams for the SiO_2-ZrO_2 system (see footnote 22) are incorrect and a modification is suggested in figure 11.

Magnesia was more effective than yttria for eliminating irregularities in the thermal length changes below 1,100° C. Above this temperature, however, the additions of MgO caused very high ex-

pansions and contractions during heating and cooling, respectively, the average linear coefficients ranging from 19.2×10^{-6} to 132×10^{-6}. The zirconia-magnesia compositions were dense and appeared very strong. The only nonabsorbent specimens obtained in this investigation contained equimolar proportions of zirconia C and periclase and were heated at 1,700° C.

The CaO additions were not only the most effective means noted in this work for producing the cubic zirconia, but they also provided an interesting demonstration of the radical changes in properties which may be caused by small changes in composition. As was observed, a 4-percent addition of CaO and preheating as high as 1,850° C had little effect on the inversions of the zirconia, whereas an addition of 5 percent and heating at 1,550° C brought about an almost complete transformation to the cubic form. A suggested explanation for the seemingly inordinate effect of the 1-percent addition of CaO is based on the large volume of the Ca ion compared to the Zr ion, or to the other ions which produced the cubic zirconia. One may assume that when a comparatively large ion enters the framework of the zirconia crystal, its effect will be more pronounced than the effect of a small ion. Thus, for example, increasing additions of the Mg ion, which has a volume 12 percent smaller than the Zr ion, should effect a more gradual change to the cubic form than increasing additions of the Ca ion, which occupies a volume 72 percent larger than the Zr ion.

In general, the results show that the irregular thermal length changes accompanying phase transformations in zirconia may be prevented by changing the crystal to the stable cubic form. This was accomplished by (a) 11.5- and 15-percent additions of Y_2O_3 and heating at 1,700° C or higher; (b) 8- and 15-percent additions of MgO and heating at 1,550° C or higher, but only in the range from room temperature to 1,200° C; and (c) 5-, 6-, 8-, and 15-percent additions of CaO and heating at 1,550° C or higher, but additions of more than 6 percent caused the specimens to be very porous and proportionately weak. In all cases, however, the expansion during heating and contraction during cooling was relatively high. The coefficients of linear thermal expansion ranged from 8.8 to 11.8×10^{-6} for specimens that were all, or nearly all, cubic. Also, zirconia has a low thermal conductivity relative to such materials of high thermal expansion as alumina, magnesia, and beryllia (unpublished data). Consequently, a high resistance to thermal shock cannot be expected of the stabilized product, even though it is not subject to the structural disintegration characteristic of the commercially pure material.

In order to apply the findings of this study, some shapes were cast of 94 percent zirconia and 6 percent lime, and installed in the furnace shown in figure 1. Only 29 tests have been made with the furnace since that time, but so far no tendency of the shapes to disintegrate has been noted.

The authors are indebted to B. L. Steierman and to H. F. McMurdie for the petrographic examinations and for the X-ray patterns and their interpretations.

WASHINGTON, April 13, 1945.

U. S. DEPARTMENT OF COMMERCE · NATIONAL BUREAU OF STANDARDS

RESEARCH PAPER RP1663

Part of Journal of Research of the National Bureau of Standards, Volume 34, July 1945

ACETYL DERIVATIVES OF CERTAIN HEPTOSES, OF GULOSE, AND OF LACTULOSE

By Harriet L. Frush and Horace S. Isbell

ABSTRACT

In the course of an investigation of the stereomeric factors that influence the course of replacement reactions, several new acetyl derivatives of the sugars were prepared. Inasmuch as the sugar acetates are of importance for analytical purposes, for the synthesis of other substances, and for the elucidation of structure, the new compounds are reported, even though the study of the reaction mechanisms has been temporarily discontinued. The preparation and properties are given for several new acetates of the heptoses, and for acetates of D-gulose, D-glucoheptulose, and lactulose.

The following new compounds are reported: Hexaacetyl-D-*glycero*-β-D-*ido*-aldoheptose, melting point 136° C, $[\alpha]_D^{20}$, −9.1°; pentaacetyl-D-*glycero*-α-D-*ido*-aldoheptosyl bromide, melting point 114° C, $[\alpha]_D^{20}$, +143°; methyl pentaacetyl-D-*glycero*-β-D-*ido*-aldoheptoside, melting point 136° to 137° C, $[\alpha]_D^{20}$, −31.3°; hexaacetyl-D-*glycero*-α-D-*talo*-aldoheptose, melting point 137° C, $[\alpha]_D^{20}$, +88.8°; hexaacetyl-D-*glycero*-L-*galacto*-aldoheptoses (crystalline mixture); pentaacetyl-D-gulose, melting point 113° C, $[\alpha]_D^{20}$, +86.2° (needle form), and melting point 105° to 106° C, $[\alpha]_D^{20}$, +86.2° (prismatic form); pentaacetyl-D-glucoheptulose, melting point 114° to 115° C, $[\alpha]_D^{20}$, +45.9°; octaacetyllactulose, melting point 138° C, $[\alpha]_D^{20}$, −6.6°.

CONTENTS

		Page
I.	Introduction	111
II.	Derivatives of D-*glycero*-D-*ido*-aldoheptose (D-β-glucoheptose)	114
	1. Hexaacetyl-D-*glycero*-β-D-*ido*-aldoheptose	115
	2. Pentaacetyl-D-*glycero*-α-D-*ido*-aldoheptosyl bromide (pentaacetyl-α-D-β-glucoheptosyl bromide)	116
	3. Methyl pentaacetyl-D-*glycero*-β-D-*ido*-aldoheptoside	116
III.	Hexaacetyl-D-*glycero*-α-D-*talo*-aldoheptose (hexaacetyl-α-D-β-mannoheptose)	117
IV.	Hexaacetyl-D-*glycero*-L-*galacto*-aldoheptoses (hexaacetyl-D-β-guloheptoses)	118
V.	Pentaacetyl-D-gulose	119
VI.	Pentaacetyl-D-glucoheptulose	121
VII.	Octaacetyllactulose	122
VIII.	References	124

I. INTRODUCTION

In the cyclic sugar derivatives the carbon atoms have known configurations and are united in a ring, so that rotation about the individual carbon-carbon bonds cannot take place. Consequently, the spheres of influence of the various groups attached to the ring are definitely fixed in relation to one another. For this reason the cyclic sugar derivatives are particularly suitable for studying the

effect of the relative position in space of the groups within the molecule upon the course and mechanism of replacement reactions.

Several years ago an investigation was begun in this laboratory of the influence of acetyl groups attached to the pyranose ring on the course of replacement reactions [1, 2].[1] At that time it was planned to prepare a large number of acetylglycosyl halides and to study their behavior in the Koenigs-Knorr reaction in order to ascertain the part which acetyl groups of neighboring carbons play in replacement reactions. A sufficient number of compounds was studied to warrant the formulation of the hypothesis that when an acetyl group is capable of approaching the face of the glycosidic carbon opposite the attached halogen, cleavage of the halogen occurs with Walden inversion and the formation of an orthoester.[2] Further study of the Koenigs-Knorr reaction has been in progress for some time, but because of the national emergency this work has been discontinued for the present. It seems desirable, however, to report the preparation and properties of certain new compounds that have been obtained, even though the work is not complete.

According to the premise on which the investigation was based, an acetylglycosyl halide having a *trans* configuration for the halogen of the glycosidic carbon and the acetyl group of the adjacent carbon can yield, on application of the Koenigs-Knorr reaction, the alpha and beta glycosides, and a methyl orthoacetate. Reaction 1 shows the formation of a glycoside with inversion of the glycosidic carbon; reaction 2 shows the formation of a methyl orthoacetate; whereas reaction 3 shows the formation of a methyl glycoside having the same configuration as the parent acetylglycosyl halide. Reaction 3 involves the formation of an intermediate of the orthoester type; as it includes two inversions, the configuration of the glycosidic carbon is retained. Although reaction 3 is illustrated in the diagram with a transient intermediate of the orthoester type, other transient intermediates are possible and might be formed from nucleophilic (electron-sharing) groups in the environment.

In an acetylglycosyl halide having a *cis* configuration for the halogen and the neighboring acetyl group, the acetyl cannot approach the face of the glycosidic carbon opposite the attached halogen, and consequently it cannot directly undergo reactions of the orthoester type. The halogen can be replaced readily, with inversion, by nucleophilic groups from the environment. The formation, in some cases, of small quantities of the glycoside having the same configuration as the parent acetylglycosyl halide may arise from an even number of successive displacements with inversion involving one or more unstable intermediates. In addition to the mechanisms outlined above, reactions resulting in racemization may take place by the formation of free carbonium ions. This course seems, however, to be of little importance under the conditions used in the present investigation.

---

[1] Figures in brackets indicate the literature references at the end of this paper.

[2] An excellent review of the subject of carbohydrate orthoesters is given by H. W. Post in The chemistry of aliphatic orthoesters, p. 106–114 (Reinhold Publishing Corporation, New York, N. Y., 1943).

In the aldoses, carbon 1 is bound in a ring, and consequently only those acetylglycosyl halides having the acetyl group of carbon 2 and the halide of carbon 1 in the *trans* position form orthoesters. In the ketoses, the halogen of the acetylglycosyl halide is located on carbon 2, and may be replaced by the acetyl groups of either carbon 1 or carbon 3. Presumably, reaction of an acetyl group of carbon 3 is

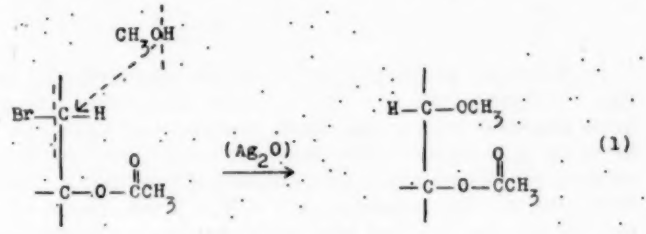

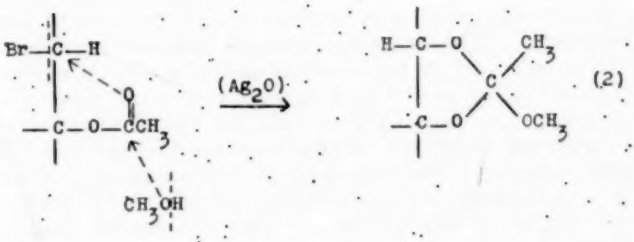

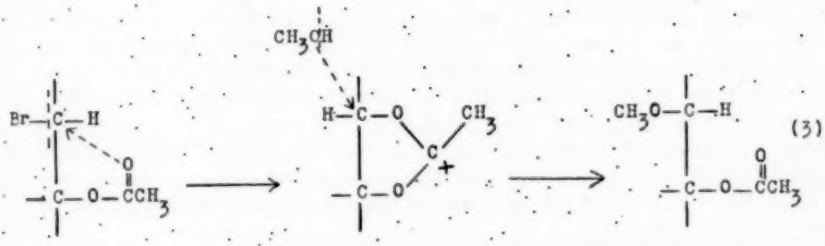

possible only when the group is *trans* to the halogen of carbon 2. As carbon 1 of the ketoses is not bound in the ring, and rotation about the carbon-carbon bond is possible, an acetyl group attached to carbon 1 can always approach carbon 2 from the direction favorable for orthoester formation. Consequently, all the ketoses should be capable of forming 1,2-orthoesters. Several orthoesters of ketoses have been reported in the literature [3], but none has been proved to have the 2,3-structure, and further investigation seems desirable.

II. DERIVATIVES OF D-*GLYCERO*-D-*IDO*-ALDOHEPTOSE (D-β-GLUCOHEPTOSE)[3] [4]

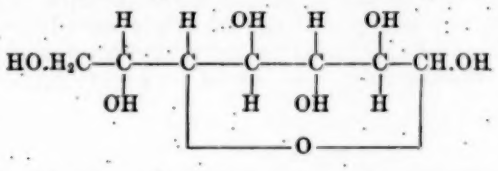

In previous publications [5, 6] the similarity of substances having like configurations for the carbons comprising the pyranose ring has been stressed, and it has been pointed out that any sugar capable of forming a pyranose ring may be considered to be configurationally related to one of the eight aldohexopyranoses. The pyranose modifications of the aldoheptoses differ from those of the aldohexoses merely in the number and stereoisomeric arrangement of the atoms in the side chain attached to the pyranose ring.

Little is known concerning the properties of the compounds of idose, the only aldohexose which has not been obtained in the crystalline state.[4] However, D-*glycero*-D-*ido*-aldoheptose (D-β-glucoheptose), one of the two aldoheptoses having the idose configuration, has been crystallized [8]. In this investigation a crystalline acetate, acetylglycosyl bromide, and methyl acetylglycoside of the sugar have been prepared. The acetyl-α-glycosyl bromide is of particular interest to the present study because the acetyl group of carbon 2 is *trans* to the halogen of carbon 1 and can approach the face of carbon 1 from the direction presumably favorable for the production of orthoesters.

The experimental study was complicated by the fact that the acetylglycosyl bromide is relatively unstable. When it was dissolved in chloroform, a mutarotation reaction took place with gradual discoloration of the solution. The compound could not be reclaimed from the chloroform solution, which turned black overnight, as did also the mother liquors of recrystallization. The compound keeps fairly well if a thin layer is stored over sodium hydroxide in a vacuum desiccator, at a low temperature. Without these precautions even the pure substance decomposes with the liberation of hydrogen bromide. The relative instability of the bromide might arise from the fact that the oxygen of the acetyl group of carbon 2 can approach the face of carbon 1 opposite the attached bromide. This stereomeric condition would make possible intramolecular elimination of the bromide ion by a reaction of the orthoester type. Application of the

[3] The systematic names used in this paper are derived by a procedure which is applicable to substances containing more than four contiguous asymmetric carbon atoms. The horizontal formula is written in the Fischer conventional manner with the lowest-numbered asymmetric carbon at the right. Configurational units are set off in order, beginning with the lowest-numbered asymmetric carbon, and the name is read from left to right in manner analogous to setting off and reading a large number. The derivation of the systematic name for D-β-glucoheptose is illustrated below:

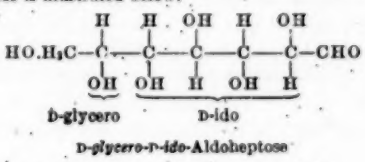

D-*glycero*-D-*ido*-Aldoheptose

[4] Gulose has been crystallized only in the form of a calcium chloride compound [7

Koenigs-Knorr reaction [9] to the acetylglycosyl bromide gave a product that was obviously a mixture. From this mixture a crystalline glycoside, tentatively classified as the beta pyranose modification, was obtained in 43-percent yield; the residual products of the reaction have not yet been identified, but will be the subject of future investigation.

A comparison by means of Hudson's isorotation principle [10] of the molecular rotations of the three new derivatives of D-*glycero*-D-*ido*-aldoheptose with molecular rotations of previously known pyranose derivatives of the epimeric sugar, D-*glycero*-D-*gulo*-aldoheptose is of interest.

	$[\alpha]_D$	$[M]_D$	Reference
Hexaacetyl-D-*glycero*-β-D-*gulo*-aldoheptose	+4. 8°	+2, 200	[11]
Hexaacetyl-D-*glycero*-D-*ido*-aldoheptose	−9. 1°	−4, 200	
Difference		+6, 400	
Pentaacetyl-D-*glycero*-α-D-*gulo*-aldoheptosyl bromide	+156°	+75, 400	[12]
Pentaacetyl-D-*glycero*-D-*ido*-aldoheptosyl bromide	+143°	+69, 100	
Difference		+6, 300	
Methyl pentaacetyl-D-*glycero*-β-D-*gulo*-aldoheptoside	−16°	−6, 950	[12]
Methyl pentaacetyl-D-*glycero*-D-*ido*-aldoheptoside	−31. 3°	−13, 600	
Difference		+6, 650	

The fact that pyranoses are ordinarily obtained by the methods used for preparing the new compounds, and the approximate agreement of the epimeric differences, seem to support the classification of the new compounds as pyranose derivatives. Apparently the acetate and acetylglycoside are beta compounds, and the bromide is an alpha compound. Additional work is necessary for the rigorous classification of these substances, but they are tentatively designated:

Hexaacetyl-D-*glycero*-β-D-*ido*-aldoheptose.
Pentaacetyl-D-*glycero*-α-D-*ido*-aldoheptosyl bromide.
Methyl pentaacetyl-D-*glycero*-β-D-*ido*-aldoheptoside.

1. HEXAACETYL-D-*GLYCERO*-β-D-*IDO*-ALDOHEPTOSE

Twenty-five grams of finely powdered D-*glycero*-D-*ido*-aldoheptose (D-β-glucoheptose) [8] was added to a mixture of 300 ml of acetic anhydride and 250 ml of pyridine previously cooled to 0° C and contained in a flask equipped with a sealed mechanical stirrer. The mixture was stirred at 0° C until solution was complete (about 2 days) and then poured with stirring into 6 liters of ice water. After half an hour, the product was extracted with chloroform, and the chloroform extract was washed several times with an aqueous solution of cupric nitrate and finally with water. The chloroform solution was dried, filtered, and finally concentrated in vacuum to a sirup from which the acetate crystallized. After the addition of ether the crystals were separated by filtration. By concentrating the mother liquor, a second crop of crystals was obtained, making a total yield of 36.7 g of crude acetate. Three successive crystallizations from warm ethyl alcohol

yielded pure hexaacetyl-D-*glycero*-D-*ido*-aldoheptose, mp, 136° C. $[\alpha]_D^{20}=-9.1°$ (chloroform, $c=4$).[5] The melting point and optical rotation were unchanged by recrystallization. A microphotograph of the crystals is given in figure 1, *A*.

Analysis: Calculated for $C_{19}H_{26}O_{13}$: C, 49.35; H, 5.67; CH_3CO, 55.85. *Found:* C, 49.2; H, 5.6; CH_3CO, 55.8.

2. PENTAACETYL-D-*GLYCERO*-α-D-*IDO*-ALDOHEPTOSYL BROMIDE (PENTAACETYL-α-D-β-GLUCOHEPTOSYL BROMIDE)

One gram of finely powdered hexaacetyl-D-*glycero*-β-D-*ido*-aldoheptose was brominated at 0° C by treating it with 5 ml of a saturated solution of hydrogen bromide in acetic acid, to which 0.5 ml of acetic anhydride had been added. The sugar dissolved in about 10 minutes. The solution was kept at 0° C for 3 hours, after which time it was poured into ice water, and extracted quickly with benzene. The benzene extract was washed six times with ice water, dried with Drierite, and after filtration, concentrated in vacuum to a thin sirup, which crystalsized upon the addition of ether. The preparation was repeated on leveral 5-g quantities of hexaacetyl-D-*glycero*-β-D-*ido*-aldoheptose, which yielded about 4 g each of the crude bromide. The compound was recrystallized several times by dissolving it in ether, and adding petroleum ether to saturation. When pure, it melts at 114° C.

Analysis: Calculated for $C_{17}H_{23}O_{11}Br$: C, 42.25; H, 4.80; Br, 16.54. Found: C, 42.9; H, 4.8; Br, 16.3.

A 0.0490-g sample of the substance dissolved in purified chloroform to give a volume of 1.511 ml showed an optical rotation in a 1-dm tube of +13.39°S 10 minutes after dissolution. The optical rotation decreased in 5 hours to +10.43° S; after 18 hours the solution was too dark to read. The reading 10 minutes after dissolution corresponds to $[\alpha]_D^{20}=+143°$ (chloroform, $c=3.2$). A microphotograph of the the crystals is given in figure 1, *B*.

3. METHYL PENTAACETYL-D-*GLYCERO*-β-D-*IDO*-ALDOHEPTOSIDE

Four grams of D-*glycero*-α-D-*ido*-aldoheptosyl bromide was added to a cold reaction mixture consisting of 200 ml of anhydrous methyl alcohol, 16 g of freshly prepared silver carbonate, and 8 g of powdered Drierite. The mixture was stirred continuously at 0° C for about 1 day, and then filtered. The filtrate was concentrated in vacuum to a sirup, from which approximately 3 g of crystals was separated. Examination of the material under the microscope revealed two types of crystals. After two recrystallizations from ethyl alcohol, 1.55 g of homogeneous material, mp 136° to 137° C, was obtained. $[\alpha]_D^{20}=-31.3°$ (chloroform, $c=2$). The constants were not changed by further recrystallization. A microphotograph of the crystals is given in figure 1, *C*.

Analysis: Calculated for $C_{18}H_{26}O_{12}$: C, 49.77; H, 6.03; CH_3CO, 49.56; CH_3O, 7.14. Found: C, 50.0; H, 6.1; CH_3CO, 49.7; CH_3O, 7.1.

In order to ascertain whether or not the substance is an orthoester, it was treated with a 0.5-percent solution of hydrogen chloride in dry chloroform under conditions which have been shown to cause the rapid conversion of orthoesters to acetylglycosyl chlorides [13]. See also page 420 of [2]. No rapid change in optical rotation was ob-

[5] The constants for this substance were previously reported on page 724 of reference [10b].

served, and after 10 minutes the hydrogen chloride was removed by the addition of dry silver carbonate and filtration. After evaporation of the filtrate, crystalline methyl pentaacetyl-D-*glycero*-β-D-*ido*-aldoheptoside was reclaimed unchanged. As the substance in chloroform solution is not sensitive to hydrogen chloride, it does not have an orthoester structure.

III. HEXAACETYL-D-*GLYCERO*-α-D-TALO-ALDOHEPTOSE (HEXAACETYL-α-D-β-MANNOHEPTOSE)

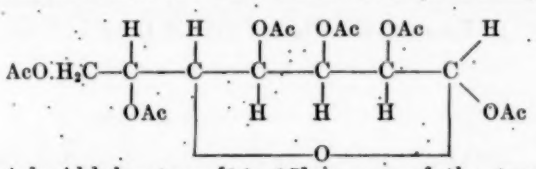

D-*glycero*-D-*talo*-Aldoheptose [14, 15] is one of the two sugars obtained by application of the cyanhydrin synthesis to mannose. The free sugar has the α-D-talose configuration for the atoms comprising the pyranose ring, and its properties show a parallelism to those of α-D-talose. As tetraacetyl-α-D-talosyl bromide is readily obtained in the crystalline state and gives rise by the Koenigs-Knorr reaction to a methyl orthoacetate [16], it was of interest to attempt the successive preparation of the acetate, acetylglycosyl bromide, and the methyl orthoacetate of D-*glycero*-D-*talo*-aldoheptose. The acetate has been prepared, and its properties are reported here, but the preparation of the acetylglycosyl bromide and the study of its behavior in the Koenigs-Knorr reaction must await a more opportune time.

Inasmuch as the new acetate was prepared from D-*glycero*-α-D-*talo*-aldoheptopyranose, and contains six acetyl groups, it is presumably hexaacetyl-D-*glycero*-α-D-*talo*-aldoheptopyranose. This classification is supported by the agreement of its optical rotation with that calculated from the rotations of compounds affording a comparison of "epimeric differences" [17]. D-*glycero*-D-*talo*-Aldoheptose (D-β-mannoheptose) has the D-talose structure, and D-*glycero*-D-*galacto*-aldoheptose (D-α-mannoheptose) has the D-galactose structure. The molecular rotation of pentaacetyl-α-D-talopyranose (+27,400) [16] is 14,250 units less than that of pentaacetyl-α-D-galactopyranose (+41,650) [18]. Assuming that this epimeric difference applies in the heptose series, the molecular rotation of hexaacetyl-D-*glycero*-α-D-*talo*-aldoheptopyranose should be 14,250 units less than that of hexaacetyl-D-*glycero*-α-D-*galacto*-aldoheptopyranose (+55,850) [19], or +41,600. This value corresponds to a specific rotation of +90.0° in comparison with the observed value of +88.8°.

Acetylation of D-*glycero*-α-D-*talo*-*aldoheptose*.—A finely powdered sample of D-*glycero*-α-D-*talo*-aldoheptose monohydrate (2.35 g) was acetylated at 0° C with a mixture of 13 ml of acetic anhydride and 20 ml of pyridine. The mixture was stirred at 0° C for 18 hours, and then poured with stirring into 400 ml of ice water. In the course of half an hour the product crystallized in small needles or slender prisms, which, when separated, weighed 3.6 g and melted at 128° to 132° C. The crude product was recrystallized from 15 ml of hot ethyl alcohol. The first crop of crystals weighed 2.7 g and melted at

135° to 137° C. Recrystallization from 10 ml of hot ethyl alcohol gave 2.5 g, melting at 137° C (fig. 1, *A*). $[\alpha]_D^{20}=+88.8°$ (chloroform, $c=4$). The melting point and optical rotation were unchanged by further recrystallization of the compound.

Analysis: Calculated for $C_{19}H_{26}O_{13}$: C, 49.35; H, 5.67; CH_3CO, 55.85. Found: C, 49.6; H, 5.7; CH_3CO, 55.6.

IV. HEXAACETYL-D-*GLYCERO*-L-*GALACTO*-ALDOHEPTOSES

(HEXAACETYL-D-β-GULOHEPTOSES)

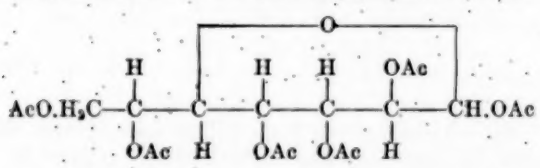

Acetylation of D-*glycero*-L-*galacto*-*aldoheptose.*—A 1.35 gm sample of finely powdered D-*glycero*-α-L-*galacto*-aldoheptose (α-D-β-guloheptose)[6] was acetylated at 0° C with 9 ml of acetic anhdride and 14 ml of pyridine. The sugar went into solution slowly; when solution was complete the mixture was poured with stirring into 10 volumes of ice water. In the course of about half an hour, crystals separated from the water mixture; they were collected on a filter and the filtrate was extracted with benzene. The benzene solution was evaporated to a sirup, which was brought to crystallization by the addition of alcohol. The crystals obtained both from water and from the benzene extract melted over a wide range and appeared to be mixtures. By numerous recrystallizations of the combined products from ethyl, isopropyl, and isoamyl alcohols, and finally from ligroin, two fractions were obtained, the larger of which melted at 117° to 118° C and had a specific rotation of −65°. A smaller fraction melted at 150° to 155° C and had a specific rotation of approximately −15°. Microscopic examination of the fractions showed that they were not homogeneous and consisted of mixtures of large flat plates and slender needles. However, it has been impossible with the amount of material at hand to effect a complete separation and purification of these acetates. The analysis of the larger fraction (mp, 117° to 118° C, $[\alpha]_D^{20}$, −65°) agrees with that of a hexaacetylheptose. Hence it is assumed that the material consists of two crystalline isomeric hexaacetates of D-*glycero*-L-*galacto*-aldoheptose. The formation of two crystalline acetates shows that the conversion of the parent sugar to other modifications takes place during the acetylation, even under the mild conditions employed here.

Analysis of the fraction melting at 117° to 118° C: Calculated for $C_{19}H_{26}O_{13}$: C, 49.35; H, 5.67; CH_3CO, 55.85. Found: C, 49.3; H, 5.7; CH_3CO, 55.3.

---

[6] LaForge [20], who was the first to prepare this sugar in the crystalline state, called it α-*d*-guloheptose. For reasons pointed out in [21] the name was subsequently changed by Isbell to *d*-β-guloheptose. The systematic name for the alpha modification of the sugar is D-*glycero*-α-L-*galacto*-aldoheptose.

V. PENTAACETYL-D-GULOSE [7]

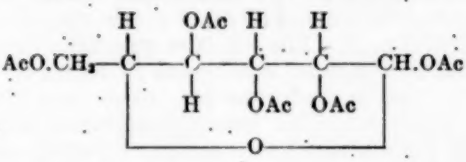

The aldohexose, gulose, has been crystallized only in the form of the calcium chloride compounds, α-D-gulose.$CaCl_2$.H_2O and (D-gulose)$_2$.$CaCl_2$ [7]. Numerous attempts to obtain a crystalline acetate by acetylation of α-D-gulose.$CaCl_2$.H_2O either with acetic anhydride and pyridine or with acetic anhydride and sodium acetate gave sirups that failed to crystallize. Acetylation of the calcium chloride compound with acetic anhydride and sulfuric acid at 0° C gave a small quantity of a crystalline gulose pentaacetate. The material was obtained in somewhat higher yield by the zinc chloride method.

A comparison, by means of Hudson's principle of isorotation, of the molecular rotation of pentaacetyl-D-gulose with the molecular rotations of some configurationally related substances may be used for the tentative assignment of structure to the compound. Thus $[M]_D$ of hexaacetyl-D-*glycero*-α-D-*gulo*-aldoheptopyranose minus $[M]_D$ of methyl pentaacetyl-D-*glycero*-α-D-*gulo*-aldoheptopyranoside should equal $[M]_D$ of pentaacetyl-α-D-gulopyranose minus $[M]_D$ of methyl tetraacetyl-α-D-gulopyranoside.

Unfortunately, two values are reported in the literature for the molecular rotation of methyl pentaacetyl-D-*glycero*-α-D-*gulo*-aldoheptopyranoside. One of these was obtained for a product derived by application of the Koenigs-Knorr reaction to pentaacetyl-D-*glycero*-β-D-*gulo*-aldoheptopyranosyl chloride [12] and the other for a product derived by acetylation of crystalline methyl D-*glycero*-α-D-*gulo*-aldoheptopyranoside [6]. It is of interest to calculate the optical rotation of pentaacetyl-α-D-gulopyranose from the relation indicated above by the use of each of the two values for the molecular rotation of methyl pentaacetyl-D-*glycero*-α-D-*gulo*-aldoheptopyranoside. The following values of $[M]_D$ are employed:

Hexaacetyl-D-*glycero*-α-D-*gulo*-aldoheptopyranose	+40,250 [11]
Methyl pentaacetyl-D-*glycero*-α-D-*gulo*-aldoheptopyranoside	+39,550 [12] +46,650 [6]
Methyl tetraacetyl-α-D-gulopyranoside	+35,250 [22]

These values give a molecular rotation for pentaacetyl-α-D-gulopyranose of +35,950 based on the value of Haworth, Hirst, and Stacey [12], and of +28,850 based on the value of Isbell and Frush [6]. They correspond to specific rotations of +92.1° and +73.9°, respectively, in comparison with the observed specific rotation of +86.2°. The observed rotation lies sufficiently close to the calculated rotations to warrant the tentative assignment of the alpha pyranose structure to the crystalline pentaacetate of gulose. The difference in the values may arise from the different ring conformations previously suggested by us as a possible explanation of other discrepancies in the optical rotations of substances in the gulose and D-*glycero*-D-*gulo*-aldoheptose series [6, p. 134].

[7] The structure shown here is to be considered as tentative.

Acetylation of α-D-gulose.$CaCl_2.H_2O$ with acetic anhydride and sulfuric acid.—Ten grams of finely powdered α-D-gulose.$CaCl_2.H_2O$ was added to a previously cooled mixture of 60 ml of acetic anhydride and 2.5 ml of concentrated sulfuric acid. The mixture was kept in an ice bath and stirred for 24 hours. After an additional 24 hours at room temperature the mixture was poured into ice water and the product was extracted with benzene. The benzene solution was washed with water, dried, and concentrated to a sirup. By extraction of the sirup with hot water and evaporation of the water solution, a small quantity of crystalline gulose pentaacetate was obtained.[8] This material was used for seeding the sirups obtained by the zinc chloride method.

Acetylation of α-D-gulose.$CaCl_2.H_2O$ with acetic anhydride and zinc chloride.—Ten grams of finely powdered α-D-gulose-$CaCl_2.H_2O$ was added to 50 ml of ice-cold acetic anhydride containing 15 g of anhydrous zinc chloride and 20 g of dry sand. The mixture was placed in an ice bath and stirred until the gulose calcium chloride went into solution (24 hr). The solution was then poured into ice water and the product was extracted with chloroform. The chloroform solution was washed with water and dried with sodium sulfate. On evaporation it gave a nearly colorless sirup which was diluted with 20 ml of secondary amyl alcohol and seeded with crystalline gulose pentaacetate. The solution was placed in a refrigerator and was allowed to stand until crystallization was complete, after which the crystals were separated and washed with amyl alcohol. The yield by this procedure varied from 1 to 4 g, and efforts to obtain higher yields and more consistent results were unsuccessful.

In order to obtain a larger quantity of the acetate, 150 g of α-D-gulose.$CaCl_2.H_2O$ was treated with 700 ml of acetic anhydride and 225 g of freshly fused zinc chloride. The mixture was mechanically stirred at 0° C for 5 days, and at room temperature for 5 days, and then poured with stirring into 8 liters of ice and water. The product was extracted with benzene and the benzene solution was washed with water, dried, and concentrated under reduced pressure to a sirup. The sirupy acetate was dissolved in 10 liters of boiling water; the solution was cooled, seeded with the crystalline acetate, and allowed to evaporate in air at room temperature. As evaporation proceeded, large crystals grew in the solution and a thin layer of sirupy acetate formed on the surface of the liquid. From time to time this layer was mechanically removed to avoid mixing with the crystals. Ultimately a total of 50 g of the crystalline gulose pentaacetate was separated from the liquid in the form of transparent hexagonal plates, some of which were nearly one-fourth inch in diameter.

When the compound was recrystallized from warm ethyl alcohol it formed slender needles (mp, 113° C, $[\alpha]_D^{20}$,+86.2°). However, the needle crystals (fig. 2, *A*) were unstable and upon standing, or occasionally even during separation by filtration, changed to chunky truncated prisms (mp, 105° to 106° C; fig. 2, *B*). Because of the difficulty in obtaining a single crystalline modification, alcohol was abandoned as a solvent, and the acetate was recrystallized from water.

[8] This compound was first crystallized in 1931, but was not closely investigated. The melting point of one form and the optical rotation were reported on page 736 of reference [10b].

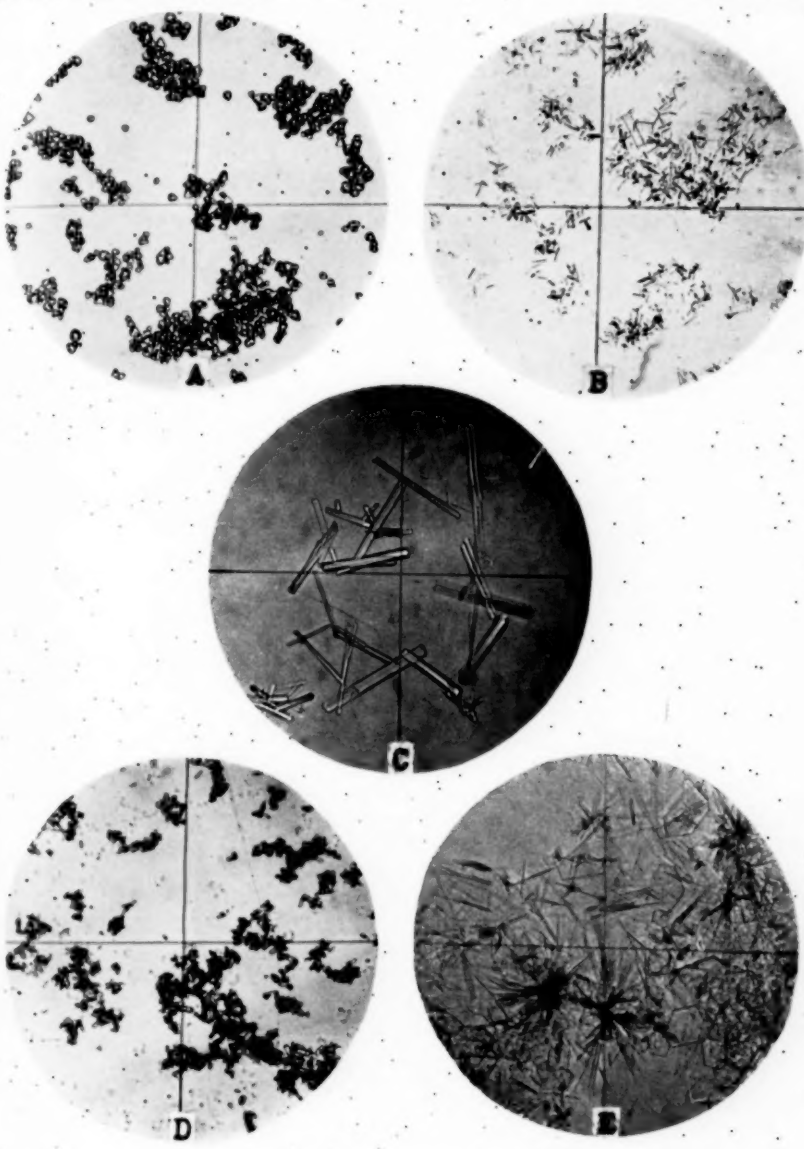

FIGURE 1.—*Photomicrographs of new compounds.*

A, Hexaacetyl-D-*glycero*-β-D-*ido*-aldoheptose (hexaacetyl-β-D-β-glucoheptose); *B*, pentaacetyl-D-*glycero*-α-D-*ido*-aldoheptosyl bromide (pentaacetyl-α-D-β-glucoheptosyl bromide); *C*, methyl pentaacetyl-D-*glycero*-β-D-*ido*-aldoheptoside (methyl pentaacetyl-β-D-β-glucoheptoside); *D*, hexaacetyl-D-*glycero*-α-D-*talo*-aldoheptose (hexaacetyl-α-D-β-mannoheptose); *E*, exaacetyl-D-*glycero*-L-*galacto*-aldoheptoses (hexaacetyl-D-β-guloheptoses).

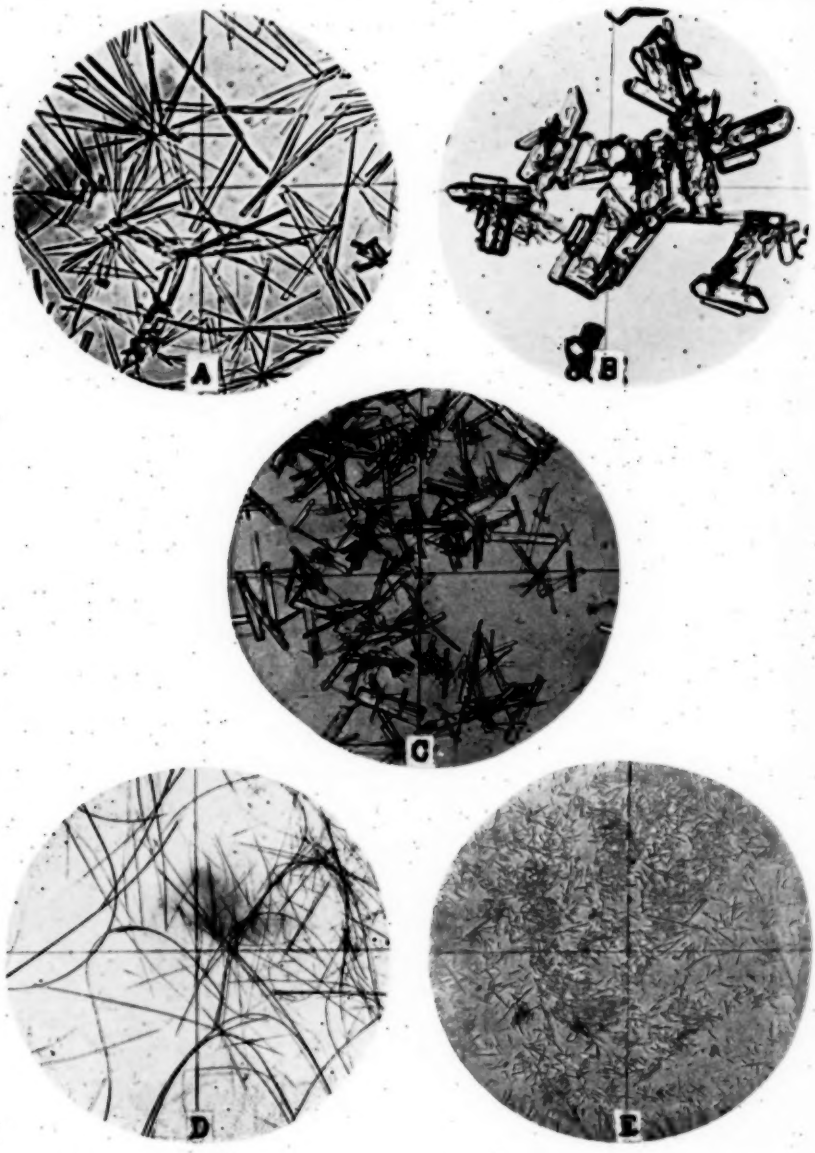

FIGURE 2.—*Photomicrographs of new compounds.*

A, Pentaacetyl-D-gulose (needle form); *B*, pentaacetyl-D-gulose (prismatic form); *C*, pentaacetyl-D-glycero-heptulose; *D*, octaacetyllactulose; *E*, octaacetyllactulose (crystallized in motion).

The material was dissolved in hot water and the solution was concentrated in vacuum to approximately one-fourth of its volume. On cooling, it yielded exclusively the modification melting at 105° to 106° C. $[\alpha]_D^{20} = +86.2°$ (chloroform, $c=2$).

Analysis: Calculated for $C_{16}H_{22}O_{11}$: C, 49.23; H, 5.68; CH_3CO, 55.14. Found for the needle crystals (mp, 113° C): C, 49.3; H, 5.6. Found for the prismatic crystals (mp, 105° to 106° C): C, 49.4; H, 5.6; CH_3CO, 55.3.

VI. PENTAACETYL-D-GLUCOHEPTULOSE [9]

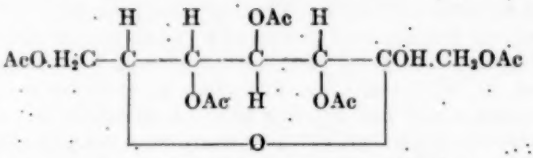

Prior to this investigation, Austin [23] had reported the preparation of hexaacetyl-α-D-glucoheptulopyranose from the corresponding sugar by the sodium acetate method of acetylation. It was expected that the same acetate would be formed by application of the milder pyridine method. However, the crystalline product obtained by the latter method proved to be a mixture from which has been isolated, in addition to hexaacetyl-α-D-glucoheptulose, a new pentaacetate and a crude fraction having an optical rotation lower than that of either. Acetylation of the new pentaacetate gave the previously known hexaacetyl-α-D-glucoheptulopyranose. Hence the pentaacetylglucoheptulose has the pyranose ring.

The pyranose modifications of D-glucoheptulose and D-sorbose have the same configuration for the atoms comprising the ring, but differ in that the heptose has a CH_2OH group attached to carbon 6 in place of a hydrogen atom. By acetylation of sorbose under approximately the same conditions used in acetylating D-glucoheptulose, a tetraacetate having a free glycosidic hydroxyl group is formed [24]. By analogy, one might expect the new compound of glucoheptulose to have a free hydroxyl group on carbon 2 and to be 1,3,4,5,7-pentaacetyl-D-glucoheptulose. Assuming that the glycosidic hydroxyl is free, an indication of the configuration of the glycosidic carbon may be gained through a comparison of molecular rotations. By application of Hudson's isorotation principle to the molecular rotations of methyl tetraacetyl-α-D-sorbopyranoside (+19,050) [24], 1,3,4,5-tetraacetyl-α-D-sorbose (+7,400) [24],[10] and methyl pentaacetyl-α-D-gluco-heptulopyranoside (+34,100) [23], the molecular rotation of 1,3,4,5,7-pentaacetyl-α-D-glucoheptulose is calculated to be +22,450. This value corresponds to a specific rotation of +53.4°, in comparison with the observed value of +45.9°. The agreement between the observed value and the calculated rotation is not sufficiently close to warrant a definite assignment of structure, although the compound is probably 1,3,4,5,7-pentaacetyl-α-D-glucoheptulose. The assignment of the acetyl groups to definite positions, however, is left to future investigation, and the compound is designated merely as pentaacetyl-D-glucoheptulopyranose.

[9] Structure is tentative.

[10] The molecular rotations of the D-sorbose derivatives were derived from those of the corresponding derivatives of L-sorbose.

Acetylation of D-*glucoheptulose.*—Twenty grams of powdered D-glucoheptulose was added to 92 ml of acetic anhydride and 140 ml of pyridine, previously cooled to 0° C. The mixture was stirred at 0° C for 3 days and at room temperature for 2 days. It was then poured, with stirring, into ice water and the produce was extracted with chloroform. The chloroform solution was concentrated in vacuum to a thick sirup, which was brought to crystallization by the addition of ether and petroleum ether. The crude acetate weighed about 30 g and the melting point was approximately 80° C. The material, which proved to be a mixture, was recrystallized several times from 50-percent aqueous alcohol. During this process some slender prisms were obtained which had a specific rotation of +48°. They were obviously different from the previously known hexaacetate, which crystallizes in silky needles and has a specific rotation of +87°. Aqueous alcohol did not appear to be a suitable solvent for the separation of the acetates, but after numerous crystallizations from carbon tetrachloride, and determinations of optical rotation, the material was separated into three fractions consisting of the previously known hexaacetyl-α-D-glucoheptulose, a new pentaacetate, and a fraction having a specific rotation lower than that of either (+10°). The new pentaacetate crystallizes in slender prisms (fig. 2, *C*), which melt at 114° to 115° C. $[\alpha]_D^{20}=+45.9°$ (chloroform, $c=4$).

Analysis: Calculated for $C_{17}H_{24}O_{12}$: C, 48.57; H, 5.74; CH_3CO, 51.20. Found: C, 48.4; H, 5.6; CH_3CO, 51.4.

To show the relation of the new pentaacetate to the previously known hexaacetate, 1 g of the pentaacetate was acetylated at room temperature with 6 ml of acetic anhydride and 7 ml of pyridine. The product crystallized when poured into ice water with stirring. After recrystallization from alcohol, the compound gave a specific rotation of +86° in comparison with a specific rotation of +87° for hexaacetyl-α-D-glucoheptulose. The pentaacetate therefore appears to be a derivative of the pyranose modification of the sugar.

VII. OCTAACETYLLACTULOSE [11]

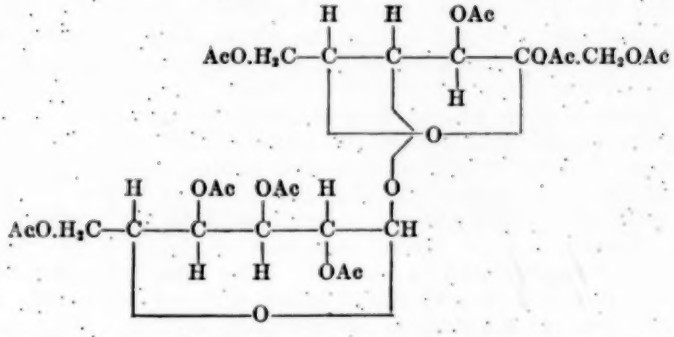

The ketose obtained from lactose by means of the Lobry de Bruyn-Van Ekenstein interconversion reaction was first prepared by Montgomery and Hudson and called lactulose [25]. In a previous publication from this laboratory [26] data were presented that indicate that lactulose crystallizes from solution in the form of a furanose modifica-

[11] Formula is tentative.

tion. The crystallization of a furanose from a pyranose-furanose equilibrium mixture is unique, and confirmation of the furanose structure is desirable. The determination of the structure of a crystalline sugar is complicated by the fact that isomeric changes take place on dissolution. During acetylation with pyridine and acetic anhydride at low temperatures, isomeric changes occur to only a limited degree, and the product usually contains the same modification as the parent sugar. Acetylation of finely powered lactulose with pyridine gave a crystalline octaacetate. As the parent sugar has been shown to be a furanose, it is probable that the acetate is a furanose derivative. Data are not available for calculating the optical rotation of the furanose acetate, but comparisons with certain pyranose derivatives appear to indicate that the compound is not a pyranose. The molecular rotation of octaacetyl-α-lactulopyranose may be calculated from the molecular rotations of octaacetyl-α-lactose (+36,400) [27], pentaacetyl-α-D-glucopyranose (+39,700) [28], and of pentaacetyl-α-D-fructopyranose (+18,500) [29], to be +15,200. This value corresponds to a specific rotation of +22.4°. From the molecular rotations of the corresponding beta compounds (octaacetyl-β lactose (−3,200) [27], pentaacetyl-β-D-glucopyranose (+1,500) [28], and pentaacetyl-β-D-fructopyranose (−47,200) [30]), the specific rotation of octaacetyl-β-lactulopyranose is calculated to be −76.5°. Hence the specific rotation of our acetate, −6.6°, does not agree with either of the rotations calculated for the pyranose derivatives. Although it seems possible that the compound, like the parent sugar, is a furanose derivative, assignment of a definite structure is not attempted at this time.

Preparation of octaacetyllactulose.—Twenty grams of finely powdered crystalline lactulose was acetylated at approximately −15° C with a mixture consisting of 92 ml of acetic anhydride and 140 ml of pyridine. After 2 days the reaction mixture was poured into ice water and the product was extracted with chloroform. The chloroform extract was concentrated in a vacuum still, and the sirupy residue was dissolved in acetone. The acetone solution was concentrated to a sirup, from which a crystalline product was obtained by the addition of ethyl alcohol. The new acetate formed mats of long hair-like crystals (fig. 2, *D*) which were difficult to separate by filtration. However, when the substance was allowed to crystallize slowly and in motion from hot ethyl alcohol, or from hot water, it formed short needles (fig. 2, *E*) which could be separated easily. The acetate, when dry, readily acquired an electrostatic charge, and tended to scatter. After several recrystallizations from hot ethyl alcohol, it melted at 138° C. $[\alpha]_D^{20} = -6.6°$ (chloroform, $c=4$). These constants were unchanged by further recrystallization from ethyl alcohol, isopropyl alcohol, carbon tetrachloride, or water.

Analysis: Calculated for $C_{28}H_{38}O_{19}$: C, 49.56; H, 5.64; CH_3CO, 50.75. Found: C, 49.5; H, 5.5; CH_3CO, 50.9.

The authors express their appreciation to Kenneth Fleischer for making the carbon, hydrogen, acetyl, and methoxyl determinations reported in this paper.

VIII. REFERENCES

[1] H. S. Isbell, Ann. Rev. Biochem. **9,** 65 (1940).
[2] H. L. Frush and H. S. Isbell, J. Research NBS **27,** 413 (1941) RP1429.
[3] E. Pacsu, J. Am. Chem. Soc. **55,** 2451 (1933); **57,** 745 (1935); **61,** 1654 (1939).
[4] E. Fischer, Liebigs Ann. Chem. **270,** 87 (1892).
[5] H. S. Isbell, J. Research NBS **18,** 505 (1937) RP990.
[6] H. S. Isbell and H. L. Frush, J. Research NBS **24,** 125 (1940) RP1274.
[7] H. S. Isbell, BS J. Research **5,** 741 (1930) RP226.
[8] H. S. Isbell, J. Am. Chem. Soc. **56,** 2789 (1934).
[9] W. Koenigs and E. Knorr, Ber. deut. chem. Ges. **34,** 957 (1901).
[10a] C. S. Hudson, BS Sci. Pap. **21,** 241 (1926) S533.
[10b] F. J. Bates and Associates, Polarimetry, saccharimetry, and the sugars, Circular National Bureau of Standards C440 (1942).
[11] C. S. Hudson and E. Yanovsky, J. Am. Chem. Soc. **38,** 1575 (1916).
[12] W. N. Haworth, E. L. Hirst, and M. Stacey, J. Chem. Soc. **1931,** 2864.
[13] H. S. Isbell, BS J. Research **7,** 1115 (1931) RP392.
[14] V. Ettel, Collection Czechoslov. Chem. Commun. **4,** 504 (1932).
[15] H. S. Isbell, J. Research NBS **20,** 97 (1938) RP1069.
[16] W. W. Pigman and H. S. Isbell, J. Research NBS **19,** 189 (1937) RP1021.
[17] C. S. Hudson, J. Am. Chem. Soc. **48,** 1434 (1926).
[18] C. S. Hudson and H. O. Parker, J. Am. Chem. Soc. **37,** 1589 (1915).
[19] E. M. Montgomery and C. S. Hudson, J. Am. Chem. Soc. **56,** 2463 (1934).
[20] F. B. LaForge, J. Biol. Chem. **41,** 251 (1920).
[21] H. S. Isbell, J. Research NBS **19,** 644 (1937) RP1052.
[22] H. S. Isbell, BS J. Research **8,** 1 (1932) RP396.
[23] W. C. Austin, J. Am. Chem. Soc. **54,** 1925 (1932).
[24] H. H. Schlubach and G. Graefe, Liebigs Ann. Chem. **532,** 211 (1937).
[25] E. M. Montgomery and C. S. Hudson, J. Am. Chem. Soc. **52,** 2101 (1930).
[26] H. S. Isbell and W. W. Pigman, J. Research NBS **20,** 773 (1938) RP1104.
[27] C. S. Hudson and J. M. Johnson, J. Am. Chem. Soc. **37,** 1270 (1915).
[28] C. S. Hudson and J. K. Dale, J. Am. Chem. Soc. **37,** 1264 (1915).
[29] E. Pacsu and F. B. Cramer, J. Am. Chem. Soc. **57,** 1945 (1935).
[30] C. S. Hudson and D. H. Brauns, J. Am. Chem. Soc. **37,** 1283 (1915).

WASHINGTON, MARCH 20, 1945.

○